2012

The evaluation of the sedimentation behavior of magnesium hydroxide in the never dried state

Sri Ramya Punnamaraju
The University of Toledo

A Thesis

entitled

The Evaluation of the Sedimentation Behavior of Magnesium Hydroxide in the Never Dried State

by

Sri Ramya Punnamaraju

Submitted to the Graduate Faculty as partial fulfillment of the requirements for the Master of Science Degree in Pharmaceutical Sciences with Industrial Pharmacy option

_____
Kenneth Alexander, PhD., Committee Chair

_____
Sai Hanuman Sagar Boddu, PhD., Committee Member

_____
Ming-Cheh Liu, PhD., Committee Member

_____
Patricia R. Komuniecki, PhD, Dean
College of Graduate Studies

The University of Toledo
December, 2012

An Abstract of

The Evaluation of the Sedimentation Behavior of Magnesium Hydroxide in the Never Dried State

by

Sri Ramya Punnamaraju

Submitted to the Graduate Faculty as partial fulfillment of the requirements for the Master of Science Degree in Pharmaceutical Sciences with Industrial Pharmacy option

The University of Toledo

The objective of this study is to prepare and evaluate the effect of Poloxamer 407 on the sedimentation behavior of never dried magnesium hydroxide suspensions. Never dried magnesium hydroxide suspensions have been prepared stoichiometrically by adding sodium hydroxide to magnesium sulfate. The effect of rate of addition of sodium hydroxide on particle size has also been studied. The hindered settling behavior of these suspensions was observed by adding various concentrations of Poloxamer, such as 0.025%, 0.05% and 0.075% (w/v). Particle size was determined using modified Stoke's equations along with laser diffraction and SEM for surface morphology. It was found that the particle size increased upon flocculation and with an increase in Poloxamer concentration. Laser diffraction was not consistent with hindered settling results and will be explained.

Permeability studies indicate a decreased permeability with increased flocculation because of reduced pore sizes. Zeta potential studies demonstrated the mechanism of action of Poloxamer in flocculating the system. Thermal analysis studies have been performed to determine the bound and unbound water content of the suspensions. It has been observed that increasing flocculation brought about a decrease in bound water

content. PXRD studies established the degradation of magnesium hydroxide to magnesium oxide at around 420^{o}C.

Acknowledgements

I would like to express my gratitude to my advisor Dr. Kenneth Alexander for his encouragement and guidance during my stay at the University of Toledo. His constant support and motivation helped me both in my study and in my life.

I would like to extend my thanks to Dr. Sai Hanuman Sagar Boddu and Dr. Ming- Cheh Liu for being a part of my defense committee and for their valuable time and advice. I would also like to thank Dr. Surya Nauli for taking time to be the Graduate Faculty Representative.

I would like to take this opportunity to thank Dr. Jerry Nesamony for allowing me to use the DLS. I would like to thank Dr. Gabriella Baki for her help with the rate of addition studies. I would like to thank Dr. Pannee Burckel for training and guidance in the SEM and PXRD.I would also like to thank Dr.Timothy Fisher, Samantha Dewald and Joseph Blockland for their assistance with the Laser Diffraction.

I would like to thank all my lab mates for their support and friendship and making the time at the University of Toledo a wonderful experience.

Finally, I am extremely grateful to my mother, father, uncle Murali, Deepu and Vicky for their love and support and for always being there for me.

Table of Contents

List of Tables

List of Figures

Chapter 1

Introduction

A concentrated suspension of magnesium hydroxide, whose synonym is Milk of Magnesia, is mainly used as an antacid and laxative. This project focuses on the preparation and characterization of never dried magnesium hydroxide suspensions produced from the chemical reaction between Magnesium sulfate heptahydrate (Epsom salt) and sodium hydroxide. In the pharmaceutical industry, magnesium hydroxide suspensions are prepared in the never dried state which implies they are prepared in situ as a suspension instead of directly suspending the dried magnesium hydroxide in the suspending medium. Never dried suspensions have many advantages over suspensions manufactured from dried powders. They do not sediment rapidly, are easily redispersible and have fewer problems compared to dried magnesium hydroxide dispersed directly in the medium [1].

Additionally, the suspensions prepared are in very high concentration and hence the sedimentation rate cannot be studied using Stokes's law. Since there are too many particles, they no longer fall independent of each other and their fall is hindered. This phenomenon is termed hindered settling. The objective of the hindered settling study on these suspensions is to determine the particle size of the aggregates of magnesium

hydroxide produced. Various modifications of Stokes law have been postulated which are utilized here to determine the mean particle size of the suspension. The equations proposed by Richardson & Zaki, Steinour and Dollimore & McBride which take porosity into consideration for particle size determination, have been used. In addition, the Kozeny-Carman equation considering permeability is also used to determine the permeability of the suspensions. These equations are discussed in further detail in subsequent chapters.SEM and Laser diffraction studies were performed to evaluate the surface morphology and particle size distribution, respectively.

The stability of these suspensions can be affected by the addition of flocculants. Flocculation is achieved by employing Poloxamer 407 as the flocculant. These polymers bring about flocculation by a bridging process, which is discussed in the chapter three. The effect of concentration and nonionic nature of the flocculant on the suspension is assessed by zeta potential measurements.

Thermal analytical techniques are used in this study to determine the bound and unbound water associated with the magnesium hydroxide produced. This associated liquid affects the final settled volume and sedimentation rate of the suspension. This study involves the use of Thermogravimetry (TG) and Differential Scanning Calorimeter (DSC) to determine any bound and unbound liquid associated with the suspensions produced. X-ray powder diffraction (PXRD) studies were performed to analyze the degradation product of magnesium hydroxide.

Chapter 2

Preparation and properties of Magnesium Hydroxide

2.1 Preparation of Magnesium Hydroxide

A suspension of magnesium hydroxide is usually not prepared by directly suspending magnesium hydroxide in water or other medium. It can be prepared in a number of different ways.

Magnesium compounds are usually produced from the following four raw materials [1]

(1) Sea water

(2) Dolomite

(3) Ores other than Dolomite

(4) Evaporite deposits and lake & well brines

The commercial manufacture of magnesium hydroxide is usually accomplished by the hydration of magnesium oxide [2]

$$MgO\ (s) + H_2O\ (l) \rightarrow Mg\ (OH)_2(s) \downarrow \qquad \text{Eq. 2.1}$$

The magnesium hydroxide produced is collected and washed on a filter and dried at 100^{o}C. This preparation is done on a large scale by mixing freshly calcined magnesium oxide with purified water in proper proportion. This reaction involves the evolution of

heat. After hydration, the precipitate is passed through a colloid mill equipped with a special steel rotor to avoid contamination due to wear.

Another method of preparation involves burning magnesium in the presence of a current of steam, producing magnesium hydroxide with the evolution of hydrogen gas.

$$Mg\ (s) + 2H_2O\ (l) \rightarrow Mg\ (OH)_2\ (s) \downarrow + H_2\ (g) \uparrow \qquad \text{Eq. 2.2}$$

Magnesium hydroxide can also be prepared by treating sea water or other natural brines with sufficient calcium hydroxide to precipitate magnesium hydroxide. The precipitate is then washed, filtered and dried.

Sometimes it is obtained as the initial material in the manufacture of magnesium carbonate or oxide from sea water which is a good source of magnesium. Magnesium hydroxide produced this way forms stable suspensions with water and makes possible the production of the milk by merely suspending the powder in water.

Dow Chemical Company produces magnesium hydroxide from sea water and oyster shells which is a source of calcium hydroxide [3].

Magnesium hydroxide is also produced by the decomposition of magnesium sulfide with water.

This reaction involves the liberation of hydrogen sulfide.

$$MgS\ (s) + 2H_2O\ (l) \rightarrow Mg\ (OH)_2 \downarrow + H_2S\ (g) \uparrow \qquad \text{Eq. 2.3}$$

It is most commonly produced as a precipitate when sodium hydroxide or barium hydroxide is added to any soluble salt of magnesium. However, it is not precipitated if in the presence of ammonium salts.

A simplified procedure of making magnesium hydroxide in the laboratory is to add a sufficient volume of 1M magnesium chloride to 1M sodium hydroxide to get a precipitate of magnesium hydroxide.

The reaction is represented as:

$$MgCl_2\ (aq) + 2NaOH\ (aq) \rightarrow Mg(OH)_2\downarrow + 2NaCl\ (aq) \qquad \text{Eq. 2.4}$$

In this study, we produced magnesium hydroxide using Epsom salts and Sodium hydroxide. A molar solution of sodium hydroxide is added to two molar solution of Epsom salts, the reaction of which is given in Eq. 2.5. The solution is allowed to stand for a period of 24 hours. The supernatant is decanted and then purified water added, mixed and allowed to settle. The suspension is washed until it is free of sodium sulfate. The presence of sodium sulphate is determined by treating the supernatant with barium chloride and observing is a precipitate of Barium sulfate is produced.

$$MgSO_4\ (aq) + 2NaOH\ (aq) \rightarrow Mg(OH)_2\downarrow + NaSO_4\ (aq) \qquad \text{Eq. 2.5}$$

2.2 Properties of Magnesium Hydroxide

2.2.1 Physical and Chemical Properties

Magnesium hydroxide appears as a white, amorphous, odorless, tasteless very fine bulky powder. The molecular weight of magnesium hydroxide is 58.34. Magnesium hydroxide dried at 105^{o}C for 2 hours should contain not less than 95 percent of $Mg(OH)_2$. It is practically insoluble in water and alcohol but soluble in dilute acids. The aqueous solubility of magnesium hydroxide is 1gm in 80,000/mL. It slowly absorbs carbon dioxide on exposure to air.

Milk of magnesia appears as a white, opaque viscous suspension from which varying proportions of water separate on standing [4].

A solution of magnesium hydroxide is faintly alkaline. Acid reducing salts are neutralized and alkaloids are liberated from solutions of their salts. It ionizes into magnesium and hydroxyl ions in aqueous solution.

$$Mg(OH)_2 \leftrightarrow Mg^{2+} + 2OH^- \qquad \text{Eq. 2.6}$$

2.2.2 Physiological properties

Magnesium hydroxide is an antacid used in the treatment of gastric and duodenal ulcer and in hyperchlorhydria. As an antacid, it works by simple neutralization of acids in the stomach leading to the formation of magnesium chloride. When taken orally as a laxative, the osmotic force of the magnesia suspension acts to draw body fluids from the body and to retain those already within the lumen of the intestine, serving to distend the bowel resulting in evacuation of colonic contents.

As an antacid it has advantages over bicarbonates and carbonates in that carbon dioxide is not evolved. However, it has some adverse effects such as nausea, vomiting and diarrhea. Magnesium is mainly excreted by the kidneys so long-term daily consumption of milk of magnesia by someone suffering from renal failure could lead, in theory, to hypomagnesaemia [5].

2.2.3 Uses

Milk of magnesia is marketed for medical use as chewable tablets, capsules and as liquids with various added flavors. It is primarily used to alleviate constipation but also to relieve indigestion and heartburn [6].

Dose- as an antacid 500 to 750 mg repeated as necessary. As a laxative it is usually given as a dose of 2 to 4 gms.

Magnesium hydroxide can be administered as tablets and as suspension.

Magnesium hydroxide mixture is used as a mouthwash to neutralize acidity and has been given in the treatment of poisoning by mineral acids or arsenic.

Some marketed formulations of magnesium hydroxide include:

Philips Milk of Magnesia	Today's Health Milk of Magnesia
Dulcolax Milk of Magnesia	Ex-Lax Milk of Magnesia

It is manufactured and distributed by a large number of generic OTC companies.

Chapter 3

Theory of hindered settling

3.1 Introduction

Suspensions are coarse dispersions of solids in liquids. Pharmaceutical suspensions are dispersions of solid particles of different sizes in liquid medium, usually water. Two distinct theories may be considered during the settling of particles in a liquid under the force of gravity, depending on the concentration of these dispersed solids in the liquid. For low concentrations of solids in the liquids, it is statistically possible to consider each particle falling unhindered from its initial position to the bottom of the container. The velocity of sedimentation can be determined by Stoke's law for these suspensions. However, for antacid suspensions, solids are dispersed in much higher concentrations and Stoke's law cannot be applied. At higher concentrations, the fall of any single particle is hindered by other particles in its path, in other words they do not settle independent of one another. There is one single observation which allows this transition in behavior to be noted, namely that under hindered fall the suspension settles "en bloc" with an interface, above which is a clear supernatant liquid. This phenomenon is termed hindered settling [1].

It should be established at what concentration the system departs from obeying Stoke's law and a clear interface can be seen in the system. However, in most cases there is no sharp transition between these two extremes. The two observations that should be made in the experiments of hindered settling are the rate of fall of the interface and final settled volume of the sediment. When fall is hindered then the mode of settling may be affected by the following factors [2]:

1. Concentration of the suspension;
2. Particle size, shape and density of the suspension;
3. Tendency of the particles to flocculate;
4. Physical properties of the suspending liquids (e.g. viscosity, surface tension and dielectric constant);
5. Chemical properties of the suspending liquid;
6. Size relation between the smallest range of particles present and the larger particles (fitting of smaller particles between close packed larger particles);
7. The lapse of time since settling began (a consequence of compression or increase in concentration in the lower levels).

The apparatus and technique used for hindered settling determination is very simple. The apparatus consists of a 250 cm^3 measuring cylinder. It involves measuring the interface with time. The suspension is allowed to settle down and the final volume of the sediment is also noted. The data obtained is plotted with time on the x-axis and height of the sediment on y-axis. The slope of the straight line portion is the rate of fall of the interface (Q) or the hindered settling rate.

In concentrated suspensions, the obvious parameter to measure is the rate of fall of the interface or sludge line. The normal curve of the position of the interface plotted against time is seen in Figure 3-1. However, an alternative curve which often occurs is seen in Figure 3-2 and a qualitative analysis indicates three regions,

1. An initial region (Region A)
2. A linear region (Region B) and a
3. Final compressive region in which no great change takes place with time (Region C)

Figure 3-1 differs from Figure 3-2 only in that the initial region is absent.

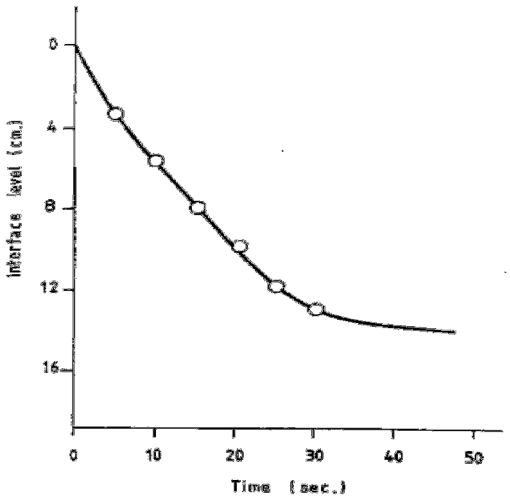

Figure 3-1 A normal plot of the position of position of the interface against time in hindered settling [2]

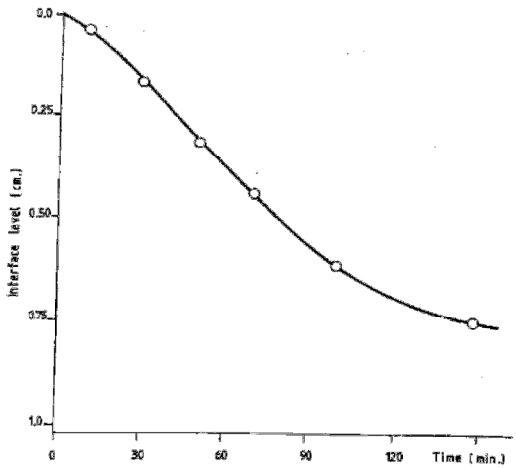

Figure 3-2 An alternative plot of the interface against time in hindered settling [2]

The initial region A in Figure 3-1 may be seen in flocculated systems. The explanation provided is that in this region the suspension is adjusting itself to a steady state. Since there is shaking of the suspension prior to the sedimentation, the agitation

causes breakage of the flocs. In the initial zone (A), reflocculation is taking place with a corresponding increase in rate of fall of interface. The second region (B) which is linear should be considered the hindered settling region from which particle size is calculated. The final compressive region (C) represents the approach to saturation and the final settled volume. At low concentrations, there may be no compressive region during sedimentation. But, as concentration increases, the initial region (A) merges into the compressive region. The rate of fall of these solid particles then depends on the concentration of the solid particles in the suspension [3].

3.2 Sedimentation

For solids with a concentration less than 0.1% of the dispersed phase in a liquid medium, the particles fall unhindered by gravitational force. The rate of sedimentation for these particles is determined by Stoke's law, which is given as:

$$V_s = \frac{2gr^2(\rho_s - \rho_l)}{9\eta} \qquad \text{Eq. 3.1}$$

where (V_s) is the stokes limiting velocity for a spherical particle;

(r) is the radius of the particle;

(g) is the acceleration due to gravity;

(ρ_s) is the density of the solid;

(ρ_l) is the density of the liquid medium; and

(η) is the coefficient of viscosity.

Gravity and concentration processes rarely involve perfect spherical particles and it is well known that the free settling velocity of a particle is also strongly influenced by its shape and the orientation of the particle to the direction of the fluid flow [4]. Lack of an

unambiguous measure of particle size, shape and orientation presents an obstacle in developing universally applicable correlations for determining the free settling velocities of non-spherical particles. An attempt has been made to extend Stoke's law to non-spherical particles but it involves a dimensionless shape factor. This appears sensibly constant over a wide range of suspension concentrations for systems of low interactions, but its value changes markedly when high interaction is present. Generally, for non-spherical particles, the particle size is defined in terms of the diameter of the sphere having the same volume as the particle to modify the drag coefficient equation.

There is no sharp transition from dilute to concentrated suspensions where it follows hindered settling. As the concentration increases from dilute suspensions, but at a concentration below hindered settling, there is an immediate state called 'Haze formation' [5]. This haze formation has two boundaries, one diffused boundary where the suspension was separating from the supernatant and another boundary at the bottom where sediment was building up. The upper boundary was observed to be moving rapidly downwards, while the lower was moving slowly upwards. They eventually merge, after which there is little or no more decrease in sediment volume. This suggests that all particles do not settle together as in hindered settling, but rather they fall depending on their size. These conditions are observed when there is an insufficient concentration of solid particles and also when there is high viscosity or a high dielectric constant of the liquid medium. McKay [6] has interpreted this as being due to the fine particles escaping from the hindered settling cloud. A second diffused boundary has been reported which settled slowly behind the main boundary which McKay has considered to be a region of uniform particle size settling according to Stoke's law. In between the limits of

concentration for Stoke's law and hindered settling, particle clustering occurs which is characterized by sedimentation rates rather than those predicted by Stoke's law. It has been postulated that the enhancement is due to hydrodynamic demixing, with equilibrium cluster size distribution being reached only after settling distances of several hundred particle diameters.

Bhatty [7] examined the behavior of particles at low concentrations in the free settling as well as the cluster forming region. It was found that almost every solid particle carried a bubble attached to its top. Individual particles falling freely showed rotation only if their shapes were not spherical. Vortices were observed behind bigger particles settling at relative high velocities and other particles were found to move into this vortex to form a temporary cluster. If the settling velocities differed greatly, the vortex force was not able to keep these particles together and the cluster was observed to break apart. It is said that the variation in settling rate changes with the extent of the degree of clustering. They [7] studied clusters of a different number of particles. Doublets were found to form more readily than bigger clusters. Cluster formations larger than four were rarely found. In the case of doublets, if the particles were equisized, they would settle in two different horizontal planes. Basically, the same phenomenon was reported with two and four particle clusters. If equisized, they fell as a triangle or as a tetrahedron, respectively. If of different sizes, they settled in different planes. Hawksley [8] noted that a proper correction factor could be applied to those cluster formations in which particles are very close and that the distance between particles is smaller than their distance from the container wall. The ultimate effect noticed was a greater terminal velocity of the cluster owing to reduction in drag on the individual particles.

When concentration increases, the settling rate of a particle is always less than the settling rate of a single particle in isolation due to the hindrance effect. According to Zimmels [9], this hindrance effect with an increase in concentration is due to:

- a decrease in the available cross section for the upward flow of the liquid, which results in an increased fluid approach velocity;
- an increase in apparent viscosity of the suspension;
- a decrease in the gravitational driving force due to a decrease in the difference in apparent specific gravity between the particles and the medium; and
- an increase in the wall hindrance.

Particle size can then be determined from various equations which have been proposed as representations of relationships between settling rate and such variables such as initial suspension concentration, Stoke's law limiting velocity, container dimensions and concentration of settling sediment.

3.2.1 Steinour's equation

Steinour developed a detailed theory of hindered settling for non-porous particles of uniform radius [10]. He modified Stoke's law by the introduction of a single function [ø(ε)] to account for hindered fall and a term for the porosity (ε):

$$V_l = \frac{2gr^2(\rho_s - \rho_l)\varepsilon\, ø(\varepsilon)}{9\eta} \qquad \text{Eq. 3.2}$$

where (ε) is the liquid volume fraction of the uniformly mixed suspension (the initial porosity of the suspension).

At infinite dilution, ($\varepsilon \rightarrow 1$) and [$\phi(\varepsilon)$] also equals unity when Eq. 3.2 reduces to Eq. 3.1. The term (V_l) in Eq. 3.2 is the average relative velocity between the spherical particles and the liquid.

The measured velocity is that of the particle relative to a fixed horizontal plane and it is represented by (Q). The relationship between (Q) and (V) may be derived by equating the volumes of the solid and fluid that move in opposite directions past a unit of horizontal cross section in unit time, i.e.

$$(1-\varepsilon)\, Q = \varepsilon\, (V_l - Q) \qquad \text{Eq. 3.3}$$

or

$$Q = \varepsilon V_l \qquad \text{Eq. 3.4}$$

Substituting this into Eq. 3.2 gives:

$$Q = \frac{2gr^2(\rho_s - \rho_l)\varepsilon^2 \phi(\varepsilon)}{9\eta} \qquad \text{Eq. 3.5}$$

Steinour derived another equation for the relationship between (V_s) and (Q) by equating the loss in potential energy attending the fall of a sphere against various resistances as:

$$\frac{4}{3}\pi r^3(\rho_s - \rho_l)gQ = \frac{4}{3}\pi r^3(\rho_s - \rho_b)gV_s \qquad \text{Eq. 3.6}$$

which reduces to:

$$\frac{Q}{V_s} = \frac{(\rho_s - \rho_b)}{(\rho_s - \rho_l)} \qquad \text{Eq. 3.7}$$

where (ρ_b)is the density used in computing buoyancy

Steinour deduced an expression for [$\phi(\varepsilon)$] from consideration of the hydraulic radius of the suspension:

$$\phi(\varepsilon) = \left[\frac{\varepsilon}{1-\varepsilon}\right]\theta(\varepsilon) \qquad \text{Eq. 3.8}$$

where $\theta(\varepsilon)$ represents those effects of shape that are not evaluated by using the hydraulic radius.

Substituting of Eq.3.8 in Eq 3.5 gives,

$$Q = \frac{2gr^2(\rho_s - \rho_l)\varepsilon^3\theta(\varepsilon)}{9\eta(1-\varepsilon)} \qquad \text{Eq. 3.9}$$

or

$$Q = \frac{V_s\varepsilon^3\theta(\varepsilon)}{1-\varepsilon} \qquad \text{Eq. 3.10}$$

Rearrangement of Eq.3.9 gives:

$$r = \left\{\frac{9Q\eta(1-\varepsilon)}{2g(\rho_s - \rho_l)\varepsilon^3\theta(\varepsilon)}\right\}^{1/2} \qquad \text{Eq. 3.11}$$

Steinour further modified this equation to allow for a situation in which there are spherical particles settling in the presence of an attached layer of immobile liquid [11] Thus modifying the equation to:

$$Q = V_s \frac{(\varepsilon - W_1)^3\theta(\varepsilon)}{(1-W_1)^2-(1-\varepsilon)} \qquad \text{Eq. 3.12}$$

The term (W_1) is the ratio of the volume of the immobile liquid to the total volume of solid (including the volume of the pores) plus immobile liquid as:

$$W_1 = \frac{\alpha}{1+\alpha} \qquad \text{Eq. 3.13}$$

where (α) is the quantity of liquid in millimeters per unit bulk volume of solid.

Steinour expressed this equation in another form:

$$Q = V_s\varepsilon^2 10^{A(1-\varepsilon)} \qquad \text{Eq. 3.14}$$

where (A) is a characteristic constant. It can be calculated from plots of log $(Q/\varepsilon)^2$ against (ε) for each experiment and fitted his experimental results with A=1.8

Comparison of coefficients in Eq. 3.14 and Eq. 3.5 gives

$$\left[\frac{1-\varepsilon}{\varepsilon}\right] 10^{A(1-\varepsilon)} = \theta(\varepsilon) \qquad \text{Eq. 3.15}$$

This can be rearranged to give:

$$\frac{1-\varepsilon}{\varepsilon\theta(\varepsilon)} = 10^{A(1-\varepsilon)} \qquad \text{Eq. 3.16}$$

which may be inserted into Eq.3.11 to give

$$r = \left\{\frac{9Q\eta 10^{A(1-\varepsilon)}}{2g(\rho_s-\rho_l)\varepsilon^2}\right\}^{1/2} \qquad \text{Eq. 3.17}$$

Taking the log of both sides and rearranging, Eq.3.14 gives the following:

$$\log\frac{Q}{\varepsilon^2} = A\varepsilon + (\log V_s - A) \qquad \text{Eq. 3.18}$$

When log (Q/ε^2) is plotted against (ε), the intercept of the equation is [$\log V_s$-A] and slope is (A). The particle size is calculated by extrapolating the relationship to unit porosity where $Q=V_s$. Low values of (A) were observed with tapioca in hydrocarbon oil and glass spheres in aqueous medium.

3.2.2 Richardson and Zaki's equation

Richardson and Zaki proposed an empirical equation as follows:

$$Q = V_s\varepsilon^n \qquad \text{Eq. 3.19}$$

where (n) is a dimensionless number which is mathematically more adaptable than Steinour's equation.

A plot of [Q (1-ε)] against (ε) will pass through a maximum at some initial porosity (ε_1) because (1-ε) decreases to zero as (ε) increases. The term ([Q (1-ε)] ρ_s) is known as the solid flux and indicates the mass transfer of solid per unit cross section per unit time down the sedimentation column. It is therefore important as a measure of solid transport. However, in many experimental interface settling rate experiments, it is often observed

that only the increasing slope is produced and the maximum value of (ε) is not produced [12].

The maximum value for [Q (1-ε)] occurs when:

$$\frac{d[Q(1-\varepsilon)]}{d\varepsilon} = 0 \qquad \text{Eq. 3.20}$$

Defining the porosity at this point as (ε_1) gives:

$$V_s\varepsilon_1^n = V_s\varepsilon_1^n \, n\varepsilon_1^{-1}(1-\varepsilon_1) \qquad \text{Eq. 3.21}$$

from which we get the following:

$$\varepsilon_1 = \frac{n}{n+1} \qquad \text{Eq. 3.22}$$

Hence, (n) which was assumed to be of no significance is in fact a function of the porosity (ε_1) where [Q (1-ε)]. Therefore solid flux has a maximum value for a system.

Richardson and Zaki's equation can now be given as:

$$Q = V_s\varepsilon^{\varepsilon_1/(1-\varepsilon_1)} \qquad \text{Eq. 3.23}$$

Applying log to both sides of this equation gives:

$$\log Q = \log V_s + n\log\varepsilon \qquad \text{Eq. 3.24}$$

The plot of (log Q) vs. (log ε) ideally should give a straight line.

Hence (ε_1) is an important parameter in describing the settling rates of suspensions and a relationship should exist between (ε_1) and the chemical system parameters which determine its magnitude. The term, (ε_1) is just as important as the initial suspension concentration for maximum solids flux.

It is to be expected that the settling rate will decrease with increasing concentration on the basis of purely mechanical interference. Therefore the experimental relationship that

(Q/V_s) is proportional to (ε) should be expected. It is more significant than the influence of concentration is raised to a power which has the form:

(liquid volume fraction)/ (solid volume fraction) which is $[\varepsilon_1(1-\varepsilon_1)]$ Eq. 3.25

If the hindrance to settling were merely an effect of solid concentration, expressible as a multiple power law because any one particle interacts with more than one other, then it would be expected that the solid volume fraction would appear in the numerator rather than the denominator of the power term. Equation 3.25 shows that the nearer the value of (ε_1) is to its theoretical maximum value of infinity, the more rapid is the decrease of interface settling rate (Q) with a decrease of initial porosity (ε). Systems with a high concentration of solids are said to be more highly hindered. It therefore follows that the higher the value of (ε_1), the more a system may be said to be hindered [13].

Hindrance is not simply a function of particle concentration. It is also related to the range and intensity of forces acting within the system. Davies et.al [14] stated that hindrance would be expected at a maximum with charged or polar particles of large surface areas per gram in polar solvents and at a minimum with uncharged or non-polar solids of small specific surface in non-polar solvents. High values of (n), (A) and (ε_1) are observed for systems such as silica, china clay and metal carbonates in water and aqueous electrolyte solutions. It was suggested that hindrance due to settling should be interpreted as partly due to particle-liquid (including multi-centre particle-liquid-particle) interactions [15]. This fits well with the concept of long range electrostatic interactions developed earlier. However, that suggestion involved the notion of particle-particle repulsions which acts

only as the cause of hindrance. Whereas, the model also suggests particle-liquid attractions. Particle-particle repulsions implies that relatively slow settling is due to electrostatic repulsions preventing particle-particle cohesion. Particle-liquid attractions would ascribe it to particle-liquid cohesion reducing the effective density of the solid, to solvated particle-solvated particle repulsion; the settling up of relatively extensive three dimensional arrays of solid particles and liquid molecules.

3.2.3 Dollimore-McBride's equation

Dollimore and McBride [16,17] studied samples of metal carbonate suspensions of known initial concentration. An empirical equation was proposed relating to the rate of fall of the interface (Q) against the concentration (C) of the suspension which should be linear. Extrapolation of this graph to zero concentration gives the rate of fall of a single particle in an infinite fluid which is the Stoke's law limiting velocity (V_s) as:

$$\log Q = a - bC \qquad \text{Eq. 3.25}$$

where a and b are constants.

At infinite dilution, then:

$$a = \log Q \qquad \text{Eq. 3.26}$$

and also

$$Q = V_s \qquad \text{Eq. 3.27}$$

hence,

$$10^a = 10^{\log V_s} = V_s \qquad \text{Eq. 3.28}$$

and therefore,

$$Q = V_s 10^{-bC} \qquad \text{Eq. 3.29}$$

The initial porosity (ε) of a settling particulate system is given by

$$\varepsilon = \frac{V_{sn} - V_{sd}}{V_{sn}} \qquad \text{Eq. 3.30}$$

where (V_{sn}) is the volume of the suspension and V_{sd} is the volume of solid. However,

$$V_{sd} = \frac{\text{mass of the solid}}{\text{density of solid}} = \frac{M_s}{\rho_s} \qquad \text{Eq. 3.31}$$

hence,

$$\varepsilon = \frac{V_{sn} - \frac{M_s}{\rho_s}}{V_{sn}} \qquad \text{Eq. 3.32}$$

or

$$\varepsilon = 1 - \frac{M_s}{\rho_s V_{sn}} \qquad \text{Eq. 3.33}$$

since $\frac{M_s}{V_{sn}} = C$ then,

$$\varepsilon = 1 - \frac{C}{\rho_s} \qquad \text{Eq. 3.34}$$

where (ρ_s) is the density of solids.

Replacing (C) by the initial porosity (ε), the equation becomes

$$Q = V_s 10^{-b\rho_s(1-\varepsilon)} \qquad \text{Eq.3.35}$$

This equation may be compared with Steinour's Equation 3.4.

In systems where (ε) is very close to unity then (ε^2) may be approximated to unity. This means that

$$A = b\rho_s \qquad \text{Eq. 3.36}$$

The precise relationship between (A) and (b), which must be used if (ε^2) cannot be regarded as unity and may be derived as follows

If we take the log on both sides of the Equation 3.35 which gives:

$$\log Q = \log V_s - b\rho_s(1-\varepsilon) \qquad \text{Eq. 3.37}$$

while from:

$$\log Q = \log V_s + 2\log\varepsilon - A(1-\varepsilon) \qquad \text{Eq. 3.38}$$

hence,

$$b\rho_s(1-\varepsilon) = A(1-\varepsilon) - 2\log\varepsilon \qquad \text{Eq. 3.39}$$

and therefore

$$A = b\rho_s + \frac{2\log\varepsilon}{(1-\varepsilon)} \qquad \text{Eq. 3.40}$$

at infinite dilution (i.e., when log ε=0) then

$$A = b\rho_s \qquad \text{Eq. 3.41}$$

Finally from the plot of Dollimore McBride, we can calculate the weight to volume solids concentration in a uniformly mixed suspension, for maximum sedimentation mass transfer, which occurs at the initial porosity (ε_1). When the concentration (C) is such that [Q (1-ε)ρ_s] is at a maximum value (i.e., when C=$C_{\varepsilon 1}$) so that ε_1=$\varepsilon_{1,}$ it was found that:

$$C_{\varepsilon 1} = \frac{1}{2.303b} \qquad \text{Eq. 3.42}$$

which is the solids concentration ($C_{\varepsilon 1}$)(g.cm^{-3}) for maximum solid flux.

A plot of (log Q) vs. (ε) would give a slope of (B) and an intercept [log (V_s-B)].

3.3 The permeability approach

An alternative approach for explaining the sedimentation behavior during hindered settling considers the phenomenon as an example of permeability. In this approach the liquids are considered as the permeating medium progressing through the settling

suspension. The suspension is regarded as a packed bed through which a fluid is allowed to flow [18].

The permeability equations derived by Lea and Nurse [19], and by Rigden [20], have been used by Allison and Murray [21] to produce functions which described sedimentation behavior [22].

The most commonly applied permeability equation for the situation of a liquid flowing through settled beds of solid particles is that of Kozeny-Carman [7] as:

$$\upsilon = \left[\frac{\varepsilon^3}{K\eta S^2}\right]\left[\frac{\Delta P}{L}\right] \qquad \text{Eq. 3.43}$$

where

(υ) is the volume of fluid flowing through the bed per second divided by the total cross section of the container ($cm.s^{-1}$), or the apparent fluid flow velocity through a motionless bed

(ε) is the volume of pore space per unit volume of bed(i.e., the porosity)

(K) is the Kozeny constant, originally stated as 5.0

(η) is the fluid viscosity($gm.cm^{-1}.s^{-1}$)

(S) is the particle surface area per unit bed volume (cm^{-1})

(ΔP) is the pressure difference across the bed depth ($gm.cm^{-1}.s^2$)

(L) is the bed's depth

The equation may be transformed to apply to sedimentating beds of spheres.

The value of (S) can be expressed for a bed of spheres having radius (r) and porosity (ε). Let a bed volume (V) contain one sphere. The sphere volume must equal [(1-ε) V] and therefore:

$$V = \frac{(4/3)\pi r^3}{(1-\varepsilon)} \qquad \text{Eq. 3.44}$$

thus,

$$S = \frac{4\pi r^2}{V} = \frac{4\pi r^2(1-\varepsilon)}{(4/3)\pi r^3} \qquad \text{Eq. 3.45}$$

In a cubic centimeter of the bed there is an additional mass, as compared with the situation in a motionless fluid of density (ρ_l) due to an element of the volume (1-ε) having an additional density (ρ_s-ρ_l), (ρ_s) being the solid density. This will create a pressure difference [(1-ε) (ρ_s-ρ_l) g L] across the bed depth and hence:

$$\Delta P / L = (1-\varepsilon)\ (\rho_s-\rho_l)\ g \qquad \text{Eq. 3.46}$$

where (g) is the acceleration due to gravity ($cm.s^{-2}$). Substitution into Eq.3.44 for (S) and (ΔP / L) gives:

$$\upsilon = \left(\frac{1}{K}\right)\left(\frac{\varepsilon^3}{1-\varepsilon}\right)\left(\frac{gr^2(\rho_s-\rho_l)}{9\eta}\right) \qquad \text{Eq. 3.47}$$

In hindered settling, the particles move under laminar flow conditions (i.e, where the Reynold's number is 0.2, with a measured velocity (Q) relative to a fixed horizontal plane, through a liquid volume, as compared with the flow of the liquid at velocity (υ) through a motionless bed, where , υ=Q. Since the Stoke's law limiting sedimentation rate (V_s) is given by

$$V_s = \frac{2gr^2(\rho_s-\rho_l)}{9\eta} \qquad \text{Eq. 3.48}$$

we can write

$$Q = \left(\frac{1}{2K}\right)\left(\frac{\varepsilon^3}{1-\varepsilon}\right)V_s \qquad \text{Eq. 3.49}$$

This is the form of the Kozeny-Carman equation reported by Happel [23] as being appropriate to sedimentation problems.

Gaudian and Fuerstenau [7] have shown that this initial porosity (ε) is maintained in the sedimenting plug moving at velocity (Q) during the hindered settling.

Davies et.al [14] concluded from this and associated evidence that a hindered settling plug is essentially the same as a fluidized bed and that Eq.3.49 describes the flow of liquid through this plug.

Rearrangement of this equation gives

$$Q(1-\varepsilon) = \left(\frac{1}{2K}\right) V_s \varepsilon^3 \qquad \text{Eq. 3.50}$$

if K is constant then,

$$Q(1\text{-}\varepsilon) = \text{constant } \varepsilon^3 \qquad \text{Eq. 3.51}$$

Davies and Dollimore [24] have shown that (K) reaches its minimum value (K_{min}) at some value (ε_K) which is less than (ε_1). This expression $[Q(1-\varepsilon)]$ reaches it maximum as seen in Fig 2.3.The relationship between (ε_K) to (ε_1) is as follows:

$$\varepsilon_K = \frac{4\varepsilon_1 - 3}{3\varepsilon_1 - 2} \qquad \text{Eq. 3.52}$$

It follows that the values for (ε_K) and (ε_1) converge as (ε_1) increases and attain virtual identity when (ε_1) is equal to unity (i.e., in highly hindered systems).

For such suspensions, (K) varies inversely with (ε) virtually all the way up to (ε_1).

3.4 Packing factor

McKay [25] has defined flow units as part solid/part liquid and their total volume as:

$$(1\text{-}\varepsilon') = pv \qquad \text{Eq. 3.53}$$

where:

($\varepsilon^{'}$) is the corrected volume of (ε) allowing for the internal void volume fraction (v_i)

(p) is the packing factor account for the portion of liquid in the sediment that is not associated with and immobilized by the flow units in the linear settling zone

(v) is the final sediment volume fraction or the ratio of the settled sediment volume to the total suspension volume.

The initial void volume fraction of the flow units (v_i) is therefore:

$$v_i = \frac{pv-c}{pv} \qquad \text{Eq. 3.54}$$

where (c) is the solid concentration by volume = wt./ml divided by (ρ_s)

By using a series of dependent dispersions prepared by dilution of the same master dispersion and differing only in the value of (c) by McKay's equation, the packing factor (p) can be evaluated from (Q) and (v) data as follows:

$$Q = \left(\frac{2g}{9\eta}\right)(\rho_s - \rho_l)\left(\frac{c}{pv}\right)(1-\rho v_s)^2 r^2 (10^{-1.82pv}) \qquad \text{Eq. 3.55}$$

It should be noted that Equation 3.55 can be substituted by the general term (A) which Steinour had assumed A= 1.82 in all cases, however as discussed above, is not necessarily true.

Equation 3.55 can be written as:

$$Q = \frac{V_s(1-\varepsilon)(1-pv)^2(10^{-Apv})}{pv} \qquad \text{Eq. 3.56}$$

By simultaneously solving pairs of equations corresponding to different concentrations in the same way, Bhatty et al. [2,7] have calculated as the following:

$$\frac{Q_a}{Q_b} = \frac{(1-\varepsilon_a)(1-pv_a)^2 v_b\left(10^{1.82(v_a-v_b)}\right)}{(1-\varepsilon_b)(1-pv_b)^2 v_a} \qquad \text{Eq. 3.57}$$

It is required to assume the value of (p) to be constant over the entire porosity range in order to solve Equation 3.57. Therefore, a large value of (p) corresponds to a large value of (A) and McKay interprets large values of (A) represents large amounts of associated liquid in the flow units.

According to Bhatty et al.[7], if McKay's theory is valid, a suspension with p>1 (clay-water system) will result in sedimentation by a process where the sedimenting flow units become devoid of associated/bound liquid as they settle into a sediment. Davies reported that suspensions for which (p>1) (calcium carbonate –various media) are associated with less compressible and less flocculated sediments. This indicates that the associated liquid is stripped from around the flow units rather than from within them. In the case of suspensions with (p<1) (glass ballotini-water system) ,the sediment is usually compressible since the total flow unit volume is less than the settled sediment volume and an amount of free liquid stays between the flow units in the sediment. They concluded that a glass ballotini system gives a very low (p) value which is consistent with close packing of incompressible spheres with a minor proportion of associated liquid. They also suggested a relationship between (p) and (v) as:

$$p = \frac{(1-\varepsilon'')}{v} \qquad \text{Eq. 3.58}$$

where $(1-\varepsilon'')$ is the volume fraction of the flow units in a uniformly mixed suspension.

3.5 Final settled volume

The first observation performed on the settling of concentrated suspensions is the rate of fall. The second often neglected observation is the final settled volume. This volume

takes into account the voids between the particles; the actual volume occupied by the solid material; and the pore volume of the solid. Therefore, the total bulk volume is made up of a floc consisting of bound liquid and solid with the free liquid able to occupy the voids.

The solid in all suspensions will settle down to the bottom of the measuring cylinder due to its relatively greater density than that of the medium in which it is dispersed. The bulk volume of a powder consists of the total volume of the solid, volume of the spaces between the solid particles (voidage) and pore volume of the solid. The medium surrounding the powder particles has a characteristic effect on the bulk volume which depends on its interaction with the powder particles, regardless of whether it is a gas or a liquid. The bulk volume observed in these sedimentation studies is often referred to as the sedimentation volume. Bhatti et al. [7] have noted that the bulk density of the sediment is not uniform and varies with the height of the sediment. There is a lower zone of high solid concentration and an upper zone of decreasing solid concentration. The number of pores per unit volume is greater in the upper zone which gives an increased proportion of liquid in these pores. This liquid was assumed to be expelled from the lower zones of the sediment during the later stages (compressive phase) of the sedimentation.

In precipitation of fresh material, a very fine powder does not break up into a dust as easily as does a coarse but uniform powder. This is because a fine powder gives strong adhesion at the point of contact and produces a system with a large voidage. Whereas, larger particles tend to make weaker points of contact and counteract this with more points of contact, thus leading to a reduction in voidage.

Thus, in general terms small particles often mean a system of large sedimentation volume or a small bulk density. Whereas, larger particles produce a smaller sedimentation volume or a larger bulk density.

McKay [25] while working on various dispersions of organic pigments pointed out the presence of a considerable proportion of liquid which appears to be associated with the dispersed particles. As a result of this, the effective density of the dispersed particles is far less than that of the solid pigment and can lead to considerable error in measuring sedimentation parameters. The association of liquid with the particles must also reduce the volume of the free liquid through which the sedimenting material can settle. This then becomes another factor which might reduce the tendency for sedimentation.

There are three factors influencing the final settled volume of the particle bed which are

- size of the particle
- shape of the particle
- the liquid associated with the particles

The particle and attached liquid form a composite aggregate of enlarged diameter whose density is the weighted mean of its liquid and solid content. Corrections have to be made to the (ε) term to account for the liquid attached to the particles.

The density (ρ_c) of the composite particles, composed of the liquid and the solid is given by

$$\rho_c = \frac{\rho_s + \partial \rho_l}{1 + \partial} \qquad \text{Eq. 3.59}$$

where (∂) is the quantity of bound liquid per centimeter cubed of solid.

The value of (∂) is calculated by noting the final settled volume and calculating the amount of liquid contained in this volume present as liquid bound to the surface of the solid particle and free liquid filling voids left between the floc.

Since the liquid must come from the total liquid present, this modifies the nominal porosity ε to a value (ε_m) ,since as (∂) increased then for small values of (ε) , (ε_m) was apparently negative (For an amount equal to 1 , the calculated values of (ε_m) corresponding to an (ε) below 0.5 are negative)

It was thus explained that the particles do not have a sufficient quantity of water in the total suspension to have an association with the water in these ratios. The viscosity of the suspension depends on the solid in the suspension.

Einstein [26] has proposed the relationship as

$$\eta_s = \eta_l[1 + 2.5\left(\frac{C}{\rho_s}\right)] \qquad \text{Eq. 3.60}$$

where (η_s) is the viscosity of the suspension

(η_l) is the viscosity of the liquid

(C) is the concentration of the solid

(ρ_s) is the density of the solid

It should be noted that viscosity term is not that of the liquid but rather for the suspension.

Davies et.al have found that

$$C=\rho_s(1-\varepsilon) \qquad \text{Eq. 3.61}$$

then

$$\eta_s = \eta_l [1 + 2.5 (1-\varepsilon)] \qquad \text{Eq. 3.62}$$

Guth and Simhe [27] have suggested the relationship for moderately concentrated suspension systems should be:

$$\eta_s = \eta_l [1 + 2.5 (1-\varepsilon) + 14.1 (1-\varepsilon)^2] \qquad \text{Eq. 3.63}$$

However, Davies et al [14], have stressed that it is the viscosity of the sedimenting plug which is of interest as much as that of the uniformly mixed suspension.

3.6 Bound or associated liquid on sedimenting particles

In aqueous suspensions, a certain amount of water is carried down with the particles. This is often termed the immobile liquid. However, since it actually moves down the cylindrical tube with the sedimenting particles, and is clearly associated with it by means of chemical or physical forces such as adsorption or Van der Waals or London forces. It is also called associated or bound liquid. When the liquid is associated by Van der Waal or London forces, the thickness of the layer probably remains the same. The quantity of bound liquid depends on particle size, whereas the stagnant liquid is assumed to be a constant proportion of the volume of the liquid. If higher concentrations of solid are used, the pressure applied on the sediment by the weight of the upper layers may cause it to compress and drain out some of its liquid. Usually, the liquid that settles down with the particles forms a part of the sediment with very little additional liquid which may collect in spaces between the aggregates as they form a network. This bound liquid may well leave less space for the free liquid to filter through the pores and thus affect the filtration rate.

The (W_1) term introduced by Steinour represents such a fluid and McKay has also introduced a term into a modified Stoke's law equation to take into account the bound

liquid. Dollimore and Griffith [14] have found that if the particles are lyophilic, low interfacial tension generally causes attachment of large amounts of bound liquid. This should cause a reduction in the surface energy and an increase in the overall radius of the solid particle with a consequent drop in sedimentation volume. Measurement of the film thickness has shown that, in general, larger particles retain thicker films. In all cases film thickness is much greater than expected by the adsorption process.

The most obvious and simplest method to account for the bound liquid is to imagine that the falling particle and attached liquid form a composite aggregate of enlarged diameter whose density is the weighted mean of its liquid and solid content. Corrections then have to be made to the (ε) term to account for the liquid attached to the solid particles.

Bhatty et al [8] have developed an equation to determine the density (ρ_c) of the composite particle (composed of liquid and solid) which is given by:

$$\rho_c = \frac{\rho_s + \alpha\rho_l}{1+\alpha} \qquad \text{Eq. 3.64}$$

where (α) is the quantity (cm^3) of the bound liquid.

Since this liquid must come from the total liquid present, this modifies the nominal initial porosity (ε) to a value (ε_m) given by:

$$\varepsilon_m = \varepsilon - \alpha\,(1-\varepsilon) \qquad \text{Eq. 3.65}$$

The value of (α) is calculated by noting the final settled volume and determining the amount of water contained in this volume present as water bound to the surface of the solid particle and free water filling voids left between the flocs.

Substitution of these new terms (ρ_c) and (ε_m) in Eq. 3.9 gives:

$$Q = \frac{2gr^2(\rho_c - \rho_l)}{9\eta}\,\frac{\varepsilon_m^3\,\theta(\varepsilon_m)}{1-\varepsilon_m} \qquad \text{Eq. 3.66}$$

The calculation of (ρ_c) is straightforward but (ε_m) poses some problems. When (α) increases for small values of (ε), (ε_m) is apparently negative. The interpretation of conditions in this range of negative (ε_m) values is simply that the particles do not have a sufficient quantity of water in total suspension to have an association with the water in these ratios.

The final settled volume will be high if there are any voids between the settled particles. Dollimore and McBride [17] found that the total bulk volume is made up of a floc, consisting of a bound liquid and solid with free liquid able to occupy the void space as

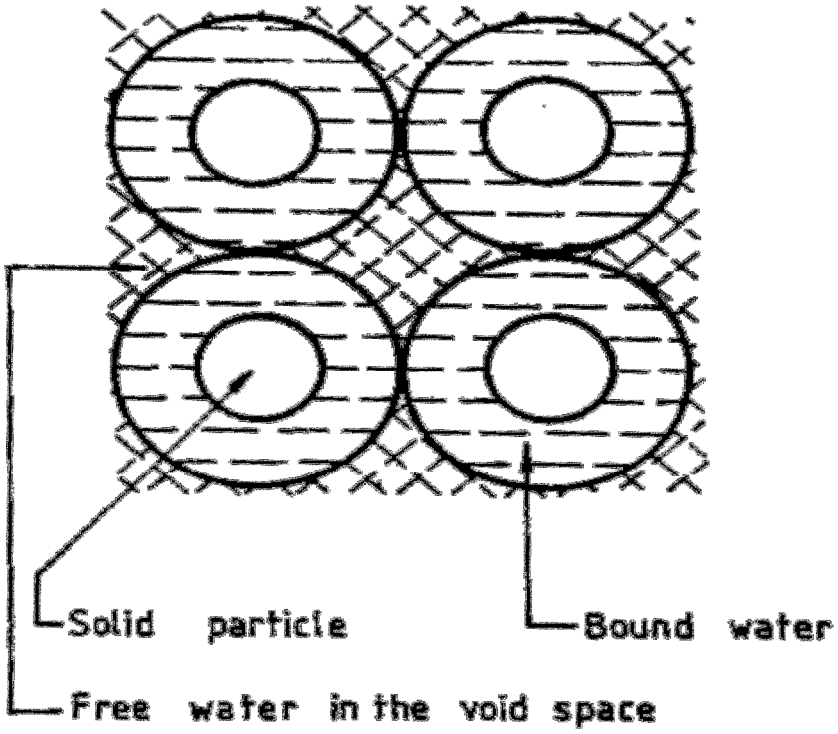

Figure 3-3: Schematic portrayal of settled bed consisting of solid particles with bound water and free water in the void space [3].

shown in the figure 3-3.The nominal coordination number for various precipitates was about four suggesting that a characteristic voidage of 0.6 could be used for the final

settled bed. Thus, the mean equivalent spherical radii refers to the mean equivalent particle or floc together with its associated liquid and not to the solid only.

3.7 Calculation of particle size

The use of hindered settling as a rapid method for particle size determination makes it suitable for laboratory study of the effect of reaction conditions on particle size. It is possible to observe the rate of settling and calculate the average particle size depending on the modifications of Stoke's law [28].

There are three methods for determining the particle size, which are as follows:

3.7.1 Method 1

Steinour's empirical equation is used in calculating the average particle size using the following equation:

$$Q=V_s\varepsilon^2 10^{-A(1-\varepsilon)} \qquad \text{Eq. 3.67}$$

Then

$$\log \frac{Q}{\varepsilon^2} = A(\varepsilon) + \log V_s - A \qquad \text{Eq. 3.68}$$

A plot of log $[(Q/\varepsilon^2)]$ against (ε) should be linear and provide data for (A) and (V_s) from the slope and the intercept. The value of (V_s) is then substituted into the Stoke's law equation to give the average particle radius of the particles in the suspension.

3.7.2 Method 2

The Richardson and Zaki [13] equation can be used to calculate (V_s) and (r) by plotting (log Q) against (log ε). The slope then gives the value of (n) and the intercept the value of (V_s), i.e.

$$\log Q = \log V_s + n \log \varepsilon \qquad \text{Eq. 3.69}$$

3.7.3 Method 3

This method is based on the experimental observations of Dollimore and McBride [17] that some plots of (log Q) against concentration were linear. This data was extrapolated to zero concentration and (Q) was equated to (V_s) to give the particle size. The equation expressing this is as follows:

$$\log Q = \log V_s + n \log(\varepsilon) \qquad \text{Eq. 3.70}$$

Chapter 4

Flocculation of suspensions

4.1 Introduction

The main properties to be considered while formulating a suspension are

1. It should remain sufficiently homogenous for at least the period between shaking the container and removing the required amount.
2. The particles that settle should not form a hard cake.
3. The suspension may be thickened to reduce the rate of settling of the particles, but the viscosity should not be so high that removal of the product from the container is difficult [1].

For pharmaceutical purposes, physical stability of suspensions may be defined as a condition in which particles do not aggregate and they remain uniformly distributed throughout the dispersion. Since this cannot be achieved, even if the particles settle they should be easily resuspended by a moderate amount of agitation.

4.2 Flocculation

As described in the earlier chapter, the rate of fall of particles follows Stoke's law. The rate of fall of particles can be decreased by reducing the particle size. The large surface area of the particles resulting from comminution is associated with a surface free energy that makes the system thermodynamically unstable. The particles are highly energetic and tend to come together in a way to decrease the surface area and reduce the surface free energy. The particles tend to come together to form light, fluffy conglomerates that are held together by weak Van der Waal's forces termed floccules [2,3]. In other conditions, such as a deflocculated suspension, a compact cake is formed where particles are held by stronger forces. This is termed aggregation. Since the attractive forces between particles in a flocculated system are relatively weak, they can be redispersed and the process is reversible. In contrast, coagulation is irreversible since attractive forces operating between particles are difficult to overcome. When electrostatic repulsion is predominant between particles in a suspension, it is called a deflocculated system. For particles with a diameter of 2-5 μm, Brownian movement counteracts sedimentation by keeping the dispersed particles in random motion. This results in a system which is physically stable with respect to sedimentation and flocculation. However, in a deflocculated suspension consisting of large particles, gravitational force counteracts Brownian movement and sedimentation occurs. At the bottom of the container compact sediment with strong attractive forces between the particles is formed and it cannot be easily redispersed. This

phenomenon is referred to as caking. The prevention of caking has been one of the main objectives in preparing stable coarse suspensions.

The formation of any type of agglomerate, either floccules or aggregates is a measure of tendency of the system to reach a thermodynamically more stable state. An increase in the work (W) or surface free energy (ΔG) brought about by dividing the solid into smaller particles and consequently increasing the total free surface area (ΔA) is given by:

$$\Delta G = \gamma_{SL}.\Delta A \qquad \text{Eq. 4.1}$$

where γ_{SL} is the interfacial tension between the liquid and solid particles.

To attain a stable state, they tend to reduce the surface free energy by a reduction of the interfacial tension or interfacial area. Interfacial tension can be reduced by the addition of a surfactant. The forces at the surface of the particle affect the degree of flocculation and agglomeration in a suspension. Forces of attraction are of the London-Van der Waal's type. Repulsive forces arise from the interaction of the electric double layers surrounding each particle [3].

Many attractive and repulsive forces that can affect flocculation behavior are Van der Waal interactions and can include:

1. Electrical interaction
2. Hydration effects
3. Hydrophobic interaction
4. Steric interaction and
5. Polymer bridging

4.3 Electrical double layer and Zeta potential

Electrical charges are developed by several mechanisms at the interface between the dispersed phase and the aqueous medium. The most common mechanisms are the ionization of surface functional groups which is a function of pH and pKa of the suspension as well as the specific adsorption of ions present in the solution. In case of water, they are mostly hydronium or hydroxyl ions. The majority of the particles dispersed in water acquire a negative charge due to the preferential adsorption of the hydroxyl ion. Another less common way by which particles acquire charge is due to the dielectric constant difference between the particle and the dispersion medium. These electrical charges play an important role in determining the interaction between particles of the dispersed phase and the resultant physical stability of the system [3].

The presence of these surface charges influences an uneven distribution of charges surrounding the particle and the development of an electrical potential between the surface and the electrically neutral bulk solution phase of the system. The surface charge and the counterions in its vicinity give rise to an electrical double layer as shown in the Figure 4-1

When a solid surface is in contact with a polar solution containing ions, some of the cations are adsorbed onto the surface giving it a positive charge. These adsorbed ions that give the surface its positive charge are referred to as potential determining ions. Some of the anions that are added to the solution are attracted to the positively charged surface by electric forces that also serve to repel the approach of any further cations. Thermal motion also tends to produce equal distribution of all the ions in the solution. An equilibrium condition is set up in which some of the anions approach the surface while

the remainder is distributed in decreasing amounts as one proceeds away from the charged surface. These ions having a charge opposite to the potential determining ions are known as counterions. Hence, the double layer is divided into two parts separated by a plane called the 'stern layer' which is located at about a hydrated ion radius from the surface [4]. Usually the anions present in the stern layer are smaller than the cations that are adsorbed onto the surface. Neutralization occurs as a Gouy-Chapman layer outside the stern layer [4]. The surface potential and the stern potential are not readily measured experimentally, instead the potential between a stationary fluid layer enveloping the particle and bulk-solution phase can be determined by measuring the mobility of the particle in an applied electric field. The potential between the tightly bound surface liquid layer (shear plane) of the particle and the bulk phase of the solution is called the zeta potential (ζ) [5].

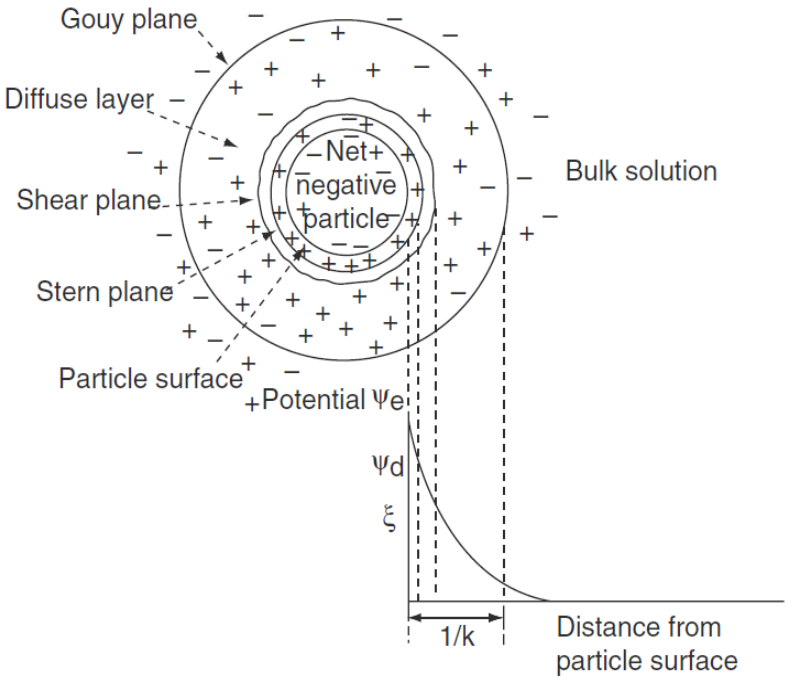

Figure 4-1: Schematic representation of the electrical double layer around a particle [5]

Zeta potential can provide a measure of the net surface charge on the particle and potential distribution at the interface. It serves as an important parameter in characterizing the electrostatic interaction between particles in dispersed systems and the properties of the dispersion as affected by this electrical phenomenon. If zeta potential is reduced below a certain value, the attractive forces exceed the repulsive forces and the particles come together, thereby causing the suspension to flocculate.

4.4 DLVO theory

The effect of surface charge or zeta potential on the physical stability of suspensions can be predicted using the DLVO theory [6]. It describes the forces between charged particles interacting through a liquid medium. According to this theory the forces on these particles in dispersion are due to electrostatic repulsion and London type Van der Waal's attraction. These forces result in potential energies of repulsion and attraction represented by (V_R) and (V_A), respectively. The stability of these particles depends upon the total potential energy (V_T). The stability of the system depends on the system as determined by the sum of these Van der Waal's attractive and electrical double layer repulsive forces between the particles. An energy barrier resulting from the repulsive forces prevents two particles from approaching one another and adhering together. But if the particles collide with sufficient energy to overcome that barrier the attractive force will pull them into contact where they adhere strongly and irreversibly together. Therefore, if the particles have sufficiently high repulsion energy, the dispersion will resist flocculation.

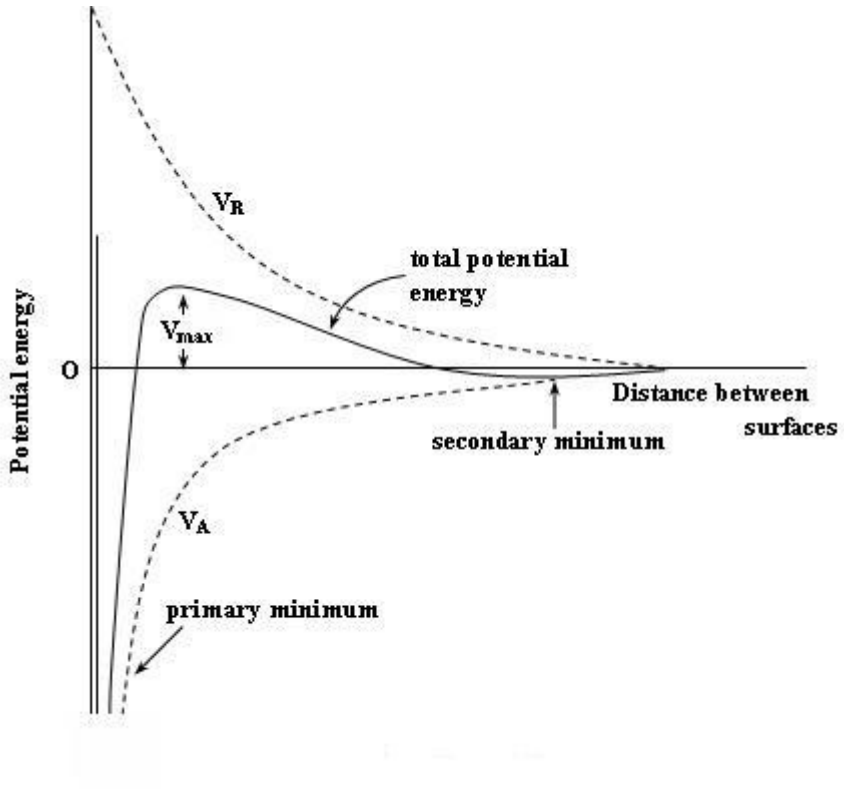

Figure 4-2: Illustration of Van der Waal's attraction potential, electric repulsion potential and the combination of the two opposite potentials as a function of distance from the surface of a spherical particle [5].

However, if a repulsion mechanism does not exist then flocculation or coagulation is likely to occur. Sometimes a shallow secondary minimum can exist at longer distances of separation. These weak forces are sufficiently stable not to be break up Brownian motion but may dissociate under an externally applied force such as vigorous agitation [7].

4.5 Flocculating agents

Flocculation of suspensions can be achieved by the addition of electrolytes, surfactants (surface active agents) and polymeric flocculants.

4.5.1 Electrolytes: Electrolytes decrease the electrical barrier between the particles and bring them together to form floccules. The solid particles in suspension possess a charge on their surface. This charge induces repulsion between particles and tends to stabilize the suspension. The overall effect of adsorption of the multi-valent ions is to create the surface charge and encourage aggregation between adjacent particles leading to the formation of flocs. There is a decrease in the zeta-potential of the particles to almost zero. There is also a formation of a bridge between the adjacent particles. Further addition of electrolytes makes the zeta potential more negative leading to deflocculation. The Schultz-Hardy Rule [8] shows that the ability of an electrolyte to flocculate hydrophobic particles depends on the valence of its counter ions. For particles having low surface charge, monovalent ions can be used to flocculate the system. For highly charged particles divalent or trivalent ions can be used. Although trivalent ions are the most efficient they are less widely used than mono or divalent electrolytes because they are more toxic. The presence of any hydrophilic polymers that are negatively charged can be precipitated by trivalent ions. The most widely used electrolytes include sodium salts of acetate, phosphates and citrates. The concentration used depends on the degree of flocculation required [9].

4.5.2 Surfactants:

Ionic and non-ionic surfactants are used in optimum concentrations and can cause flocculation of the suspended particles. These agents act by decreasing the surface free energy and reducing the surface tension between liquid medium and solid particles. The particles having less surface energy are attracted towards each other by Van der Waal's

forces and forms loose aggregates. Ionic surface active agents may cause flocculation of the suspension by neutralizing charge on each particle thus resulting in deflocculation. Non-ionic surfactants may have a negligible effect on the charge density of a particle but because of their linear configurations adsorb onto more than one particle, thereby forming a loose flocculated system [1].

4.5.3 Polymeric flocculants:

By far the largest number of pharmaceutical suspensions contains lyophilic polymers as their suspending agent. Polymers are long chain, high molecular weight compounds containing active groups spaced along their length. These soluble polymeric materials adsorb onto more than one solid particle surface. This is due to the repeating nature of the basic monomeric unit in the poymer structure and their very high molecular weight. Both synthetic and natural polymers behave as complex surfactants playing an important role in the mechanisms of stabilization or flocculation of suspended particles. Synthetic polymers are designed to fulfill some specified function. Thus, homopolymers or random copolymers are used as flocculating agents while block or graft copolymers (with two types of polymeric chains, one insoluble in the dispersion medium, attached to the solid surface and another soluble one in the dispersion medium) are currently used as stabilizing agents [10,11].

4.5.3.1 Nature of polymers

Polymers employed as flocculating agents may be nonionic, cationic or anionic in nature. The most important characteristics are the molecular weight and charge density of the

polymer. A major problem associated with these polymers is that the molecular weights quoted are average values and there may be a very broad distribution of chain lengths within a given sample.

Starch, alginates, cellulose derivatives, tragacanth, carbomers and silicates are examples of polymers that can be used to control flocculation. Some of the synthetic polymers based on their ionic character include [1]

1. Nonionic: Polyvinyl alcohol, Polyethylene oxide
2. Anionic: Sodium polystyrene sulfonate
3. Cationic: Polyethyleneimine,Polydiallyldiemthyl-ammonium chloride [12]

Adsorption of polymers onto mineral particles as well as the effectiveness of the adsorbed polymer in promoting flocculation is dependent to a large extent on polymer properties. These include molecular weight, nature and concentration of functional groups and configuration, ionic strength of the particles and the solvent system in which it is dispersed. Flocculation by the polymer depends on the charge of the polymer and the particle charge in the dispersion. Dollimore and Horridge [13] studied the effect of cationic, anionic and non-ionic polyacrylamides on aqueous china clay suspensions. The binding force for the anionic polymer is not observed because of the repulsion between the negatively charged clay and polymer. However, cationic polymers are responsible for increasing flocculation in clay suspensions. Non-ionic polymers also cause flocculation of the clay suspensions but without involving charge.

If the particles and polymer have opposite charges then electrostatic attraction occurs, which gives rise to strong adsorption. For nonionic polymers or where both the particles

and the polymer have the same charge, there should be some specific interaction responsible for the adsorption.

In principle when polymeric additives are used for flocculating suspensions the possibility of different flocs developing depends on the mechanism. Polymers strongly influence the strength of the particle-particle attraction as well as the characteristics of the suspension, such as sediment volume and viscosity.

4.5.3.2 Sensitization and protection:

Heller and Pugh [14] have discussed the protective action of the polymers in terms of steric protection. Interpenetration of these polymeric chains causes them to extend outward from neighboring particles. These protruding chains keep the particles separated sufficiently to avoid large interactions from the dispersion forces. These polymers have a structural protective action in the layer around the particle.

Sensitization results because the polymer molecules can form bridges between two particles. They adsorb different proportions of themselves onto each of the two particles. Excess polymer reduces the uncoated area so that the probability of a link forming between two particles is reduced.

4.5.3.3 Mechanism of Action of Polymeric Flocculants

Flocculation occurs via polymer bridging in which large loose flocs are formed when long chain polymers are adsorbed onto the particles in the suspension [13]. These polymer molecules consist of active centers spaced along the backbone of the molecule. To be effective the polymer concentration must be less than that required for complete

coverage of the particles since this would result in particles being enveloped by a polymer instead of being attached to other particles via the bridging mechanism. In the region of relatively low molecular weight the amount adsorbed increases with the molecular weight of the polymer higher molecular weights, the amount adsorbed seems to be independent of the polymer molecular weight. The adsorption phenomenon is relatively insensitive to changes in temperature, solvent and even the adsorbent surface. Everett N. Hiestand [11] explains the action of polymers based on the adsorption of several adjacent segments of the polymer. The several adjacent segments form a loop out into the vehicle, followed by adsorption of another group of segments of this same molecule.

Kraugh and Langston [15] studied the effect of time of agitation. They postulated that when particles are kept apart long enough by agitation one may obtain a gradual rearrangement on the particles. This process adsorbs more free chains onto the particle so that they are no longer available to form bridges. Polymers, also called as polyelectrolytes, may influence p^H and ionic strength. However, this may or may not be negligible.

Chapter 5

Instrumentation

5.1 Laser Diffraction Analysis

Laser diffraction is the most widely used technique for particle size analysis. Instruments employing this technique are easy to use and are chosen for their capability to analyze a sample over a broad size range in a variety of dispersion media [1].

5.1.1 Principle of Laser Diffraction

When particles are passed through a laser beam, light is scattered at an angle depending on the size of the particle. As the particle size decreases, the observed scattering angle increases logarithmically [2]. Scattering intensity is also dependent on the particle size and diminishes with particle volume. Larger particles therefore scatter light at narrow angles with high intensity, whereas smaller particles scatter at wider angles but with low intensity. This behavior is exploited in the determination of particle size by laser diffraction [3,4].

In this technique, the particle size distribution is calculated by comparing a sample's scattering pattern with an appropriate optical model. Two different widely used models are the Mie theory [5] and Fraunhofer approximation theory [6,7].

The Mie theory provides a solution for the calculation of particle size distribution from light scattering data. The Mie theory is applicable for smaller particles. This theory allows for the primary scattering from the surface of the particle, using the intensity predicted by the refractive index difference between the particle and the dispersion medium. It also predicts the secondary scattering caused by light refraction within the particle.

The Fraunhofer approximation theory assumes that the particles being measured are opaque and scatter light at narrow angles, hence it is mostly applicable for the particle size distribution of larger particles [8].

5.1.2 Instrumentation

A laser diffraction system typically consists of a laser source to provide coherent intense light of fixed wavelength. A (Helium-Neon) laser is most commonly employed. The instrument consists of a sample representation system to ensure that the material under test passes through the laser beam as a homogenous stream of particles in a known, reproducible state of dispersion. The scattering produced by the particle is detected by a scattering detector and the intensity by the beam power detector [9,10]. The scattering signals are collected and converted to electrical data and processed into a computer for calculation of the particle size range, median and mode.

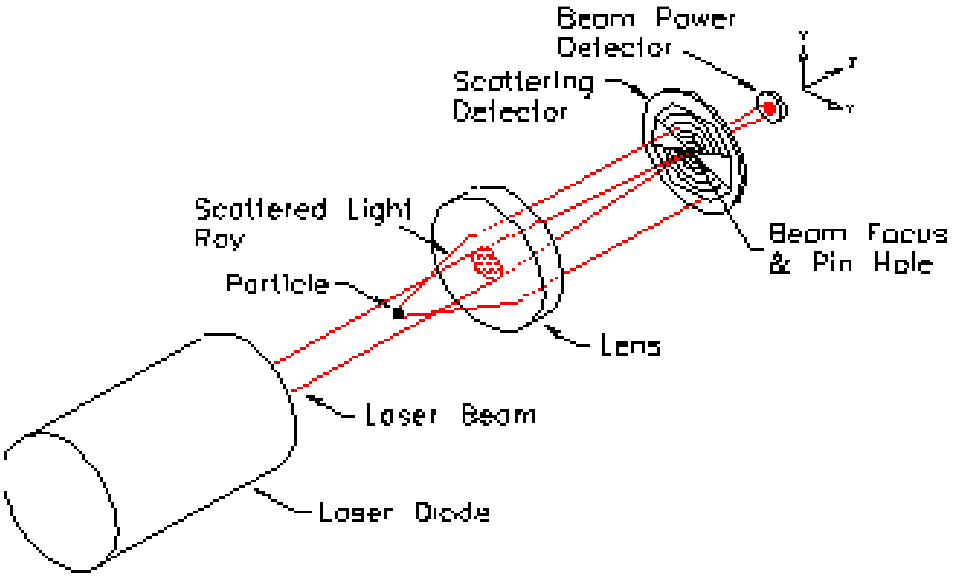

Figure 5-1: Schematics for a laser diffraction system [11]

5.1.3 Sample Preparation

No special sample preparation techniques are necessary. The particle size of any solid particle dispersed in gas or liquid can be measured. A suitable medium should be chosen to uniformly distribute the particles [10]. The sample should be sufficiently diluted for proper distribution and reproducibility. The usual concentration of solids dispersed in a liquid is between 0.001 to 1% (w/v).

5.1.4 Applications

Laser diffraction is a non-destructive, non-intrusive method that can be used for either dry or wet samples [12]. It is mainly used for the determination of mean particle size and analysis of particle size distributions of pharmaceutical solids, sprays, dry powders,

suspensions and emulsions. The data obtained is usually a volume based particle size distribution which is equivalent to a weight distribution [4].

5.2 Electrophoretic Light Scattering

Electrophoretic light scattering is a technique that is used to measure the electrophoretic mobility of particles in dispersion or molecules in solution [13]. Electrophoretic mobility is then converted to zeta potential, which is the difference in potential between the surface of the tightly bound layer and the electroneutral region of the solution as described in Chapter 4, Section 4.3.

5.2.1 Principle of Electrophoretic light scattering [14, 15]

Electrophoretic light scattering is based on the principle of electrophoresis. Electrophoretic mobility of charged particles suspended in a fluid medium is measured under the effect of an electrical field. In order to determine the speed of the particles, they are irradiated with a laser light and the scattered light emitted from the particles is detected. Since the frequency of the scattered light is shifted from the incident light in proportion to the speed of the particle's movement, the elcetrophoretic mobility of the particles can be measured from the frequency shift of the scattered light. Zeta potential is then calculated from electrophoretic mobility using the Helmholtz-Smoluchowski equation [16]

$$\zeta = \eta \mu / \varepsilon \qquad \text{Eq. 5.1}$$

where:

ζ is the zeta potential

η is the viscosity of the solvent

μ is the electrophoretic mobility of the particle

ε is the dielectric constant of the solvent.

5.2.2 Instrumentation

The main components of this instrument consist of a laser source, delivering optics, electrophoretic cell, collecting optics and a photomultiplier tube which acts as the detector as shown in the Figure 5-2. A laser beam passes through the electrophoresis cell, irradiates the particles dispersed in it and it is scattered by particles in it. The scattered light is detected by the photo multiplier tube after passing through the pin holes. In a fringe optics ELS instrument, a laser beam is divided into two beams.

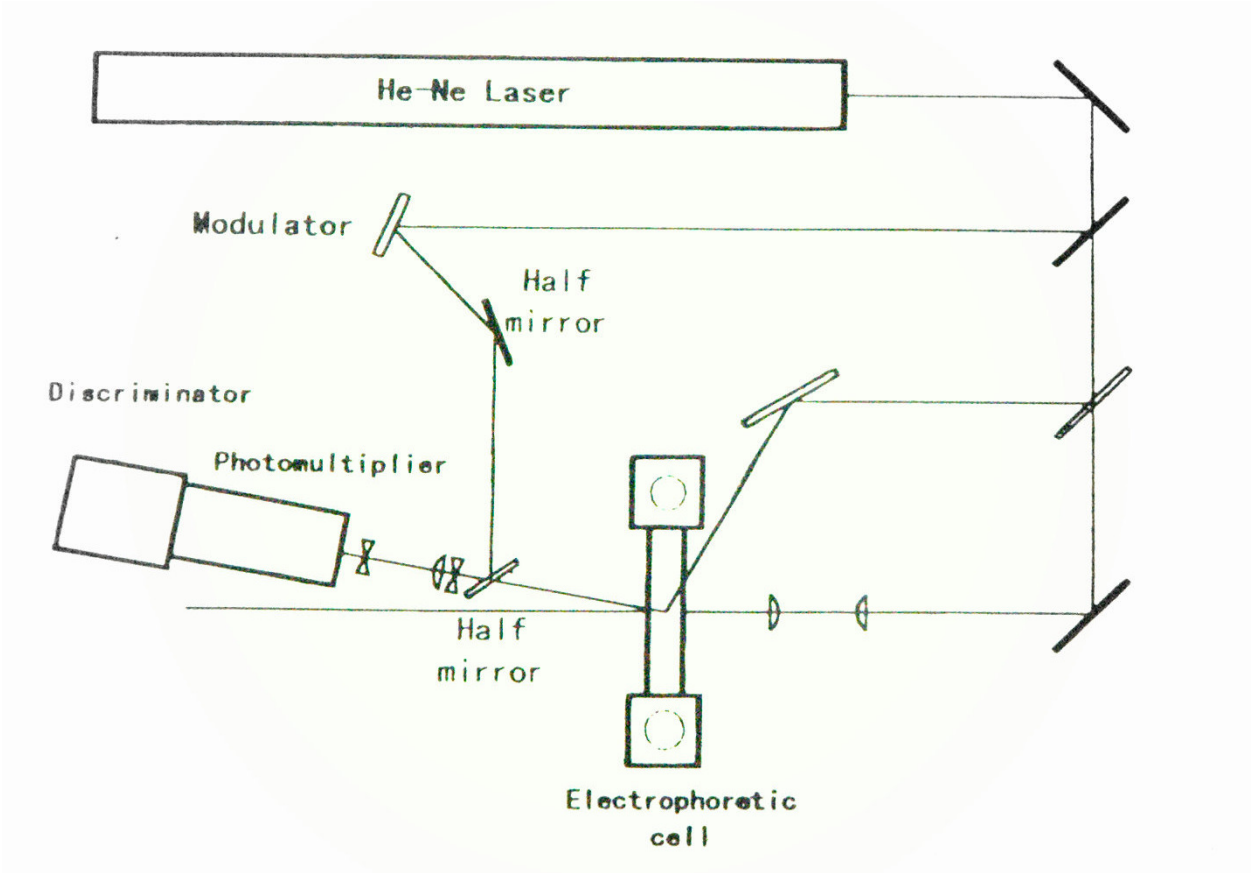

Figure 5-2: Schematics of an electrophoretic light scattering instrument [18].

The two beams cross inside the electrophoretic cell at a point called measurement volume. The beams are scattered by moving particles at the measurement volume and the scattered light reaches the detector [17].

5.2.3 Sample Preparation

No special sample preparation techniques are necessary. The sample should be dilute enough to prevent particle-particle interaction. Dry samples should be suspended in a liquid before measurement.

5.2.4 Applications

Zeta potential of a wide range of particles can be measured by this technique. Zeta potential serves as an important parameter in characterizing the electrostatic interaction between particles in dispersed systems as well as the properties of the dispersion as affected by this electrical phenomenon [16]. Zeta potential is mainly used in the formulation of particulate dispersions.

5.3 Scanning Electron Microscopy (SEM)

A scanning electron microscope permits the observation and characterization of heterogeneous organic and inorganic materials on a nanometer (nm) to micrometer (mm) scale [19]. SEM is capable of obtaining three dimensional like images of the surface for a very wide number of materials. It uses a focused beam of high energy electrons directed onto the sample to generate various signals such as secondary electrons, back-scattered electrons, characteristic electrons, characteristic x-rays, light, specimen current and transmitted electrons. These signals reveal information about the sample including

external morphology, chemical composition and crystalline structure as well as the orientation of materials in the sample [20]. SEM is also capable of performing analyses of selected point locations on the sample. This is useful in qualitatively or semi-quantitatively determining chemical compositions, crystalline structure and crystal orientations.

5.3.1 Principle of Scanning Electron Microscopy

A high energy electron beam, thermionically emitted from an electron gun, hits a limited volume of the sample. The energy exchange between the electron beam and the sample results in the reflection of high energy electrons by elastic scattering, emission of secondary electrons by inelastic scattering and the emission of electromagnetic radiation, each of which can be detected by specialized detectors [21]. X-ray radiation is produced by inelastic collisions of the incident electrons with electrons in the orbitals of the atoms in the sample. As the electrons return from the excited state to the ground state they produce x-rays of fixed wavelength. Thus, characteristic x-rays are produced for each element in a mineral that is excited by the electron beam [20]. Of all the signals that are produced, secondary electrons and backscattered electrons are commonly used for imaging samples. The resulting image is therefore a distribution map of the intensity of the signals being emitted from the scanned area of the sample.

5.3.2 Instrumentation

Essentially, a SEM consists of a lens system, the electron gun, sample stage, the electron collector, the visual and photo recording cathode ray tubes (CRT) and the associated electronics [21]. It usually has at least one detector and most have additional detectors. The electron gun is the source of the electron beam which is fitted with a tungsten filament cathode.

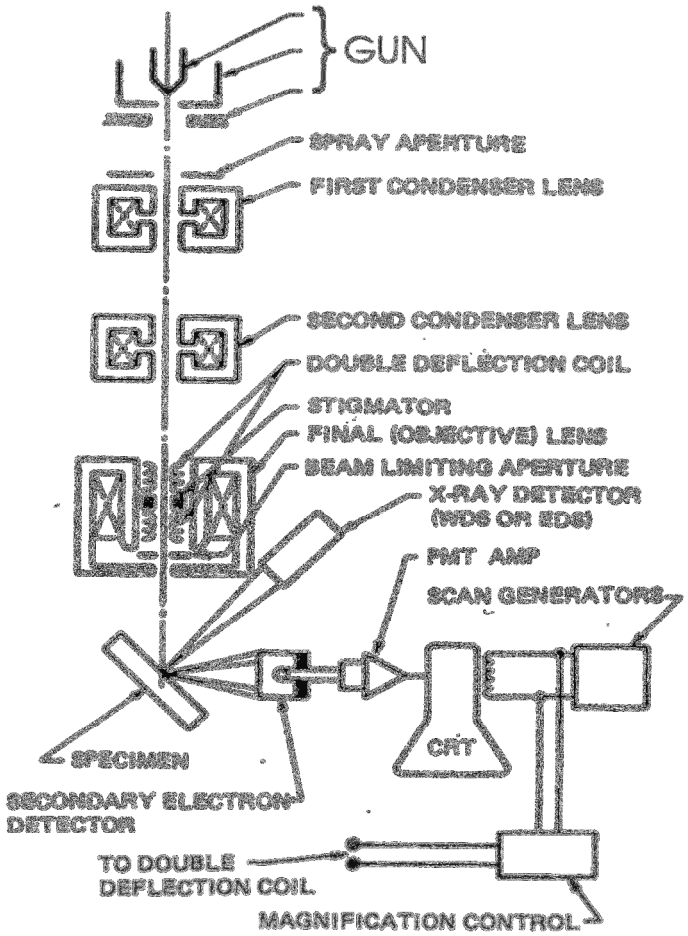

Figure 5-3: Schematic for a Scanning electron microscope [20]

The beam is focused onto the sample by a series of lenses which includes both condenser and objective. These lenses also help in maintaining the diamter of the beam. A series of

apertures of micron scale through which the beam passes, affects the beam [22,23]. The raster scanning of the CRT display is synchronised with that of the beam on the specimen. The signal produced is received by the corresponding detector. The entire system is maintained at a high vacuum level to prevent electron air-molecule interactions [22,24].

5.3.3 Sample preparation [25]

All samples must be of appropriate size to fit in the specimen chamber and are generally mounted on the specimen stub. Water must be removed form the sample because water would vaporize under vacuum [26]. Samples that contain metal are conductive and do not need any special sample preparation. Non conductive samples tend to charge when scanned by the electron beam causing scanning faults and other image artifacts. Hence, all non-metals need to be made conductive by covering the sample with a thin layer of conductive material usually gold. This is done by low vacuum sputter coating or by high vacuum evaporation [24]. Sometimes sputter coating is done for materials that have enough conductivity. This is done to increase signal and surface resolution.

5.3.4 Applications

SEM is one of the most widely used instruments in pharmaceutical research. It studies sample surface topography and composition. It is generally used to generate high resolution images of pharmaceutical solids and show spatial variations in chemical compositions. It is mainly used for the study and characterization of excipients, drugs and other adjuvants especially those of nano particle size [27].

5.4 Differential Scanning Calorimetry(DSC)

Differential scanning calorimetry is a thermoanalytical technique that studies thermal transitions in substances when they are heated. This technique was first developed by E.S. Watson and M.J. O'Neill in 1962 [28].

5.4.1 Principle of Differential Scanning Calorimetry

The principle involves the measurement of flow of the change of the difference in the heat flow rate to the sample and to a reference sample while they are subjected to a controlled temperature program [29]. Both the sample and the reference are maintained at the same temperature throughout the experiment. When there is a thermal transition such as a glass transition, crystallization or melting, more or less heat may be needed for the sample than the reference to maintain the same temperature. Hence, there is a change in heat capacity producing a peak. The peaks may be positive or negative depending on whether the thermal event is exothermic or endothermic. When a solid sample melts, it will require more heat to melt all the crystals to maintain the sample temperature as the reference. Therefore, this process is endothermic. Some exothermic processes such as crytsallization release heat and will require less heat to maintain the same temperature as the reference [30].

5.4.2 Instrumentation

A DSC usually consists of a furnace containing two identical crucibles each of which rests on a thin plate located inside the measurement head. Directly beneath the center of each crucible is the junction of a differential thermocouple. Any difference in

temperature of the two specimens is caused by differences in mass, specific heat, heats of reaction, or phase transitions [31]. The crucibles for the sample and reference pan are made of inert materials such as aluminum, quartz, glass and platinum. The pans are heated at a specific rate in an inert atmosphere of nitrogen gas purge at a constant pressure.

Two basic types of Differential Scanning Calorimeters can be distinguished depending on the heating rate, namely a constant heating rate or a variable heating rate.

Heat flux DSC [32]: In this design a single furnace heats both the sample and reference pans. This furnace is much larger than the one used in Power Compensated DSC described below. The temperature vs. time profile through a phase transition in this instrument is not linear. When there is a phase transition, there is a large change in heat capacity for the sample leading to a difference in temperatures between the sample and reference pans.

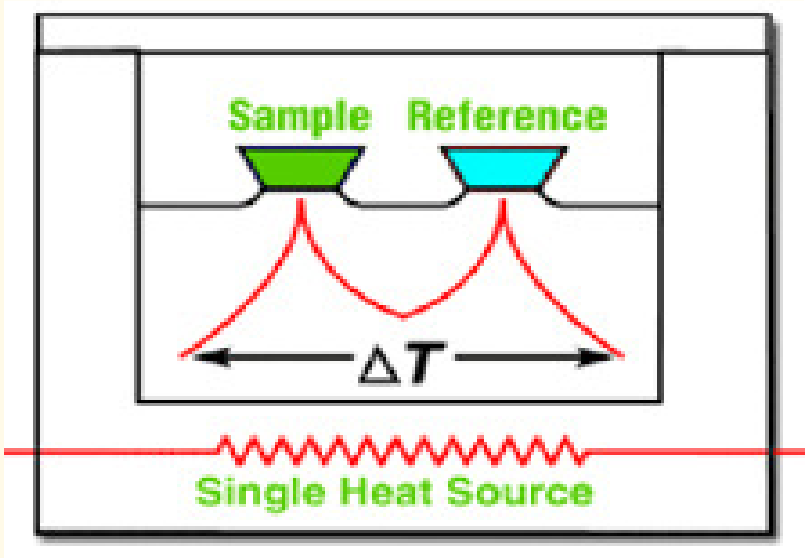

Figure 5-4: Schematic for a Heat Flux DSC [33]

Power Compensation DSC [34,35]: In this design the sample and reference pans are heated in different furnaces. Platinum Resistance Thermometers (PRTs) are sensitive and detect any small changes in temperature in the furnaces. Power is either applied or removed to compensate for the change in heat flow to or from the sample. The amount of power supplied is directly proportional to the energy changes occurring in the sample. No complex heat flux equations are necessary because the system directly measures the energy flow to and from the sample [36].

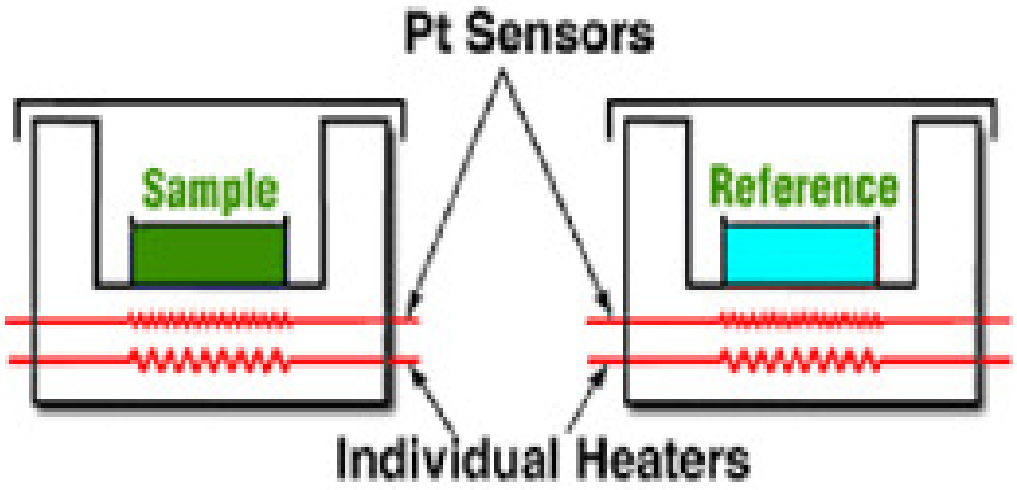

Figure 5-5: Schematics for a Power Compensated DSC [33]

5.4.3 Thermogram

A thermogram is a plot of heat flow versus temperature. The heat flow is usually the units of heat supplied per time (dQ/dt) [37]. A typical thermogram is given in Figure 5-5.The thermogram gives information about the heat capacity when heat flow (dQ/dt) is divided by the heating rate (dT/dt). It also provides information about the heat of vaporization,

heat of crystallization from the area of the melting and crystallization peaks, respectively [28].

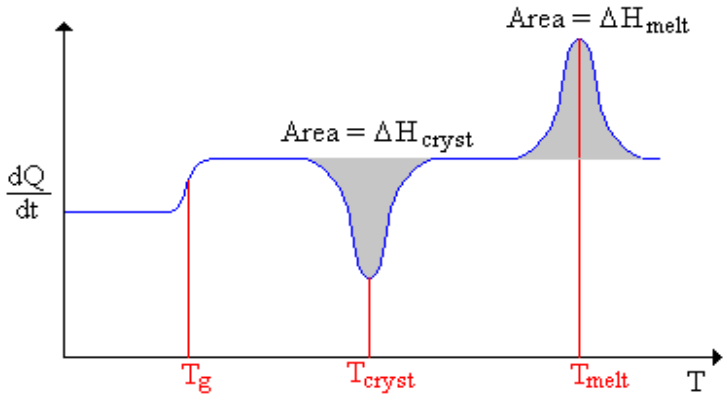

Figure 5-6: A typical thermogram of DSC [38]

5.4.4 Sample Preparation

DSC analyzes both solid and liquid samples. Solid samples can be in form of a film, powder, crystal or granular. Although quantitative accuracy will remain the same regardless of sample shape, the qualitative appearance of the experiment run may be affected by the sample configuration. Proper sample preparation, one that maximizes the contact surface between the pan and the sample, will reduce the resistance of the sample to heat flow. The DSC temperature sensors will result in maximum peak sharpness and resolution [39]. The best sample shapes for optimum performance are thin disks, or films or fine granules spread in a thin layer on the bottom of the pan. Pans are usually made of aluminum or platinum and may be open, sealed, covered or pin holed depending on the nature of the sample. The sample size can range from 3-10 mg or more.

5.4.5 Applications

DSC is the most widely used thermoanalytical technique to characterize pharmaceutical substances. It is used for the characterization of drug substances, excipients and packaging material. Pharmaceutical applications for DSC include identification, purity determination, study of polymorphism, solvation and stability determination. It is also used in the development of dosage forms to determine the choice of the salt form, phase diagrams, drug substance and excipient interactions, physical changes on processing or during storage and even in the analysis of the dosage form [40]. Other applications include the study of polymers (melting point, cyrstallization) [41], study of liquid crystals [42] and measurement of heat involved in protein folding/unfolding reactions [43].

5.5 Thermogravimetric Analysis (TGA)

Thermogravimetric analysis is another thermoanalytical technique which when used with DSC measures both heat flow and weight changes. TGA when used with DSC can differentiate between endothermic and exothermic events with no associated weight loss (e.g, melting and crystallization) and those that involve a weight loss (e.g, degradation) [44].

5.5.1 Principle of Thermogravimetric Analysis

TGA measures the amount of weight change of a material either as a function of increasing temperature or isothermally as a function of time, in an atmosphere of nitrogen, helium, air or a vacuum. The weight change sensitivity for a TGA can be

around 0.01mg. TGA essentially consists of a very sensitive balance with a pan loaded with the sample. Any change in weight of the sample during heating is recorded and interpreted as any thermal event such as decomposition, oxidation or dehydration depending on the temperature. A typical thermogram of TGA consists of weight plotted against temperature [45]. All the weight loss curves may look similar, therefore a derivative weight loss curve can identify the point where weight loss is more apparent [44].

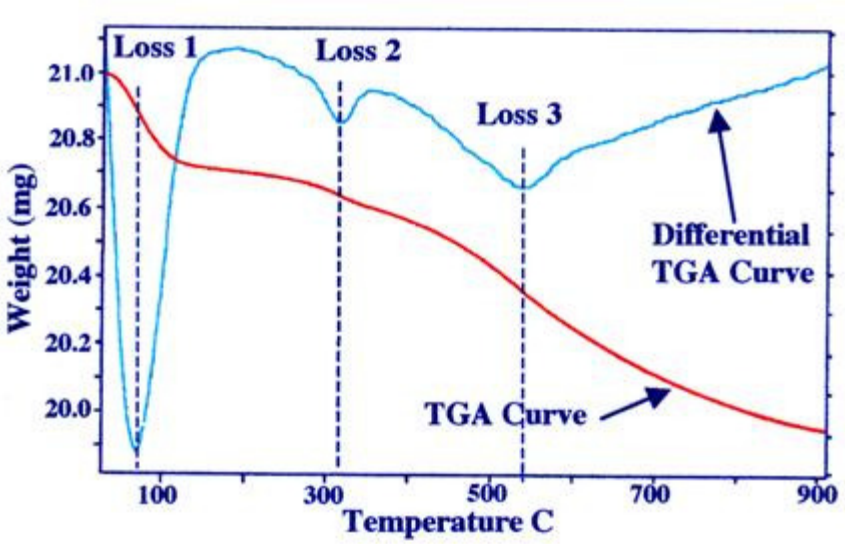

Figure 5-7: A typical thermogram for TGA [45]

5.5.2 Instrumentation

TGA usually consists of a high precision balance with a pan generally made of platinum or aluminum depending on the nature of the sample. Aluminum can with stand a temperature up to 660^0C. If higher temperatures are needed, platinum pans can be used [46]. Some processes use a quartz crystal microbalance that measures small samples in the order of micrograms (seen in Figure 5-7). The sample is placed in a small electrically heated oven with a thermocouple to accurately measure the temperature. The sample is

heated in the presence of a vacuum, or with the purging of nitrogen and/or helium or air. A water cooling system is used to cool down the furnace when required.

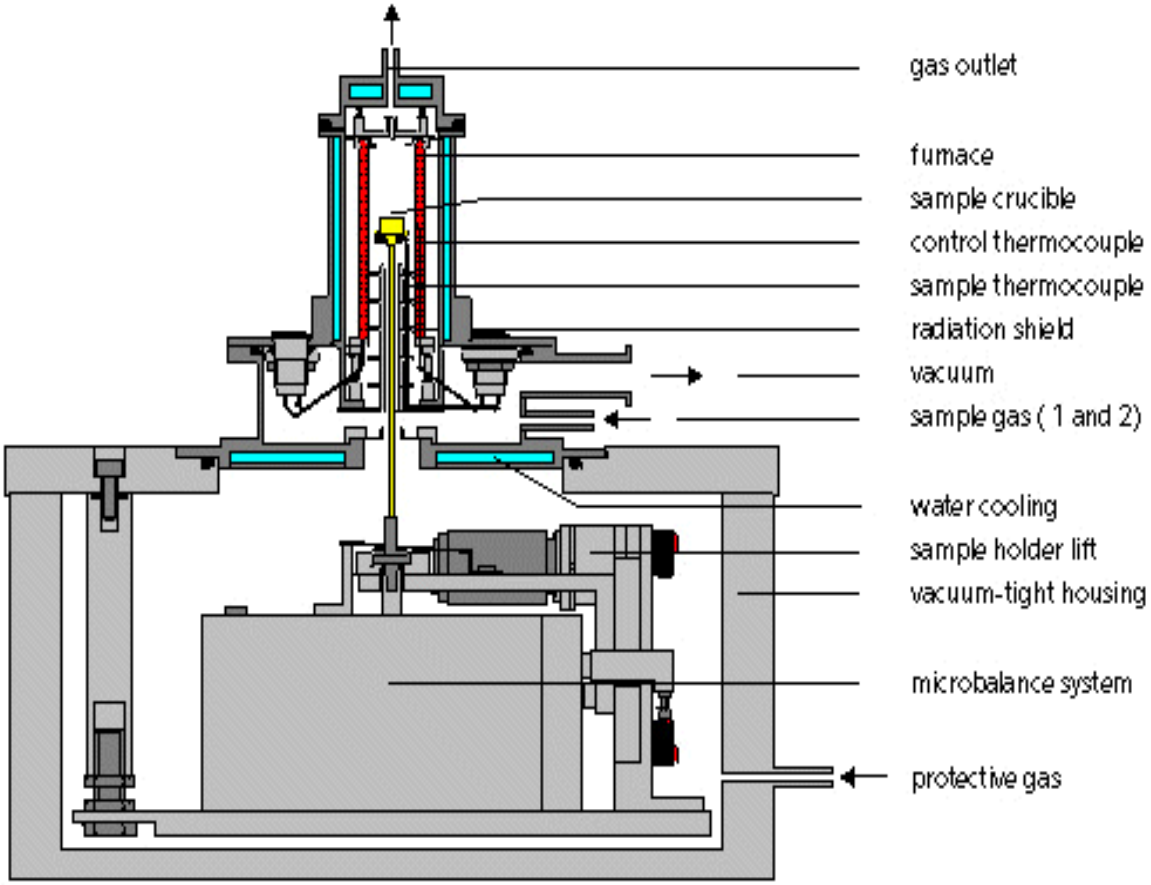

Figure 5-8: Schematics for a Thermogravimeter [48]

5.5.3 Sample preparation:

Any solid or liquid samples can be analyzed using TGA. The sample should be spread well on the pan to maximize the surface area of the sample to improve weight loss resolution and temperature reproducibility [47]. Sample weight for most substances is 10-20 mg. To measure volatile substances a sample weight of 50-100 mg is required [48].

5.5.4 Applications

TGA determines a temperature and weight change for decomposition reactions which often allows quantitative compositional analysis [50]. It can be used in the determination of bound and unbound water content in a given sample.It can also be used to measure evaporation rates and volatile emissions from liquid mixtures.TGA is helpful in the characterization of materials such as polymers, to determine degradation temperatures as well as absorbed moisture content of materials, the level of organic and inorganic components and the presence of volatile ingredients in the sample.TGA in conjunction with DSC helps in the characterization of various drugs, pharamceutical excipients and other adjuants [51].

5.6 Powder X-ray Diffraction Analysis (PXRD)

X-ray powder diffraction is a rapid analytical technique primarily used for phase identification of a crystalline material and can provide information on unit cell dimensions [52]. Each crystalline solid has its unique characteristic X-ray powder pattern which may be used as a fingerprint for its identification.

5.6.1 Principle of PXRD

X-rays are electromagnetic radiation of about 1Å which is about the same size as an atom. Since the wavelength of an X-ray is comparable to the size of atoms, they are ideally suited for probing the structural arrangement of atoms and molecules in a wide range of materials [53]. The three dimensional structure of crystalline solids consists of

repeating planes of atoms that form a crystal lattice which can be separated by a distance (d) (shown in the Figure 5-8). When a focused X-ray beam interacts with these planes of atoms, part of the beam is transmitted, part is absorbed by the sample, part is reflected and scattered and part is diffracted. Diffraction occurs when the incident X-ray waves have a wavelength that is comparable to that of the atom spacings in the crystal and this leads to constructive interference in accordance to Bragg's law [54].

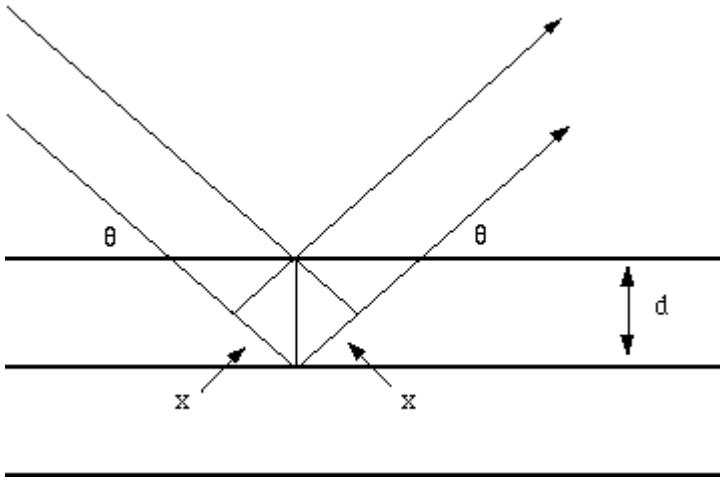

Figure 5-9: Diffraction of X-ray by crystalline material [53]

Bragg's law relates the wavelength of an X-ray to the diffraction angle and the lattice spacing in a crystalline sample which is given by:

$$n\lambda = 2dsin\theta \qquad \text{Eq. 5.1}$$

where (λ) is the wavelength of the incident wave;

(n) is an integer;

(d) is the spacing between the planes in the crystal lattice; and

(θ) is the angle between the incident ray and the scattering planes.

The diffraction of X-rays takes place only at certain angles when there is constructive interference and Bragg's law is thus satisfied. Each crystal has its own unique diffraction pattern which is used for identification purposes [55].

5.6.2 Instrumentation of PXRD [52,56]

X-ray diffractometers consist of three basic elements: an X-ray tube, a sample holder and an X-ray detector. X-rays are generated in a cathode ray tube by heating a filament to get electrons. These electrons are accelerated towards a target when a voltage is applied. The target material is bombarded with these high energy electrons. When electrons have sufficient energy to dislodge inner shell electrons of the target material, characteristic X-ray spectra are produced.

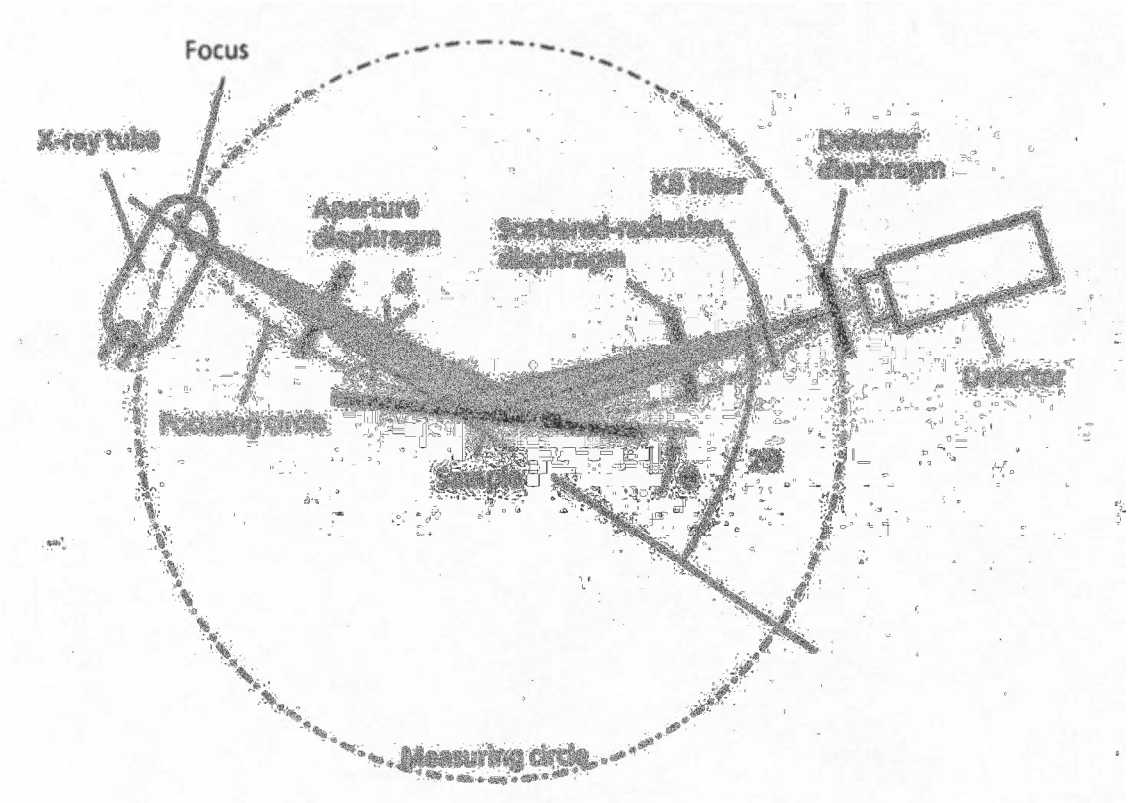

Figure 5-10: Schematic of an X-ray diffractometer [57].

The wavelength of the X-ray produced depends on the target material. Some of the most commonly used targets include copper, iron, molybdenum and chromium. The X-rays produced have 2 components (K_α) and (K_β). These X-rays are collimated and directed onto the sample by means of a slit (aperture diaphragm). A goniometer which is an angle measuring device rotates the sample. The measuring circle remains constant throughout the analysis and is defined by the position of the target, centre of the sample and the position of the receiving slit. As the sample and detector are rotated, the intensity of reflected X-rays is recorded. When the geometry of the incident X-ray impinging the sample satisfies the Bragg's equation, constructive interference occurs and a peak in intensity occurs. A filter is used to remove all the (K_α) radiation from the diffractor beam before it enters the detector. A detector records and processes this X-ray signal. The incident angle (θ) is the angle between the incident beam and the sample and (2θ) is the angle between the incident and diffracted beam before it enters the detector. The detector rotates at twice the angular rate of the sample to maintain the θ-2θ geometry [58].

5.6.3 Sample preparation

The sample should be ground to a fine powder, typically in a fluid to reduce the extra strain that can offset peak positions and to randomize orientations. Powder with a particle size less than 10 μm is preferred [56]. A 100 mg portion of the pure sample should be sufficient. The sample should be placed on the sample holder, smearing uniformly to create a flat upper surface to achieve random distribution of lattice orientations [52].

5.6.4 Applications of PXRD

PXRD is used extensively in the design and development of drug delivery systems [59]. X-ray powder diffraction is most widely used for the identification of unknown crystalline materials. It is used for the characterization and purity determination of crystalline solids [60]. Most of the pharmaceutical products are mixtures of drug and their excipients. PXRD can be used to determine the presence of a compound in a mixture. Qualitative and quantitative analysis of pharmaceuticals can be done using PXRD. Other applications include determination of drug-excipient interactions [61], properties of different polymorphs associated with various drugs and percentage crystallinity of drugs and excipients [62].

Chapter 6

Materials and methods

6.1 Materials

The materials used in this study include the following:

6.1.1 Magnesium sulfate heptahydrate

Magnesium sulfate heptahydrate is most commonly called Epsom salts. It is a colorless, odorless, bitter tasting substance with fine needle like crystals. It has a high melting point. The crystals are efflorescent and if the container remains unopened, it loses water into the atmosphere. It is partially soluble in organic solvents such as glycerin and alcohol and insoluble in acetone.

6.1.1.1 Physical properties

Source: Spectrum Chemicals, LOT No. YFO493, pH: 6

CAS No. 10034-99-8 Vapor density: <0.01

Chemical name: Magnesium (II), sulfate, Refractive index: 1.433

heptahydrate	Soluble in cold water (710gms/L)
Chemical formula: MgSO4.7H2O	Melting point: 1124^{o}C
Molecular weight: 246.46 gm/mole	Specific gravity: 1.67

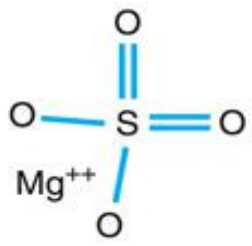

Figure 6-1:Structure of Magnesium Sulfate

6.1.1.2 Chemical properties

It reacts with arsenates, phosphates and tartrates to precipitate the corresponding magnesium salts. On exposure to dry air at ordinary temperatures it loses 1 water molecule. It loses 4 water molecules at 70-80^{o}C and at 250^{o}C it theoretically loses all water molecules to form an anhydrous salt. TG experiments done in our laboratory have shown that $MgSO_4.7H_2O$ loses water molecules in odd ways and there are ½ moles and ¾ moles water lost from 100 to 500^{o}C and it never becomes anhydrous. A magnesium sulfate solution is neither acidic nor basic. When dissolved in water magnesium sulfate splits into ions of magnesium and sulfate.

6.1.1.3 Uses

Due to its cathartic properties, it can be used as a laxative to evacuate the bowel. It is used in replacement therapy for hypomagnesemia. It is commonly administered via the IV route for the management of severe asthma attacks. Solutions of this salt may be given

for barium chloride poisoning. Topically, the paste is applied for dehydrating boils. It also finds use in the treatment of blemishes and acne. Used in the manufacture of bath salts.

6.1.2 Sodium Hydroxide

Sodium hydroxide is commonly called as lye or caustic soda. It appears as white, odorless pellets. It is hygroscopic and readily absorbs water from the air. It is very soluble in water with the liberation of heat. It is also soluble in ethanol and methanol. It is insoluble in ether and other non-polar solvents. It is usually stable at room temperature in closed containers.

6.1.2.1 Physical properties

Source: Fisher scientific, LOT No. 066852

CAS No. 1310-73-2

Chemical name: Sodium hydroxide

Chemical formula: NaOH

Molecular weight: 40gm/mole

Specific gravity: 2.13

Melting point: 318^{o}C

pH: 14 (5% solution)

Vapor density: >1

Vapor pressure: 1mmHG at 739^{o}C

Refractive index: 1.412

Soluble in water (111gms/100gms water)

Boiling point:1390^{o}C

6.1.2.2 Chemical properties

Sodium hydroxide is an extremely corrosive and reactive chemical. A solution of caustic soda reacts with metals such as aluminum, magnesium, zinc, tin and chromium. Many

non-metals also react with it, forming salts. Sodium hydroxide reacts slowly with glass to form sodium silicate. It forms salts with carboxylic acids and it is even a strong enough base to form salts with phenols. It precipitates metal hydroxides. Caustic soda reacts with protic acids to produce their corresponding sodium salts and water.

6.1.2.3 Uses

Sodium hydroxide is mainly used for the production of sodium salts, detergents and pH regulation. It is most commonly used for alumina production by the Bayer's method [1]. It is used in any scenario where there is a need to increase the alkalinity of the mixture or to neutralize acids. Lye is most commonly used in paper making. It is traditionally used in soap making

6.1.3 Lutrol F127

This hydrophilic non ionic surfactant is commonly called Poloxamer 407. This substance appears as a white colored, waxy, coarse grained powder with a faint specific odor. It is not only readily soluble in water but also in polar and non polar organic solvents. It is insoluble in ether, paraffin and fatty oils. Water solubility is due to the hydrogen bonding of its polyethylene oxide block with water. When dispersed in liquid at low concentrations, the Poloxamer exists as individual molecules, however when the concentration increases, they form multimolecular aggregates.

6.1.3.1 Physical properties

Source: BASF, LOT No. WPAF580B

CAS No. 9003-11-6

Specific gravity: 1.05

Viscosity: 3100cps

Chemical name: Triblock copolymer of polypropylene glycol and polyethylene glycol

Chemical formula: $(C_3H_6O.C_2H_4O)_X$

Molecular weight: 12,600 Daltons

Bulk density: 500kg/m^3

Soluble in cold water (>175gms/L)

Melting point: 56°C

pH: 6-9 (50gms/L of solution)

Surface tension: 41 dynes/cm (of a 0.1% solution at 25°C)

HLB value: 18-23

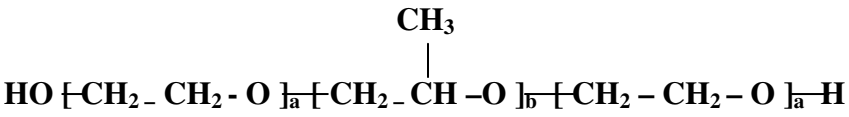

Figure 6-2: Structure of Lutrol F127 (Poloxamer 407) where a=101 and b=56

6.1.3.2 Chemical properties

They are generally regarded as non-toxic and non-irritant materials. It is incompatible with stearates. It generally contains less than 0.5% w/w water and is hygroscopic only at a relative humidity greater than 80%. Each grade of Poloxamer is usually followed by a number, the first two digits of which, when multiplied by 100 gives the molecular weight of the polyoxypropylene portion and the third digit when multiplied by 10 gives the percentage by weight of the polyoxypropylene portion.

6.1.3.3 Uses

Poloxamer has a gelling effect in lower concentrations because of their high molecular weight; hence they are used to modulate the viscosity of liquid formulations. They are mainly used as thickening agents, co-emulsifiers and consistency enhancers in creams and liquid emulsions.

It can also be used as a solubilizer for drugs such as nifedipine, naproxen and fenticonazole as well as for essential oils in pharmaceutical formulations. It is used as a flocculating agent in topical and oral suspensions and used in toothpastes, gargles and mouthwashes. In addition to its application in formulations, oil in water based microemulsions of Poloxamer can be an effective agent in the extraction of lipophilic drugs from plasma in cases of overdosing. It finds use in the manufacture of contact lens cleaning solutions.

6.1.4 Reverse osmosis (RO) water

RO water is used to prevent the impurities having an effect on the system being studied. It was obtained from the University of Toledo, RO aqueous system.

6.2 Equipment used

Measuring cylinders were used to study the rate of fall of the interface. A 250 mL measuring cylinder made of pyrex glass and manufactured by Fisher Scientific, Fairlawn, NJ was used.

A 100 mL volumetric flask was used to make the 1% polymer solution.

An electronic balance, ER 120A, made by American Scientific Products was used for all weighing.

An Ostwald-Viscometer, E.H. sergent & Co. No. S-83305, Chicago, IL was used for the viscosity measures.

A pycnometer, 25ml, Kimble brand, Item No. 15123-ST, USA was used for density and specific gravity measurements.

A stop watch, Fisher Scientific, Fairlawn, NJ was used to time the experiments

Parafilm, American National Can Co. Chicago, IL was used to prevent liquid loss through evaporation and environmental contamination.

A long glass stirring rod, pyrex was used and manufactured by the UT glass blower

Sputter Coater –Denton vacuum, Desk II and JSM 5200 Scanning Electron Microscope, The University of Toledo

Laser diffraction instrument, Malvern Metasizer 2000^{e}, The University of Toledo

Zeta potential measurement, Nicomp 380 ZLS, Particle Sizing Systems, CA, University of Toledo

Differential Scanning Calorimeter, DSC 822^{e} Mettler Toledo, University of Toledo

Thermogravimeter, TGA/SDTA 851^{e} Mettler Toledo, University of Toledo

X-ray powder diffractometer, PANalytical X'Pert Pro MPD, University Of Toledo

6.3 Methods

6.3.1 Preparation of polymer solutions

A stock solution of the polymer was prepared by dissolving 1gm of Poloxamer solution in 100 mL of distilled water to make a 1% solution. Various concentrations of Poloxamer, namely 0.025%, 0.05% and 0.75% were prepared by adding 5 mL, 10 mL and 15 mL respectively, to the measuring cylinder to make 200 mL of the dispersion

medium. The solution of Poloxamer produced froth when dissolved in water. Hence, it was left aside for a few hours before it was made up to the final volume.

6.3.2 Determination of density

A 25 mL pycnometer was used to measure the density of the polymer solution. The weight of the empty bottle is taken and then it is filled with the solution until it overflowed the stopper returned, bottle wiped off and weighed again. This procedure was repeated three times with each of the solutions. The difference in weights was calculated and the density determined using the formula

Density (gm/ml) = difference in weights/volume (25 ml) Eq. 6.1

The density of all the other solutions was also calculated. The specific gravity was calculated relative to water.

6.3.3 Determination of viscosity

The Ostwald's viscometer was used to measure the viscosity of the solutions. The principle underlying this method is the measurement of time relative to the solution falling between two calibration marks that are above and below the bulb. This is usually compared with the time it takes for water to fall between these same markings. The water was drawn up to the mark above the bulb and the time required to fall to the mark below the bulb is noted. The same procedure was repeated for all solutions of known density. The viscosity of the solutions was calculated using the formula:

$$\frac{\eta_1}{\eta_2} = \frac{\rho_1 t_1}{\rho_2 t_2} \qquad \text{Eq. 6.2}$$

where,

η_1 is the viscosity of water ρ_1 is the density of water

η_2 is the viscosity of the solution ρ_2 is the density of the solution

6.3.4 Hindered settling experiments

Magnesium hydroxide was stoichiometrically prepared using 1M sodium hydroxide and 1M magnesium sulfate heptahydrate as given in the equation. The experiments were carried out in 200 mL graduated measuring cylinders. For the hindered settling study experiments, various weights of magnesium hydroxide such as 1gm, 2 gm, 3 gm, 4 gm and 5 gm were prepared using appropriate quantities of epsom salts and sodium hydroxide. The required quantity of magnesium sulfate heptahydrate was weighed accurately and dissolved in 100 mL purified water. A solution of sodium hydroxide was prepared by adding the appropriate amount to the beaker and dissolving it in the purified water. The NaOH solution prepared was slowly added to the magnesium sulfate solution taken in a 200 mL measuring cylinder.

The precipitate formed was maintained in the never dried state. The suspension was shaken well and left overnight so that the precipitate could settle and the solid be well wetted with the medium. The next day the supernatant fluid is decanted and the suspension was again made up to 200 mL and shaken again and left for 24 hrs. The supernatant liquid was decanted and filled with the same volume of purified water. This process was repeated till the supernatant liquid is free of sodium sulfate ions. The presence of sodium sulfate is tested by its ability to precipitate barium chloride. When the suspension was free of sodium sulfate, the volume of the suspension is made up to 200

mL, the precipitate was redispersed inverting the cylinder up and down for 25-30 times to produce a uniform suspension. The suspension was left undisturbed on a flat surface and the time taken for the position of the interface to drop by 2 mm was noted.

The final settled volume of the suspension was noted after the suspension was left undisturbed for 7 days. This time interval was chosen because the final level remained constant after 7 days. The average particle size of the magnesium hydroxide produced was determined by the rate of fall of the interface, which is the straight line portion of the graph obtained by plotting the position of the interface with time.

6.3.5 Flocculation of suspensions

For this study, all the suspensions were made as above to make sure they are clear of sodium sulfate ions. A stock solution of the polymer is prepared and the required volume of the solution is added to the final suspension to achieve the desired concentration of the polymer.

6.3.6 Variation in the rate of addition of the reagent

The required volume of 1M magnesium sulfate was placed into a measuring cylinder and 1M sodium hydroxide was added to it from a burette. The rate of addition was controlled with constant stirring. The sodium hydroxide solution was added to the magnesium sulfate solution at 5 different rates namely 0.01 mL/sec, 0.03 mL/sec, 0.05 mL/sec, 0.07 mL/sec and 0.09 mL/sec.

6.3.7 Determination of percentage yield

The sediments of the various magnesium hydroxide suspensions were filtered and dried overnight in a hot air oven at 70^0C. The dried powder was weighed accurately. The percentage yield was calculated using the formula:

$$\text{Percentage yield} = \frac{\text{Actual weight}}{\text{Theoretical weight}} \times 100 \qquad \text{Eq. 6.3}$$

6.3.8 Scanning electron microscopy (SEM)

SEM was performed to study the surface and morphology of magnesium hydroxide particles. A drop of the suspension was dried on a clean glass slide. The sample was made conductive by gold coating using a low vacuum sputter coater. Images were taken using a JSM- 5200 Scanning electron microscope operated at 10 kV.

6.3.9 Laser Diffraction (LD)

A small quantity of suspension was added to the volume of pumped water in the analyzer. The aqueous dispersion was homogenized for a few some seconds at 1000 rpm. The Malvern Metasizer 2000^e provided both the particle size distribution and statistical analysis for the sample used.

6.3.10 Zeta potential measurement

The zeta potential of the suspensions was measured using the dynamic light scattering, instrument a Nicomp 380 ZLS, Particle sizing system. A small volume of the suspension

was taken and placed in a disposable Durex borosilicate glass culture tube. The zeta potential was determined by placing the sample in the path of a Helium Neon laser of wavelength 658nm at a scattering angle of 90^{o} C and a temperature of 23^{o} C.

6.3.11 Differential Scanning Calorimetry (DSC)

The suspension samples along with the dried sediments and reference media were analyzed using a DSC 822^{e} Mettler Toledo equipped with a TS0800GCI gas controller. The 1gm sample of magnesium hydroxide dispersed in various media was chosen to be analyzed using this instrument. Approximately 20 mg of the sample was weighed and placed in a 100 µL Aluminum pan and the lid was pierced. Nitrogen was used as the purge gas at a flow rate of 20 mL/min. The temperature program had the following segments: dynamic cooling segment from 25°C to -30°C at 10°C/min, isothermal segment at -30°C for 5min, dynamic heating segments from -30°C to 150°C at 10°C/min, from 150°C to 350°C at 50°C/min, and from 350°C to 500°C at 10°C/min. The results were evaluated using $STAR^{e}$ software.

6.3.12 Thermogravimetry (TG)

The 1gm magnesium hydroxide dispersed in various media was analyzed using TGA/SDTA 851^{e} Mettler Toledo. Approximately 20 mg of the sample was weighed and placed into a 100 µL aluminum pan. The lid was pierced for the evolution of water vapor. The sample was heated from 25°C to 500°C at 10°C/min. Nitrogen was used as the purge gas at a flow rate of 20 mL/min. The results were evaluated using $STAR^{e}$ software.

6.3.13 X-ray Powder Diffraction (PXRD)

Commercial powder of Magnesium hydroxide and dried magnesium hydroxide suspended in water and 0.025% Poloxamer were analyzed using PANalytical X'Pert Pro MPD. X-ray spectra were recorded using a Cu X-ray source, a voltage of 45 kV, a current of 40 mA, with 0.04 rad Soller slits, 1/4° divergence slit,10 mm mask, 1/2^{o} anti scattered slit, Nickel filter and X'Celerator detector over a 2□ range of 10^{o} to 70^{o} with a continuous speed of 4^{o}/min. The peak pattern for dried magnesium hydroxide after heating on the TG was evaluated using this instrument. Fine powder samples were obtained by grinding using a mortar and pestle and packed smoothly in the cavity of an aluminum sample holder. The results were evaluated using the X'Pert Data High Score Plus software.

Chapter 7

Results and discussion

7.1 Hindered settling experiments

7.1.1 Density and Viscosity of the suspending media

The density and viscosity of the suspending media was calculated based on the method as described in Chapter 6 Sections 6.3.2 and 6.3.3. The results are given in Table 7.1. The value for the density of magnesium hydroxide used in this study is 2.3446 gm/cm^3 and was obtained from the literature. A clear supernatant was observed for water and the three different concentrations of Poloxamer. However, when 0.1% w/v of Poloxamer was used, the system deflocculated with no clear interface.

Table 7.1: Densities and viscosities of the suspending media

Suspending media	Density(gm/cm^3)	Viscosity(poise)
Purified water	0.9857	0.0091
0.025% w/v Poloxamer	1.0282	0.02947
0.05% w/v Poloxamer	1.0323	0.03012
0.075% w/v Poloxamer	1.0354	0.03185

7.1.2 Hindered settling results:

Hindered settling experiments were performed as described in the Chapter 6 Section 6.3.4. After making sure the suspensions were free of sodium sulfate, they were shaken well and the rate of fall of the interface was recorded. For magnesium hydroxide suspensions dispersed in Poloxamer, foaming was observed as the suspensions were shaken. The interface height was measured after a clear interface was observed.

The experiments were performed in triplicate for all the suspending media namely water, 0.025%, 0.05% and 0.075% Poloxamer solutions. The hindered settling plots for all the suspensions resembled the normal plot as depicted in Figure 3-1 with an initial zone, a second linear zone and the final compressive zone. To determine the effect of the flocculating agent, the rate of fall (Q) of the suspensions were compared.

The plots of interface height (mm) against time (min) for various concentrations (1 gm to 5 gms) of magnesium hydroxide are given in Figures 7-1 to 7-4. The values for the hindered settling parameters (concentration, Q and ε) in each suspending media are given in Tables 7.2 to 7.5. The Q- values for each of these suspensions were obtained from the slope of the linear zone of the sedimentation curves. The initial porosity (ε) was calculated using the equation below:

$$\varepsilon = 1 - \frac{C}{\rho_s} \qquad \text{Eq. 7-1}$$

where C is the concentration of the suspension (gm/mL); and

ρ_s is density of the solid suspended (gm/cm^3)

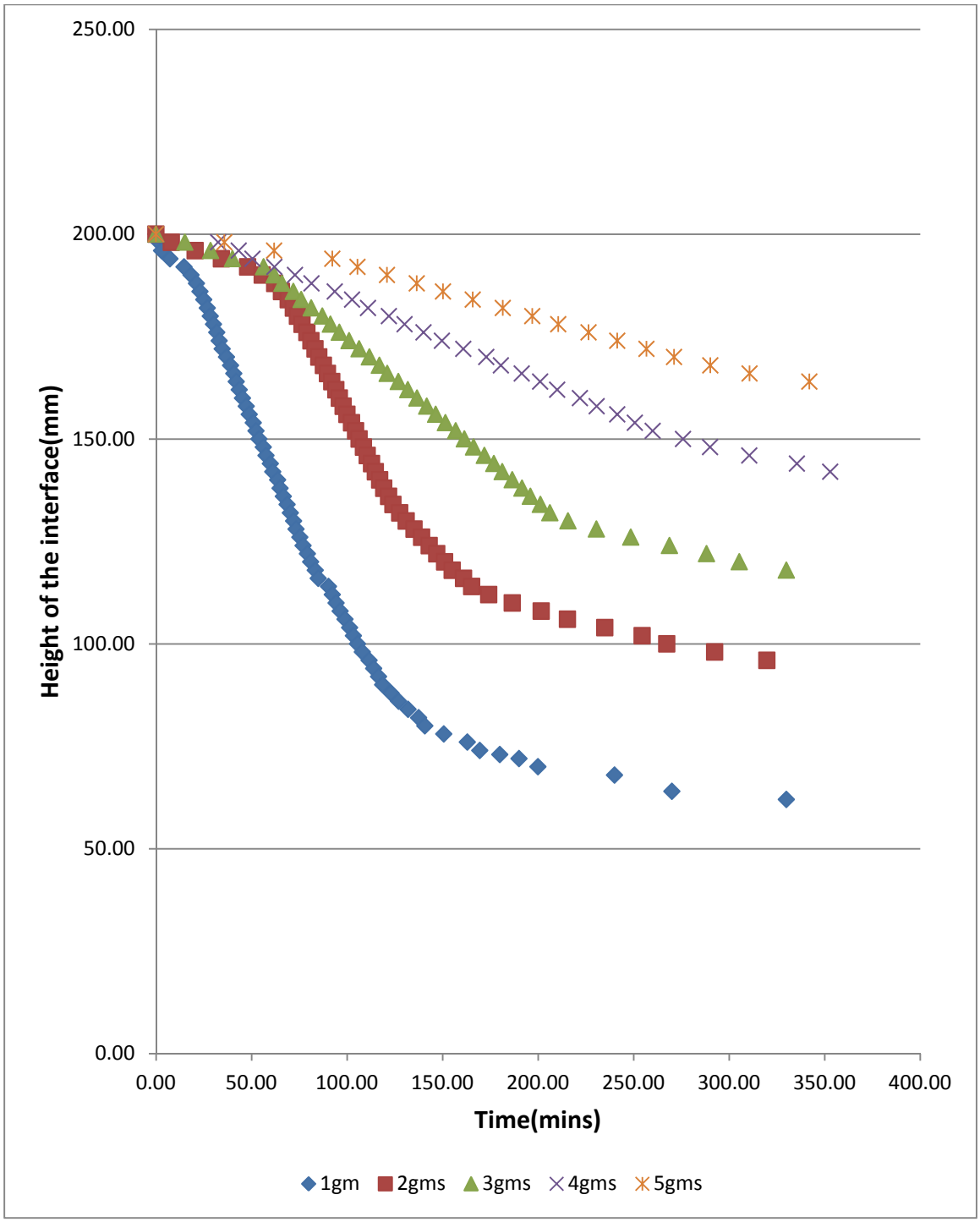

Figure 7-1: A plot of height of the interface (mm) against time (min) for magnesium hydroxide suspensions in purified water.

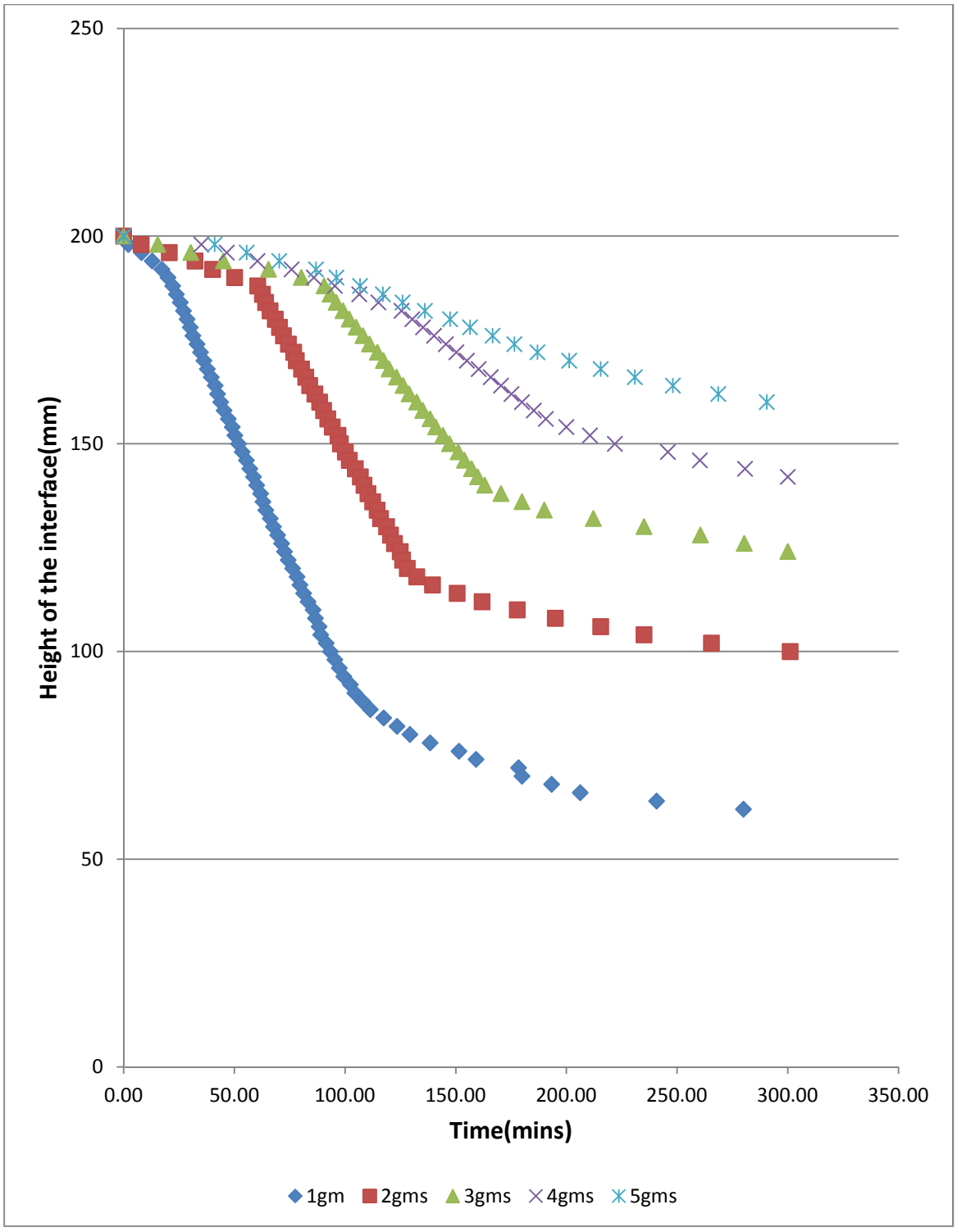

Figure 7-2: A plot of height of the interface (mm) against time (min) for magnesium hydroxide suspensions in 0.025% Poloxamer solution

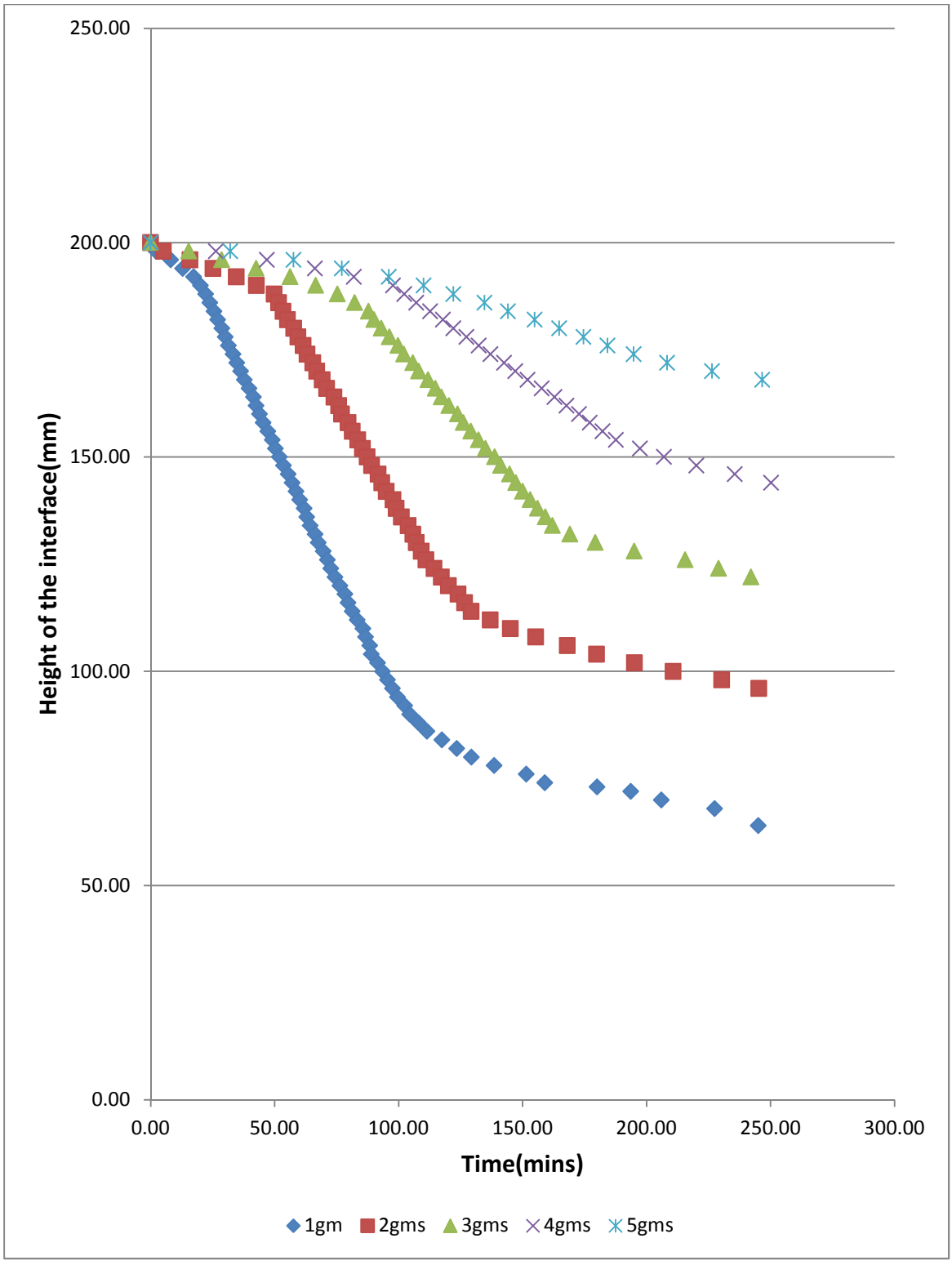

Figure 7-3: A plot of height of the interface (mm) against time (min) for magnesium hydroxide suspensions in 0.05% Poloxamer solution.

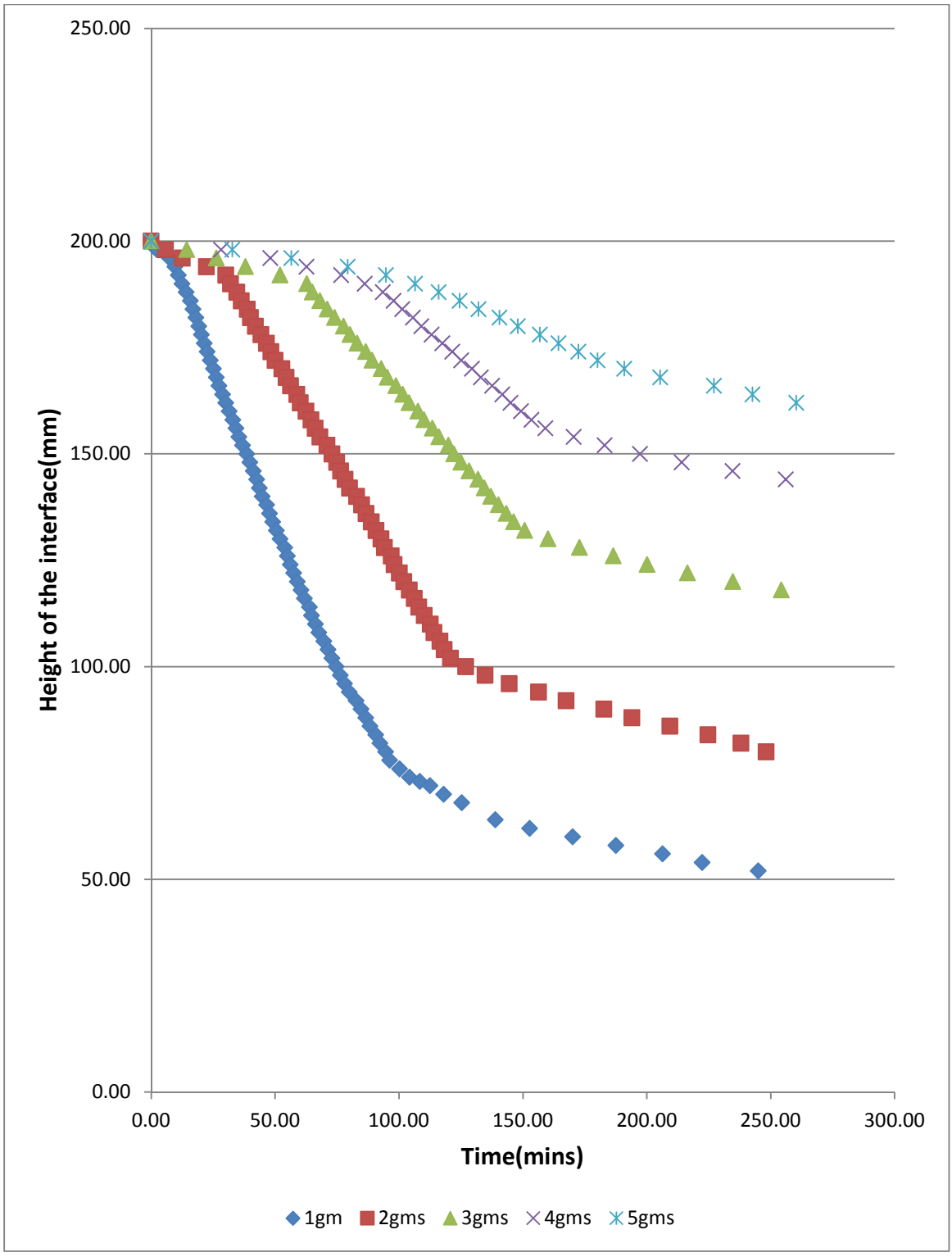

Figure 7-4: A plot of height of the interface (mm) against time (min) for magnesium hydroxide suspensions in 0.075% Poloxamer solution.

Table 7.2: Hindered settling parameters for different weights of magnesium hydroxide suspended in water

Wt (gm)	Conc. (gm/mL)	Q_1 (mm/min)	Q_2 (mm/min)	Q_3 (mm/min)	Q_{avg} (mm/min)	S.D	ε
1	0.005	1.2378	1.0864	1.1321	1.1521	0.063406	0.99786
2	0.01	0.704	0.7005	0.7066	0.7037	0.002499	0.99573
3	0.015	0.3999	0.4009	0.401	0.4006	0.000497	0.9936
4	0.02	0.2034	0.2032	0.2045	0.2037	0.000572	0.99146
5	0.025	0.1328	0.1328	0.1326	0.1327	0.000094	0.98933

Table 7.3: Hindered settling parameters for different weights of magnesium hydroxide suspended in 0.025% Poloxamer

Wt (gms)	Conc (gm/mL)	Q_1 (mm/min)	Q_2 (mm/min)	Q_3 (mm/min)	Q_{avg} (mm/min)	S.D	ε
1	0.005	1.2322	1.323	1.2206	1.2586	0.045783	0.99786
2	0.01	0.987	0.9646	1.005	0.985533	0.016526	0.99573
3	0.015	0.6639	0.6617	0.6557	0.660433	0.003465	0.9936
4	0.02	0.4006	0.4046	0.4108	0.405333	0.004196	0.99146
5	0.025	0.1993	0.1988	0.1975	0.198533	0.000759	0.98933

Table 7.4: Hindered settling parameters for different weights of magnesium hydroxide suspended in 0.05% Poloxamer

Wt (gms)	Conc. (gm/mL)	Q_1 (mm/min)	Q_2 (mm/min)	Q_3 (mm/min)	Q_{avg} (mm/min)	S.D	ε
1	0.005	1.2769	1.2206	1.1168	1.204767	0.066313	0.99876
2	0.01	1.0066	0.9941	0.9882	0.9963	0.007671	0.99573
3	0.015	0.6665	0.6658	0.6711	0.6678	0.002351	0.9936
4	0.02	0.3992	0.3944	0.4011	0.398233	0.002819	0.99146
5	0.025	0.1817	0.1814	0.1825	0.181867	0.000464	0.98933

Table 7.5: Hindered settling parameters for different weights of magnesium hydroxide suspended in 0.075% Poloxamer

Wt (gms)	Conc. (gm/mL)	Q_1 (mm/min)	Q_2 (mm/min)	Q_3 (mm/min)	Q_{avg} (mm/min)	S.D	ε
1	0.005	1.4714	1.422	1.3837	1.4257	0.035899	0.99876
2	0.01	1.0169	0.989	0.9913	0.999067	0.012645	0.99573
3	0.015	0.6728	0.6585	0.6619	0.6644	0.0061	0.9936
4	0.02	0.4981	0.4985	0.5113	0.502633	0.00613	0.99146
5	0.025	0.2433	0.2428	0.2424	0.242833	0.000368	0.98933

Hindered settling results indicate that as the concentration increased, the rate of fall (Q) decreased. This is due to greater hindrance of the particles as the concentration of the suspension increases. However, the rate of fall (Q) for each concentration increases with the increase in concentration of the polymer. This is due to the flocculation of the suspensions by the polymer, thereby increasing particle size and causing the particles to fall down rapidly.

7.1.3 Particle size determination using Steinour, Richardson & Zaki and Dollimore & McBride equations:

Particle size can be calculated using three different modifications of Stoke's law as described in Chapter-2. These equations provide a relationship between parameters such as settling rate and settling velocity. The particle size is then calculated from Stoke's law. The hindered settling parameters used for these plots are given in Tables 7.6 to 7.9

Steinour's equation:

$$\log \frac{Q}{\varepsilon^2} = A(\varepsilon) + \log V_s - A \qquad \text{Eq. 7.2}$$

A plot of log (Q/ε^2) vs ε gives a straight line with a slope of A and an intercept of (log V_s-A). The linear plots for this equation using four different media are given in Figures 7-5 to 7-8 and the parameters obtained from the plot are given in Table 7.10.

Richardson & Zaki equation:

$$\log Q = \log V_s + n \log \varepsilon \qquad \text{Eq. 7.3}$$

A plot of log Q vs log ε gives a straight line with a slope of n and an intercept of (log V_s). The linear plots for this equation using four different media are given in Figures 7-9 to 7-12 and the parameters obtained from the plot are given in Table 7.11.

Dollimore & McBride equation:

$$\log Q = \log V_s - b\rho_s(1-\varepsilon) \qquad \text{Eq. 7.4}$$

A plot of log Q vs (1-ε) gives a straight line with a slope of $-b\rho_s$ and an intercept of log V_s. The linear plots for this equation using four different media are given in Figures 7-13 to 7-16 and the parameters obtained from the plot are given in Table 7.12.

Particle size was then calculated using Stoke's law as described in Chapter -3.

$$r = \sqrt{\frac{9\eta V_s}{2g(\rho_s - \rho_l)}} \qquad \text{Eq. 7.5}$$

By substituting the values of settling velocity determined by the various equations with the density and viscosity from Section of Chapter-7 in the equations, the radii of the particles in different media are calculated and given in Table 7.13 to 7.16.

Table 7.6: The values for the hindered settling parameters for different weights of magnesium hydroxide suspended in water.

Wt(gms)	Q_{avg}(mm/min)	ε	logQ	log ε	log (Q/ε^2)	1-ε
1	1.1521	0.99786	0.06149	-0.00093	0.06335	0.00214
2	0.7037	0.99573	-0.15261	-0.00185	-0.14889	0.00427
3	0.4006	0.9936	-0.39729	-0.00278	-0.3917	0.0064
4	0.2037	0.99146	-0.69101	-0.00372	-0.6835	0.00854
5	0.1327	0.98933	-0.87702	-0.00465	-0.8677	0.01067

Table 7.7: The values for the hindered settling parameters for different weights of magnesium hydroxide suspended in 0.025% Poloxamer

Wt(gms)	Q_{avg}(mm/min)	ε	log Q	log ε	log (Q/ε^2)	1-ε
1	1.2586	0.99786	0.06149	-0.00093	0.1017	0.00214
2	0.985533	0.99573	-0.15261	-0.00185	0.0026	0.00427
3	0.660433	0.9936	-0.39729	-0.00278	-0.1746	0.0064
4	0.405333	0.99146	-0.69101	-0.00372	-0.3847	0.00854
5	0.198533	0.98933	-0.87702	-0.00465	-0.6928	0.01067

Table 7.8: The values for the hindered settling parameters for different weights of magnesium hydroxide suspended in 0.05% Poloxamer

Wt(gms)	Q_{avg}(mm/min)	ε	log Q	log ε	log (Q/ε^2)	1-ε
1	1.204767	0.99786	0.080903	-0.00093	0.08276	0.00214
2	0.9963	0.99573	-0.00161	-0.00185	0.002107	0.00427
3	0.6678	0.9936	-0.17535	-0.00278	-0.1698	0.0064
4	0.398233	0.99146	-0.39986	-0.00372	-0.3924	0.00854
5	0.181867	0.98933	-0.74025	-0.00465	-0.7309	0.01067

Table 7.9: The values for the hindered settling parameters for different weights of magnesium hydroxide suspended in 0.075% Poloxamer

Wt(gms)	Q_{avg} (mm/min)	ε	log Q	log ε	log (Q/ε^2)	1-ε
1	1.4257	0.99786	0.154028	-0.00093	0.1559	0.00214
2	0.999067	0.99573	-0.00041	0.002107	-0.0003	0.00427
3	0.6644	0.9936	-0.17757	-0.1698	-0.172	0.0064
4	0.502633	0.99146	-0.29875	-0.3924	-0.2913	0.00854
5	0.242833	0.98933	-0.61469	-0.7309	-0.6054	0.01067

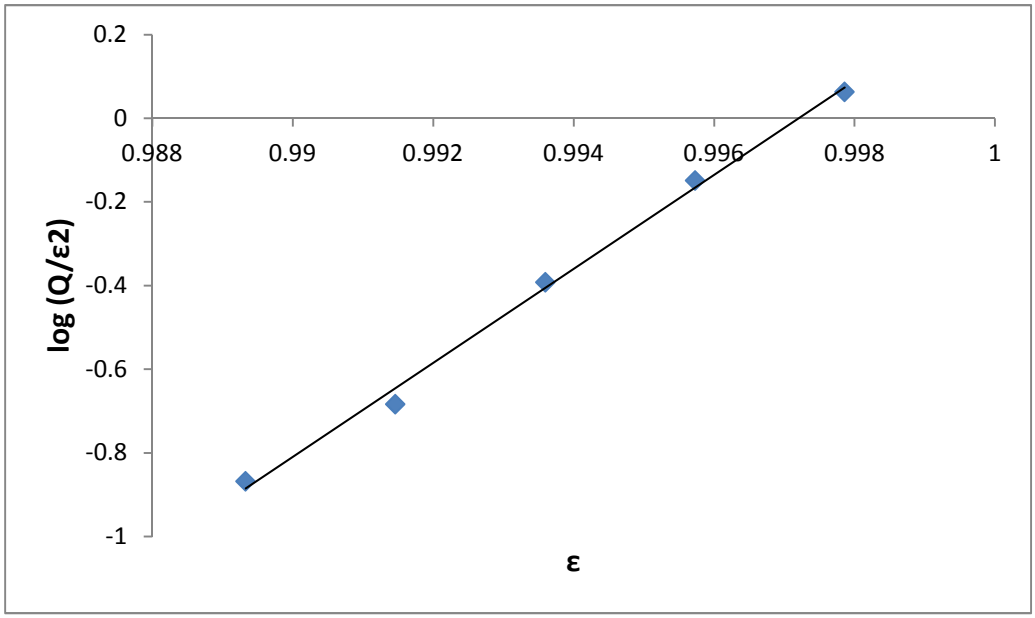

Figure 7-5: The linear plot of the Steinour's equation for different weights of magnesium hydroxide in water where slope=112.37; intercept =-112.05 and R^2=0.996

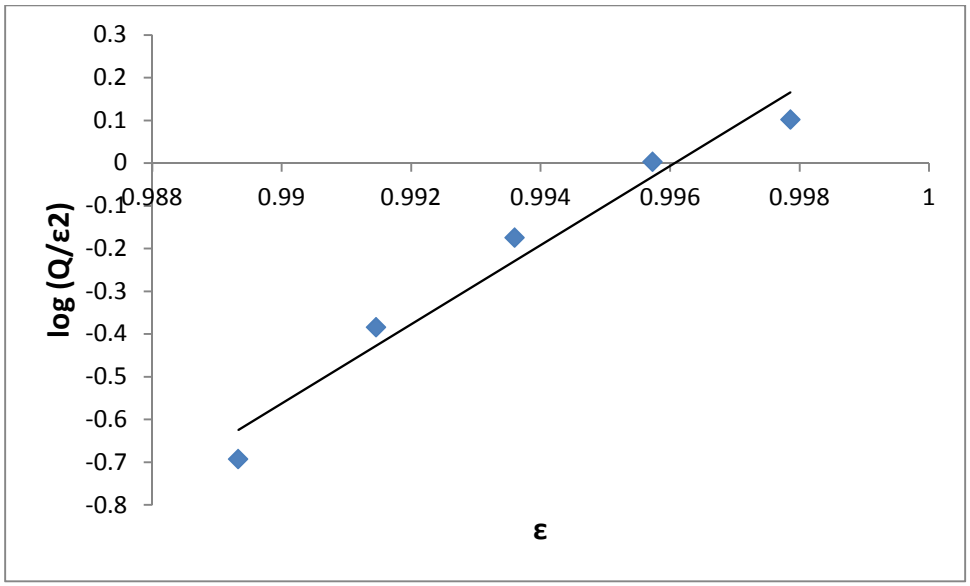

Figure 7-6: The linear plot of the Steinour's equation for different weights of magnesium hydroxide in 0.025% Poloxamer where slope=92.659; intercept=-92.295 and R^2=0.9638

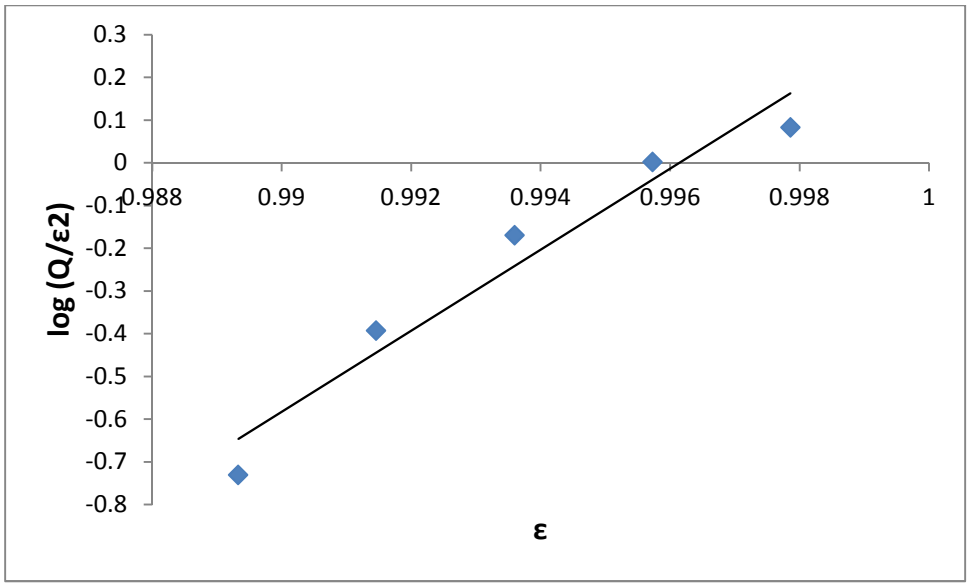

Figure 7-7: The linear plot of the Steinour's equation for different weights of magnesium hydroxide suspended in 0.05% Poloxamer where slope=94.795; intercept= -94.43 and R^2=0.9466

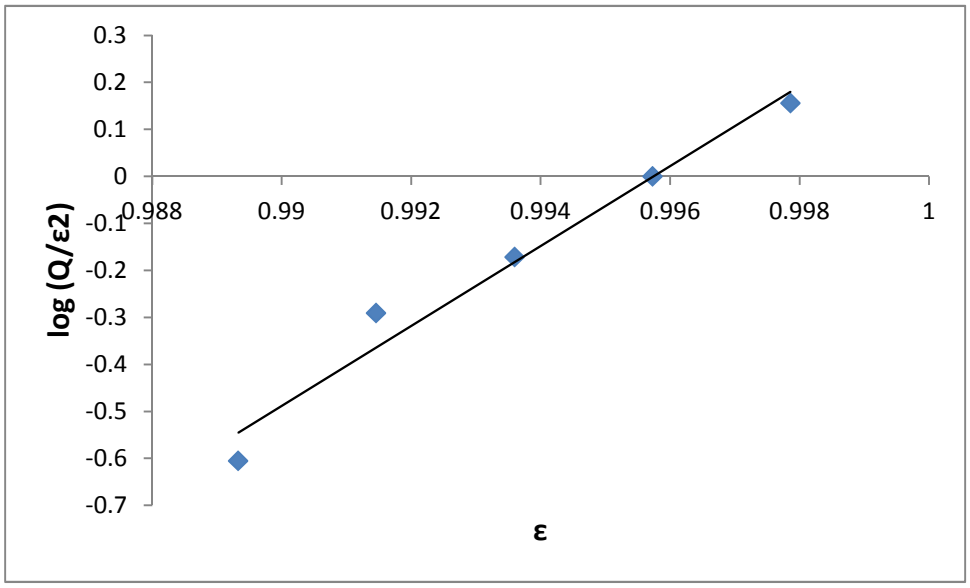

Figure 7-8: The linear plot of the Steinour's equation for different weights of magnesium hydroxide suspended in 0.075% Poloxamer where slope=85.023; intercept= -84.661 and R^2=0.9716

Table 7.10: The values for hindered settling parameters obtained by Steinour's equation for magnesium hydroxide suspended in different media

Medium	A	log V_s	V_s (mm/min)
Water	112.37	0.32	2.08929
0.025% Poloxamer	92.59	0.364	2.31206
0.05% Poloxamer	94.795	0.365	2.31740
0.075% Poloxamer	85.023	0.362	2.30144

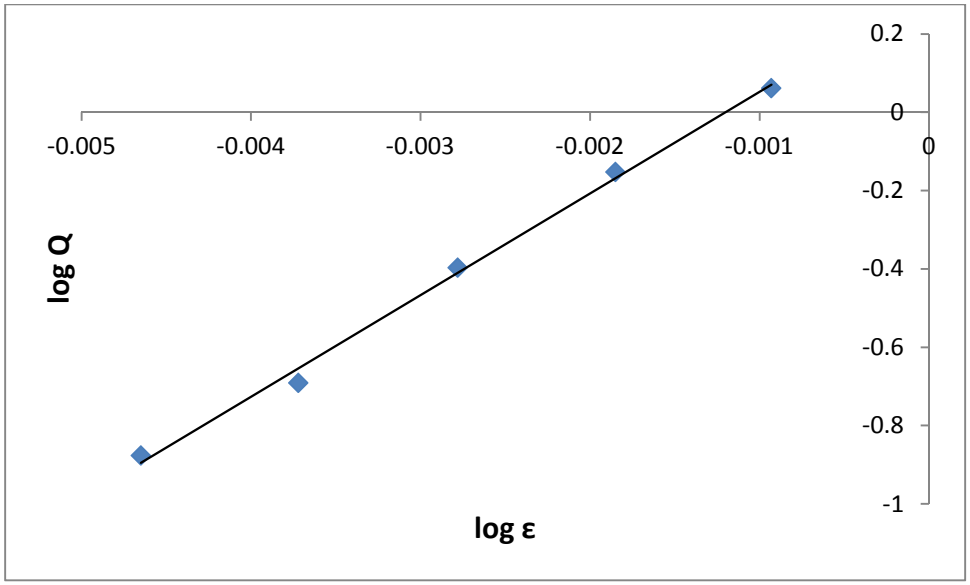

Figure 7-9: The linear plot of the Richardson & Zaki equation for different weights of magnesium hydroxide in water where slope=259.48; intercept=0.3116 and R^2=0.9962

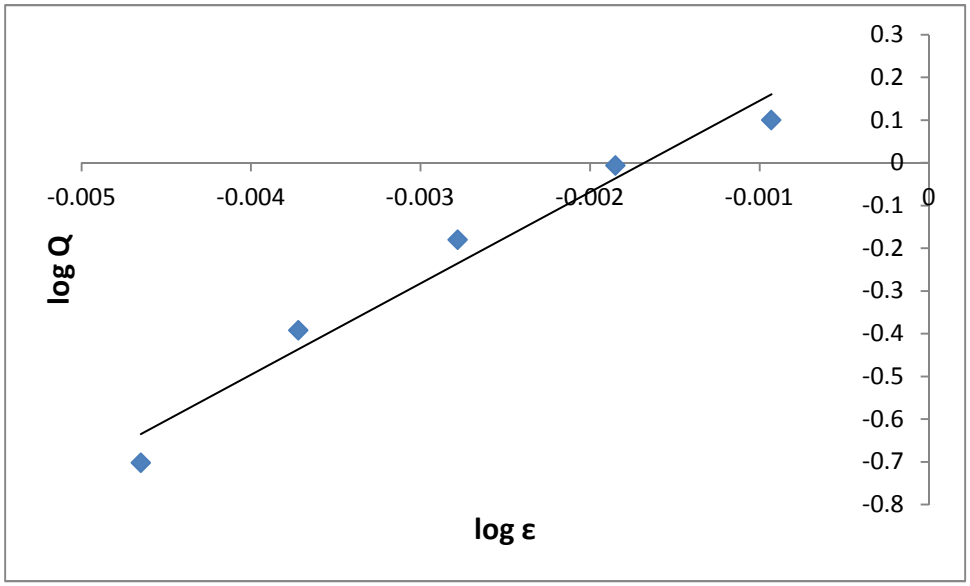

Figure 7-10: The linear plot of the Richardson & Zaki equation for different weights of magnesium hydroxide in 0.025% Poloxamer where slope=213.84; intercept=0.3596 and R^2=0.9658

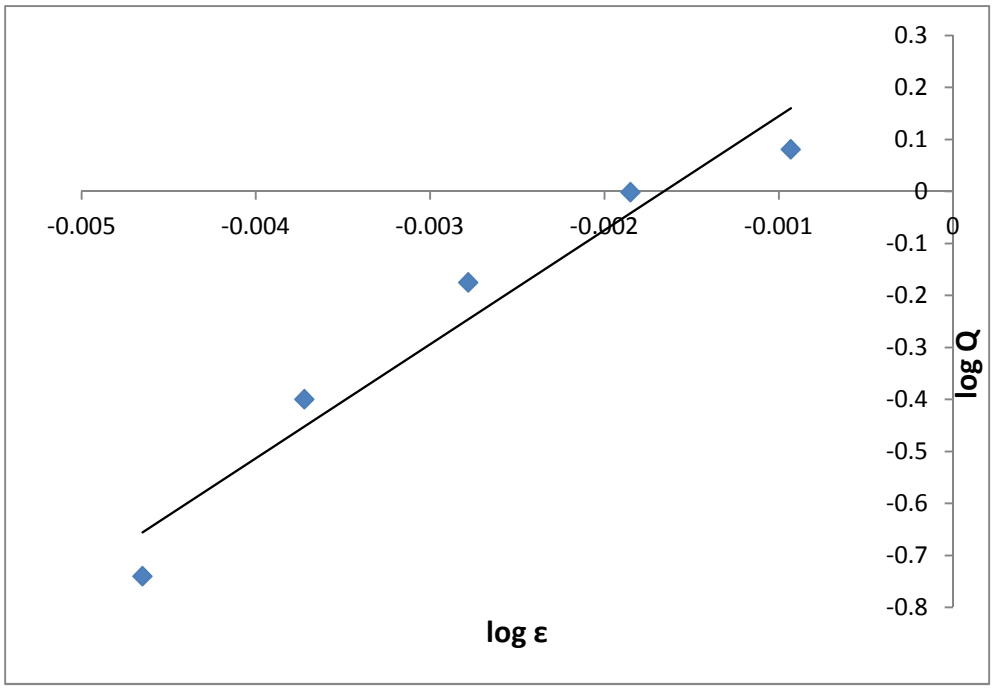

Figure 7-11: The linear plot of the Richardson & Zaki equation for different weights of magnesium hydroxide in 0.05% Poloxamer where slope=219.31; intercept=0.3638 and R^2=0.9485

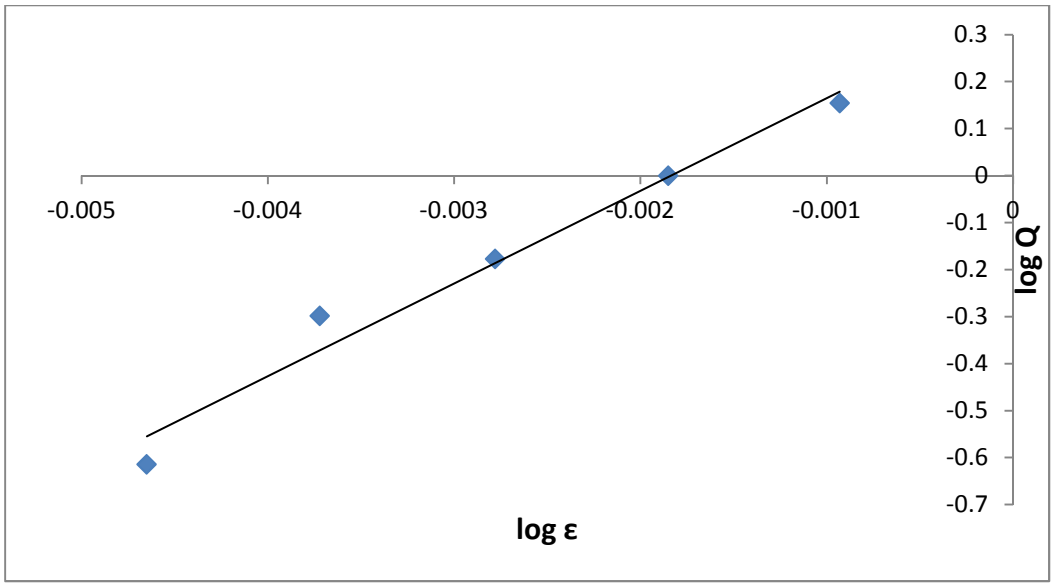

Figure 7-12: The linear plot of the Richardson & Zaki equation for different weights of magnesium hydroxide in 0.075% Poloxamer where slope=197.2; intercept=0.3619 and R^2=0.9724

Table 7.11: The values for the hindered settling parameters obtained by Richardson & Zaki equation for magnesium hydroxide suspended in different media

Medium	n	log V_s	V_s (mm/min)
Water	259.48	0.3116	2.04927
0.025% Poloxamer	213.84	0.3596	2.28870
0.05% Poloxamer	219.31	0.3638	2.31100
0.075% Poloxamer	197.20	0.3619	2.30090

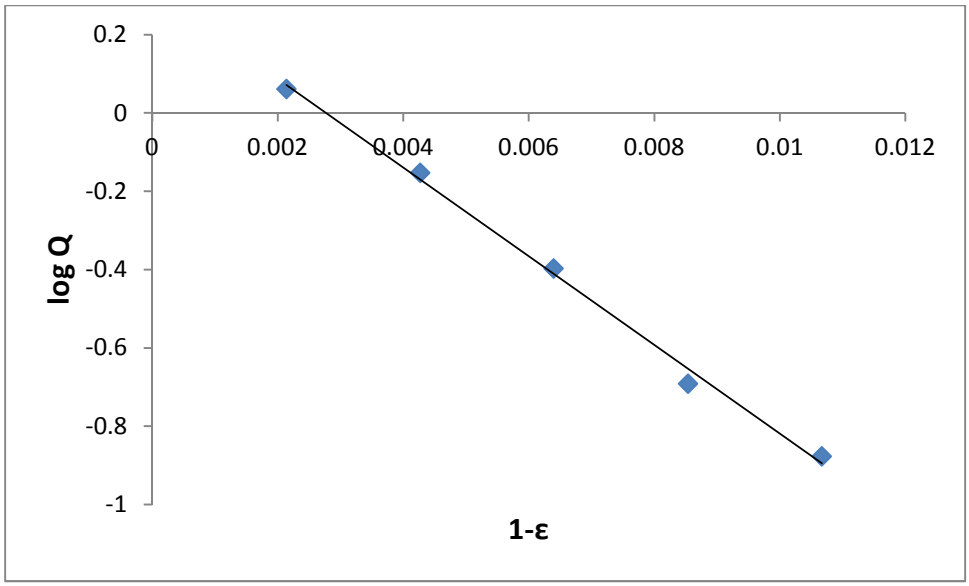

Figure 7-13: The linear plot of the Dollimore &McBride equation for different weights of magnesium hydroxide in water where slope=-113.24; intercept=0.3139 and R^2=0.9961

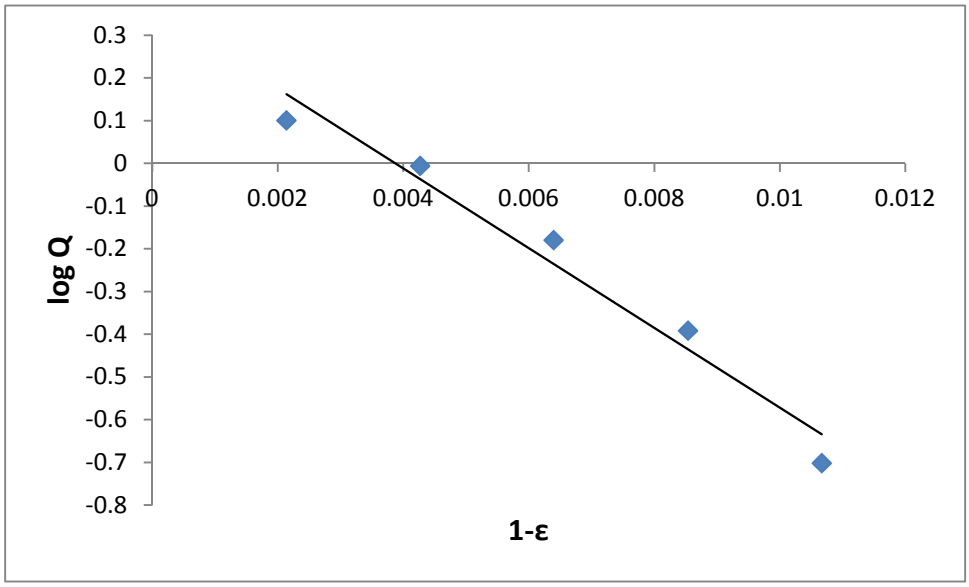

Figure 7-14: The linear plot of the Dollimore &McBride equation for different weights of magnesium hydroxide in 0.025% Poloxamer where slope=-93.3; intercept=0.3613 and R^2=0.965

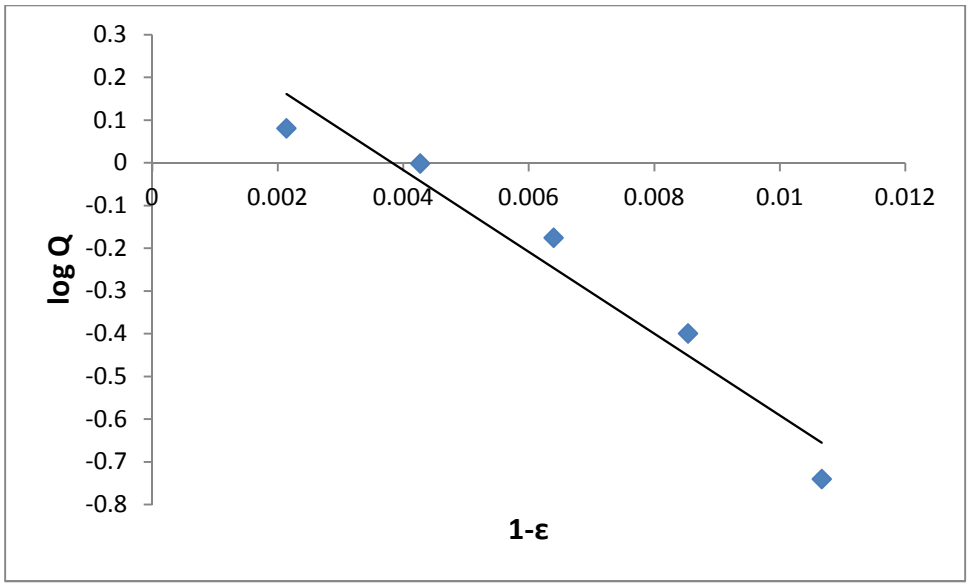

Figure 7-15: The linear plot of the Dollimore &McBride equation for different weights of magnesium hydroxide in 0.05% Poloxamer where slope=-95.673; intercept=0.3655 and R^2=0.9475

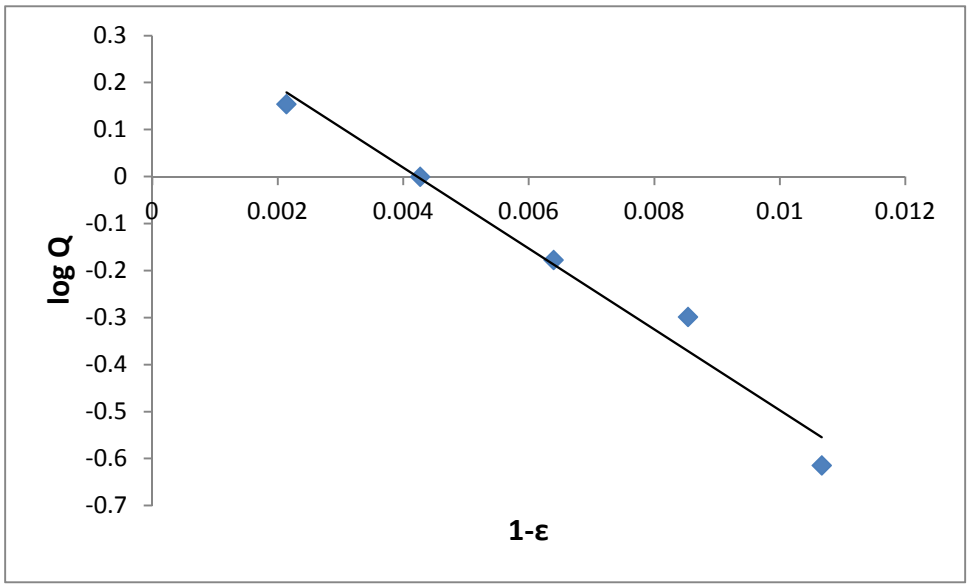

Figure 7-16: The linear plot of the Dollimore &McBride equation for different weights of magnesium hydroxide in 0.075% Poloxamer where slope=-86.063; intercept=0.3637 and R^2=0.3637

Table 7.12: The values for the hindered settling parameters obtained for the Dollimore & McBride equation for magnesium hydroxide suspended in different media

Medium	b	log V_s	V_s(mm/min)
Water	48.2982	0.3139	2.0602
0.025% Poloxamer	39.7935	0.3613	2.2977
0.05% Poloxamer	40.8057	0.3655	2.3201
0.075% Poloxamer	36.7069	0.3637	2.3105

Table 7.13: Particle size calculated using the three different equations for magnesium hydroxide suspended in water

Equation	V_s (cm/sec)	r (µm)
Steinour	0.003482	3.2724
Richardson & Zaki	0.003415	3.2407
Dollimore McBride	0.003433	3.2507
Average	0.003443	3.2538

Table 7.14: Particle size calculated using the three different equations for magnesium hydroxide suspended in 0.025% Poloxamer

Equation	V_s(cm/sec)	r (µm)
Steinour	0.003853	6.2938
Richardson & Zaki	0.003814	6.2615
Dollimore McBride	0.003829	6.2738
Average	0.003832	6.2763

Table 7.15: Particle size calculated using the three different equations for magnesium hydroxide suspended in 0.05% Poloxamer

Equation	V_s(cm/sec)	r (µm)
Steinour	0.003860	6.3782
Richardson & Zaki	0.003852	6.3716
Dollimore McBride	0.003867	6.3840
Average	0.003860	6.3782

Table 7.16: Particle size calculated using the three different equations for magnesium hydroxide suspended in 0.075% Poloxamer

Equation	V_s (cm/sec)	r (µm)
Steinour	0.003836	6.5461
Richardson & Zaki	0.003835	6.5453
Dollimore McBride	0.003850	6.5580
Average	0.003840	6.5495

It was observed from the particle size results that the average particle size of magnesium hydroxide increased with an increase in the concentration of the polymer. This is due to the flocculation of suspension by the bridging action of the polymer. Particles get adsorbed onto active sites present on the polymer thereby causing the formation of floccules.

The regression coefficients for all the linear plots were very good indicating the linearity of the plots. There was good correlation between all of the three equations for each of the suspending media.

7.1.4 Permeability Calculations

The hindered settling plug can be considered to be stationary with the fluid moving upwards through the pores in the bed of granular solids. This phenomenon is called permeability (K).

The K- value can be calculated by using the rate of fall (Q) and settling velocity (V_s) or by using (n) obtained from the Richardson Zaki method as shown in the equations below

where:

$$K = \left(\frac{1}{2Q}\right)\left(\frac{\varepsilon^3}{1-\varepsilon}\right)V_s \quad \text{Eq. 7.6}$$

$$K = \frac{1}{2\varepsilon^{n-3}(1-\varepsilon)} \quad \text{Eq. 7.7}$$

$$\varepsilon_K = \frac{n-3}{n-2} \quad \text{Eq. 7.8}$$

$$K_{min} = \frac{1}{2\varepsilon_k^{n-3}(1-\varepsilon_K)} \quad \text{Eq. 7.9}$$

In this study, the values for the Kozeny Carman constant (K) were calculated using Equation 7-7.The K-values for each suspension are plotted against ε as seen in the Figure 7-17. If K- values are plotted against ε, the curve should pass through a minimum K_{min} at a value of $\varepsilon = \varepsilon_K$.

ε_K and K_{min} are calculated from Equations 7-8 and 7-9, respectively. The K- value is inversely proportional at values of ε above ε_K and it is directly proportional to ε when ε is below ε_K.

ε_1 is the initial volume fraction of the suspension at which hindered settling commences. $\varepsilon_1$is calculated using the equation

$$\varepsilon = \frac{n}{n+1} \quad \text{Eq. 7.10}$$

The higher the value of ε_1, the more the system tends to be hindered. ε_K is always less than ε_1 and a plot of ε_K and ε_1 gives a straight line as shown in Figure 7-18.

From Figure 7-17, it can be seen that the Kozeny Carman constant for permeability (K) increases when (ε) is greater than (ε_K) and (K) increases when (ε) is less than (ε_K). This

pattern is observed for all the suspensions.

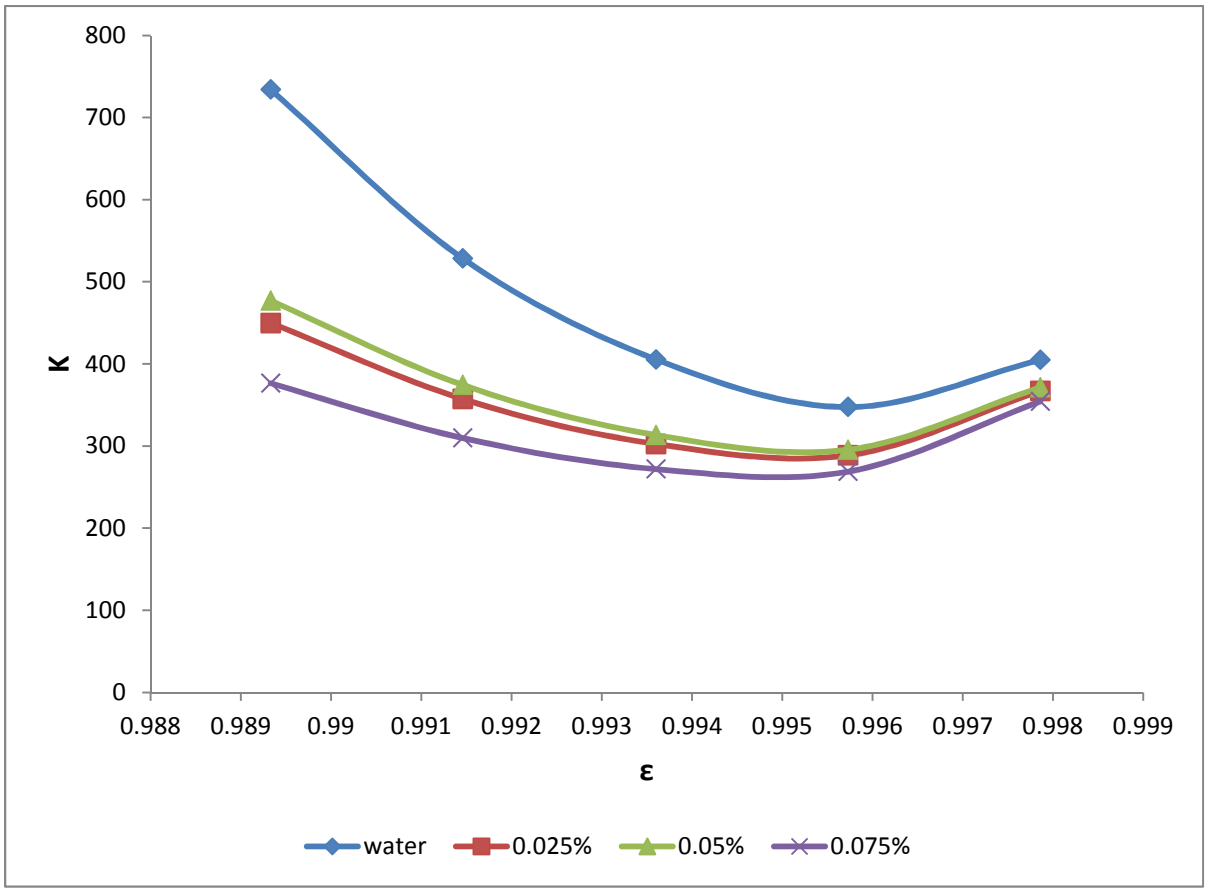

Figure 7-17: A plot of the Kozeny Carman constant for permeability (K) and porosity for magnesium hydroxide suspended in different media

From the Table 7.17, it was observed that permeability decreased when Poloxamer was added to the suspension. This could be due to the flocculation of suspensions resulting in fewer pores through which the fluid could move. However, the K value slightly increased at 0.05 %(w/v) concentration of Poloxamer but this increase was significantly less when compared to K value of water.

Table 7.17: The values for permeability parameters of magnesium hydroxide suspended in different media

Medium	Weight (gms)	K	ε_K	K_{min}
Water	1	404.745	0.996116	349.272
	2	347.476		
	3	405.465		
	4	528.269		
	5	734.028		
0.025%	1	367.045	0.995279	287.244
	2	288.648		
	3	302.482		
	4	357.150		
	5	449.858		
0.05%	1	371.371	0.9954	294.675
	2	295.484		
	3	313.294		
	4	374.305		
	5	477.042		
0.075%	1	354.191	0.994877	264.624
	2	268.810		
	3	271.833		
	4	309.648		
	5	376.313		

Table 7.18: The values of initial porosity and minimum porosity for magnesium hydroxide suspended in different media

Medium	ε_1	ε_K
Water	0.99616	0.996116
0.025%	0.995345	0.995279
0.05%	0.99546	0.9954
0.075%	0.994954	0.994877

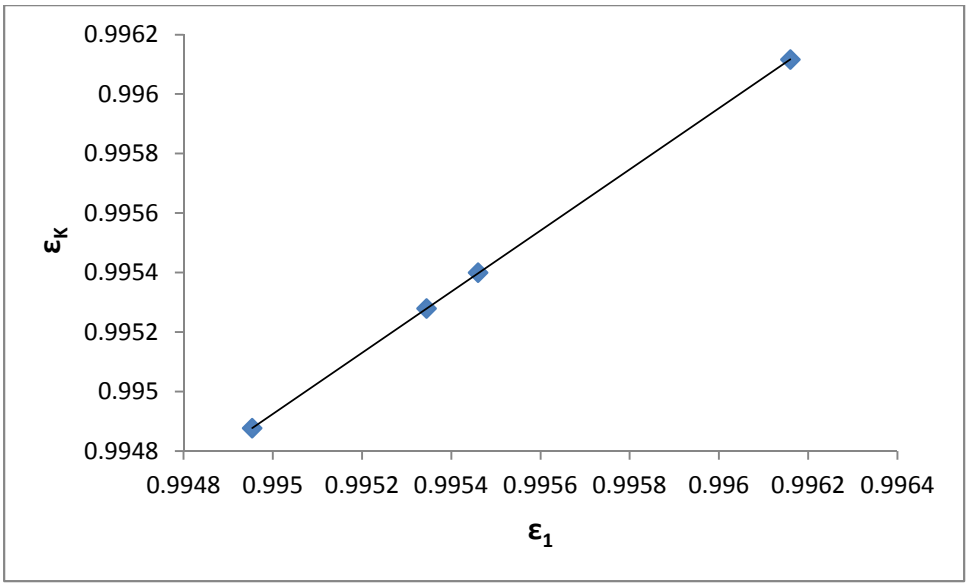

Figure 7-18: A plot of initial porosity and minimum porosity for magnesium hydroxide suspended in different media where slope=1.0272; intercept=-0.0272 and R^2=1

7.1.5 Hindered settling results obtained by varying the rate of addition of the reactants:

Five different suspensions using 1gm magnesium hydroxide were prepared by various rates of addition of sodium hydroxide as described in Chapter-6 section 6.3.6. The average rate of fall (Q) for the various rates is given in Table 7.19.

Table 7.19: The values of rate of fall at different rates of addition of sodium hydroxide for 1gm magnesium hydroxide

Rate of addition (mL/sec)	Q_{avg} (mm/min)
0.01	2.5617
0.03	1.7304
0.05	1.7052
0.07	1.2073
0.09	1.0284

From this table it was observed that as the rate of addition of sodium hydroxide increases, the rate of fall decreases. The slower the rate of addition, the larger the particle size. This

may be due to the fact that as the reagent is slowly added, larger particles are formed because there is enough time for nucleation.

7.2 Calculation of percentage yield:

The calculation for the percentage yield is done based on the method described in chapter-6, section 6.3.7. The theoretical weight along with the actual weight obtained after drying magnesium hydroxide and percentage yield calculated in given in Table 7.20. For convenience theoretical weights have been used in all the calculations for hindered settling experiments.

Table 7.20: Percentage yield calculated from actual weight and theoretical weight

Theoretical weight (gms)	Actual weight (gms)	%Yield
1	0.989±0.006	98.9
2	1.990±0.005	99.5
3	2.982±0.002	99.4
4	3.913±0.042	97.8
5	4.957±0.026	99.1

7.2 Scanning Electron Microscopy (SEM) results:

SEM was performed based on the method described in chapter-6, section 6.3.8. Figures 7-19 and 7-20 show the dried sediments of magnesium hydroxide dispersed in water and Poloxamer, respectively. It was observed from Figure 7-19 that magnesium hydroxide dispersed in water appeared as rod shaped crystals in clusters.

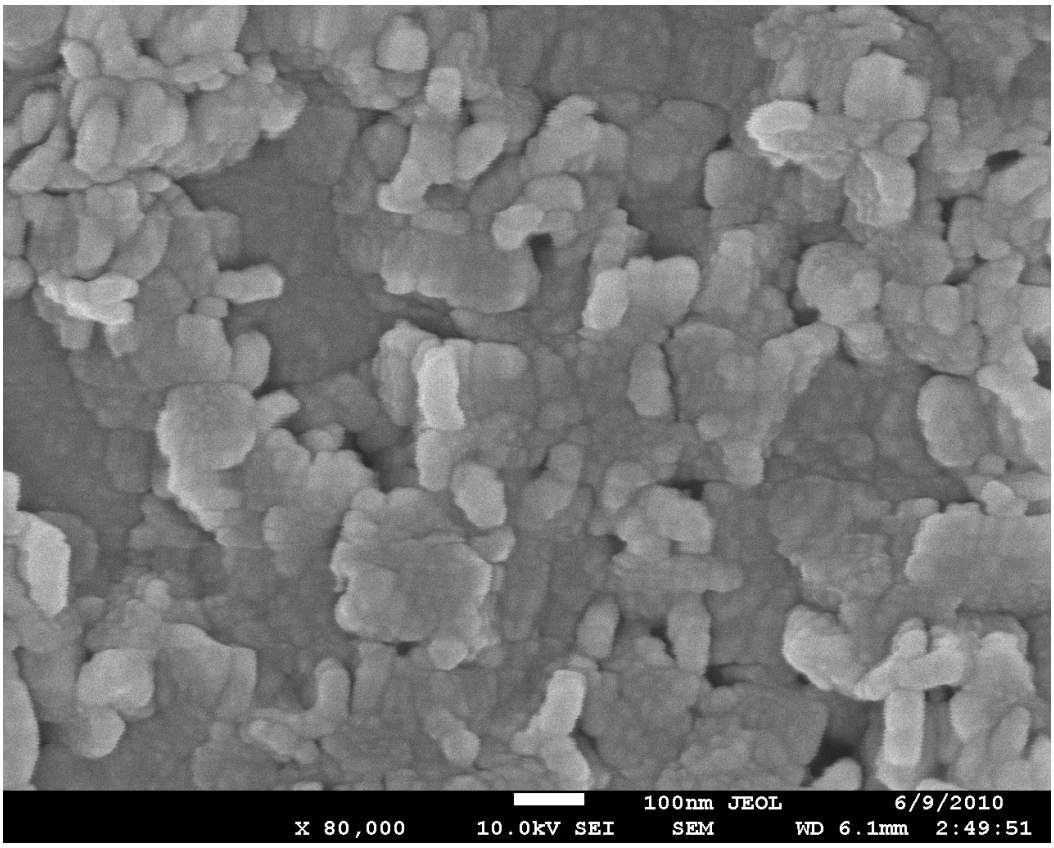

Figure 7-19: SEM image for dry magnesium hydroxide suspended in water

Magnesium hydroxide dispersed in Poloxamer appeared as clusters of magnesium hydroxide crystals indicating the floccules in the suspension as seen in Figure 7-20.

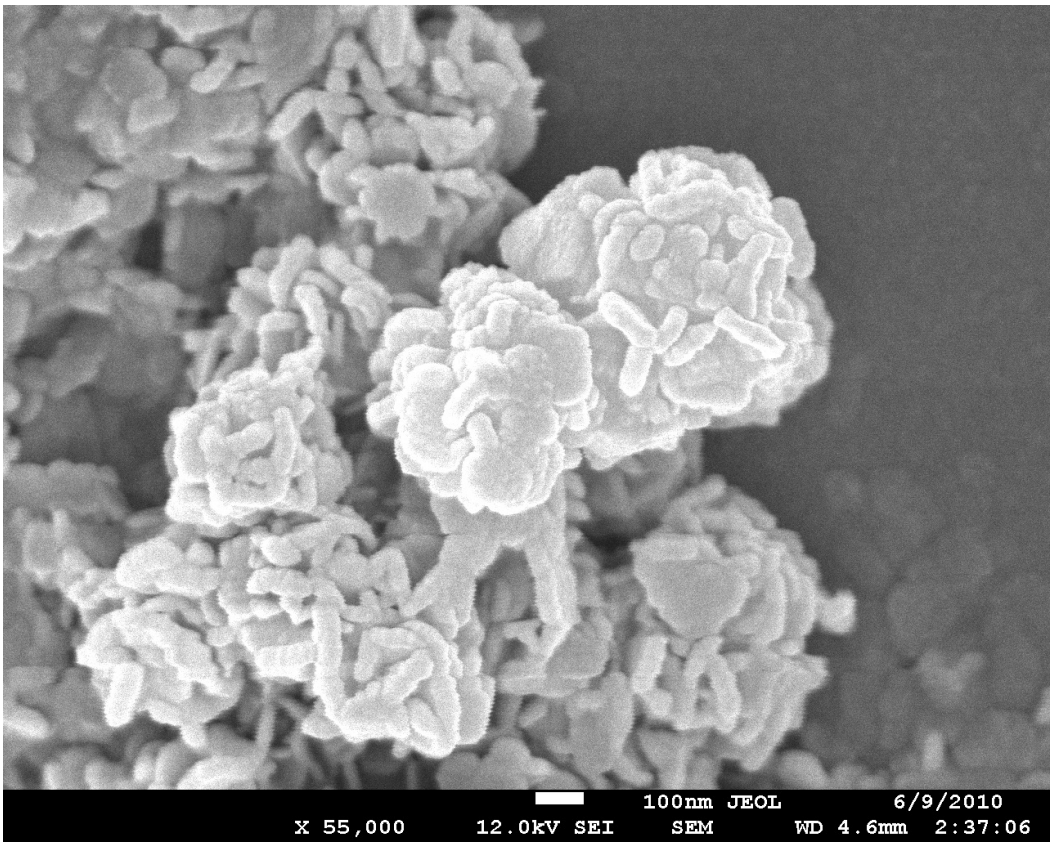

Figure 7-20: SEM image for dry magnesium hydroxide suspended in 0.025% Poloxamer solution.

7.3 Laser Diffraction (LD) results:

Laser diffraction was performed on 1gm magnesium hydroxide suspensions in different media as described in Chapter -6, Section 6.3.9. Particle size distributions for the various suspensions are given in Figures 7-21 through 7-24. The mean particle size for suspensions is given in the Table 7.21.

Concentration:	Span :	Uniformity:	Result units:
0.0031 %Vol	1.956	0.805	Volume

Specific Surface Area:	Surface Weighted Mean D[3,2]:	Vol. Weighted Mean D[4,3]:
1.8 m²/g	3.327 um	5.909 um

d(0.1):	1.832 um	d(0.5):	4.082 um	d(0.9):	9.814 um

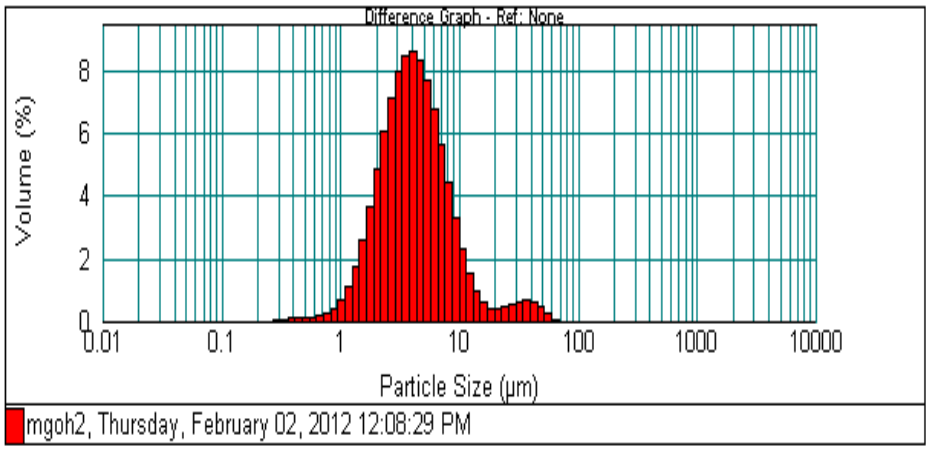

Figure 7-21: Laser diffraction results for 1gm of magnesium hydroxide suspended in water

Concentration:	Span :	Uniformity:	Result units:
0.0030 %Vol	2.270	1.06	Volume

Specific Surface Area:	Surface Weighted Mean D[3,2]:	Vol. Weighted Mean D[4,3]:
1.75 m²/g	3.438 um	7.597 um

d(0.1):	1.861 um	d(0.5):	4.539 um	d(0.9):	12.165 um

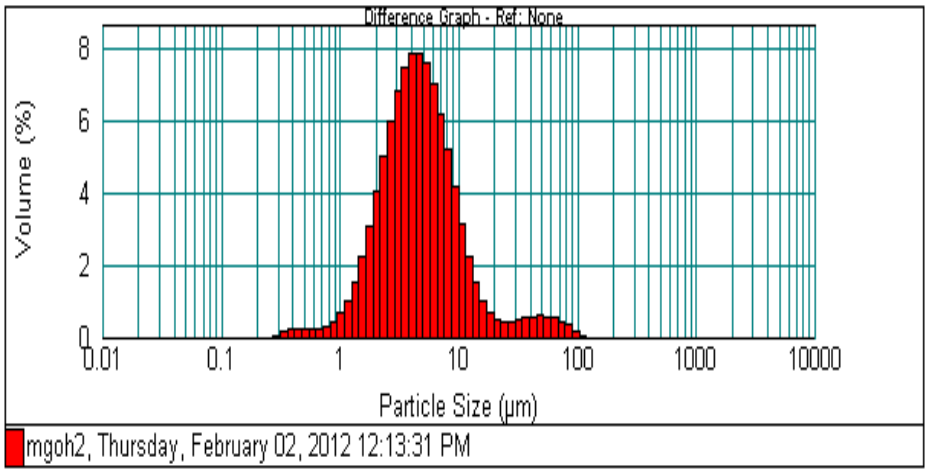

Figure 7-22: Laser diffraction results for 1gm of magnesium hydroxide suspended in 0.025% Poloxamer

Concentration:	Span :	Uniformity:	Result units:
0.0043 %Vol	1.809	0.644	Volume

Specific Surface Area:	Surface Weighted Mean D[3,2]:	Vol. Weighted Mean D[4,3]:
1.66 m²/g	3.604 um	5.813 um

d(0.1): 1.995 um d(0.5): 4.533 um d(0.9): 10.195 um

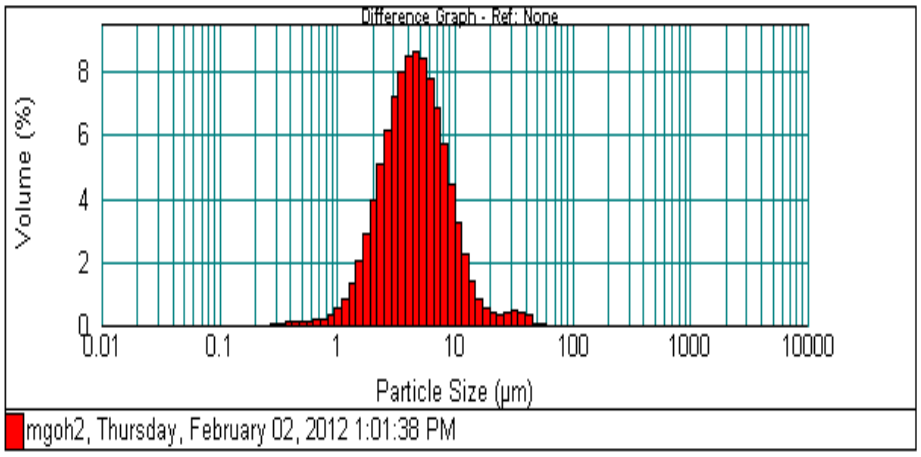

Figure 7-23: Laser diffraction results for 1gm of magnesium hydroxide suspended in 0.05% Poloxamer

Concentration:	Span :	Uniformity:	Result units:
0.0053 %Vol	4.749	3.29	Volume

Specific Surface Area:	Surface Weighted Mean D[3,2]:	Vol. Weighted Mean D[4,3]:
1.53 m²/g	3.910 um	20.498 um

d(0.1): 1.990 um d(0.5): 5.282 um d(0.9): 27.076 um

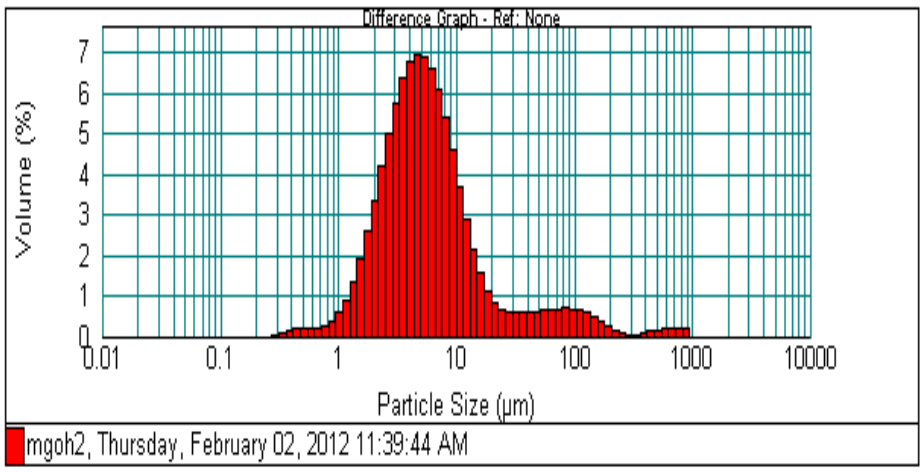

Figure 7-24: Laser diffraction results for 1gm of magnesium hydroxide suspended in 0.075% Poloxamer

Table 7.21: Mean particle size of magnesium hydroxide suspended in different media

Medium	Surface weighted mean(µm)	Volume weighted mean(µm)	d(0.1) (µm)	d(0.5) (µm)	d(0.9) (µm)
Water	3.327	5.909	1.832	4.082	9.814
0.025% Poloxamer	3.438	7.597	1.861	4.539	12.165
0.05% Poloxamer	3.604	5.813	1.995	4.533	10.195
0.075% Poloxamer	3.910	20.498	1.990	5.282	27.076

As observed from the laser diffraction results, surface weighted mean increases as Poloxamer concentration increases. There is also an increase in particle size with an increase in the concentration of Poloxamer. The mean particle size of magnesium hydroxide suspended in water is consistent with the hindered settling results. However, the results for magnesium hydroxide suspended in Poloxamer are not consistent with the hindered settling results. This may be due to the homogenizer used in the laser diffraction instrument which breaks the floccules resulting in smaller particles.

7.3 Zeta potential measurements:

Zeta potential measurements have been done on 1gm of magnesium hydroxide suspended in water and various concentrations of Poloxamer. It was performed based on the method described in chapter-6, section 6.3.10. The zeta potential values for magnesium hydroxide dispersed in different media in given in the Table 7.22.

Table 7.22: Zeta potential values for 1gm magnesium hydroxide suspended in different media

Medium	Zeta Potential (mV)
Water	23.91±0.84
0.025% Poloxamer	23.33±0.41
0.05% Poloxamer	23.27±1.03
0.075% Poloxamer	23.84±0.45

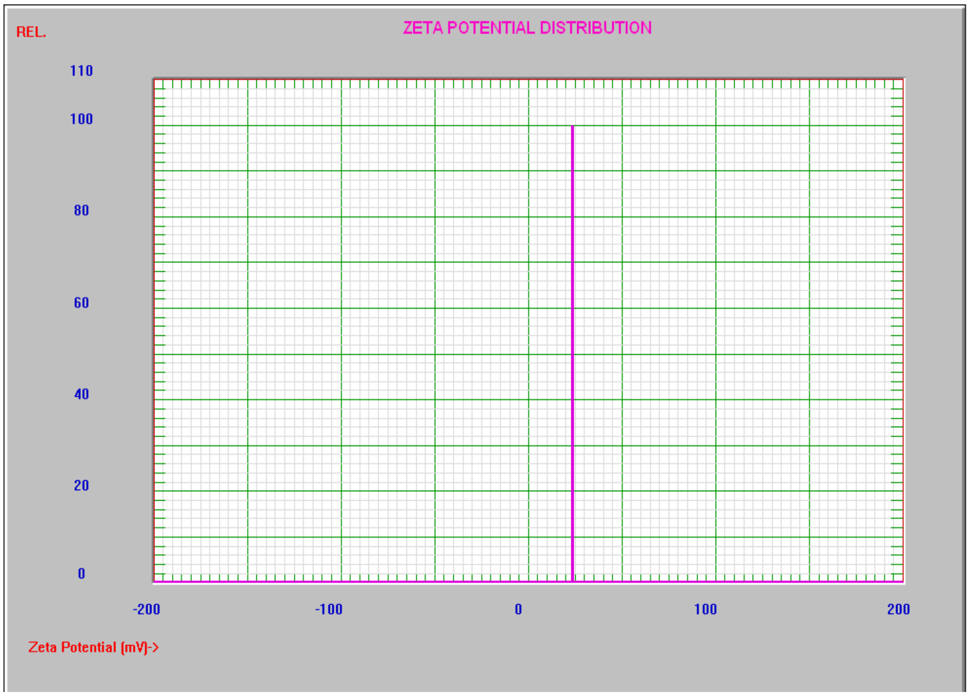

Figure7-25: Zeta potential distribution of 1gm of magnesium hydroxide suspended in water.

It was observed that the value of zeta potential remained constant when magnesium hydroxide was suspended in Poloxamer. There was no significant change in zeta potential even with an increase in concentration of Poloxamer. Since Poloxamer is a non ionic polymer, it causes flocculation of the suspension by bridging between the particles and does not interact electrostatically with the suspended particles and hence there is no change in the zeta potential.

7.4 Differential Scanning Calorimetry (DSC) results:

DSC was performed on 1gm magnesium hydroxide suspended in various media as described in Chapter-6, section 6.3.11. The DSC for the filtered sediments in the various media are given in Figures 7.26, 7.28, 7.30 and 7.32 and DSC of reference media and

dried sediments are given in Figures 7.27, 7.29, 7.31 and 7.33. As seen in the DSC of the filtered sediments there are three endothermic and an exothermic peak. The exothermic peak is due to the crystallization of water and the other endothermic peaks are due to melting and vaporization of water. The endothermic peak at higher temperature, around 420^0C might be due to the degradation of magnesium hydroxide.

The heats of crystallization (ΔH_c), fusion (ΔH_m), vaporization (ΔH_v) and degradation (ΔH_d) along with the temperatures for both filtered sediment and reference media are given in Tables 7.23 and 7.24.

Table 7.23: Summarized data for thermograms of filtered sediment in different media

Medium	ΔH_c	T_c	ΔH_f	T_m	ΔH_v	T_v	ΔH_d	T_d
Water	51.81	-20.15	-40.45	3.55	-852.56	109.19	-409.37	410.43
0.025% Poloxamer	169.76	-10.95	-160.45	1.38	-1275.83	105.47	-76.26	418.63
0.05% Poloxamer	169.56	-9.55	-210.84	1.81	-1368.90	105.36	-139.14	419.64
0.075% Poloxamer	202.97	-8.93	-243.74	1.89	-1623.58	104.75	-141.81	412.97

Table 7.24: Summarized data for thermograms of reference media and dried sediments in different media

Medium	ΔH_c	T_c	ΔH_f	T_m	ΔHv	T_v	ΔH_d	T_d
Water	328.15	-9.80	366.50	4.03	-2006.48	100.35	-1355.53	423.96
0.025% Poloxamer	325.67	-9.92	365.95	5.06	-2170.15	103.02	-1363.42	421.68
0.05% Poloxamer	339.06	-7.75	377.18	5.21	-2332.95	122.35	-1351.28	422.27
0.075% Poloxamer	321.51	-10.92	374.02	5.61	-2176.55	104.35	-1262.23	420.75

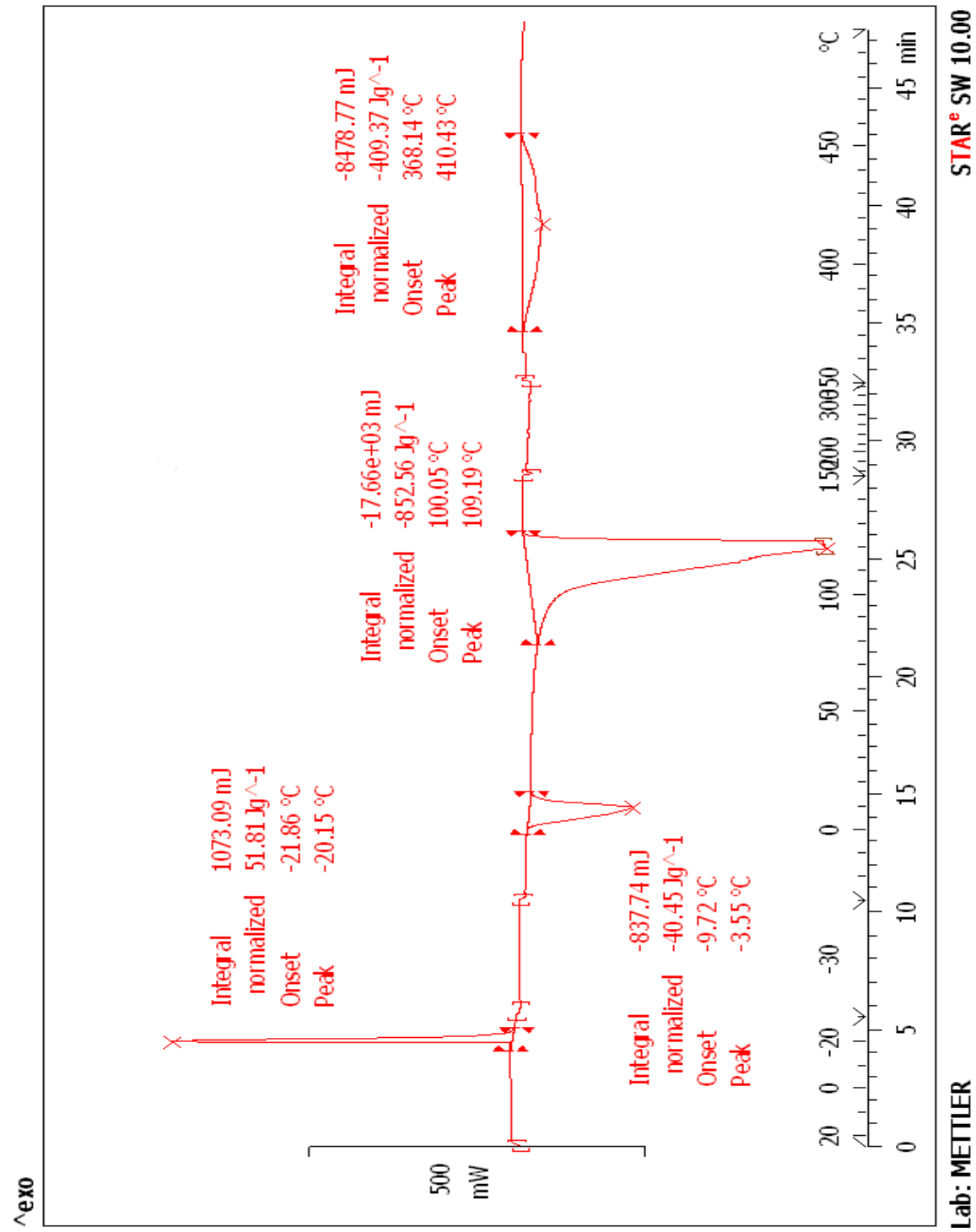

Figure 7-26: DSC thermogram of 1gm of magnesium hydroxide suspended in water

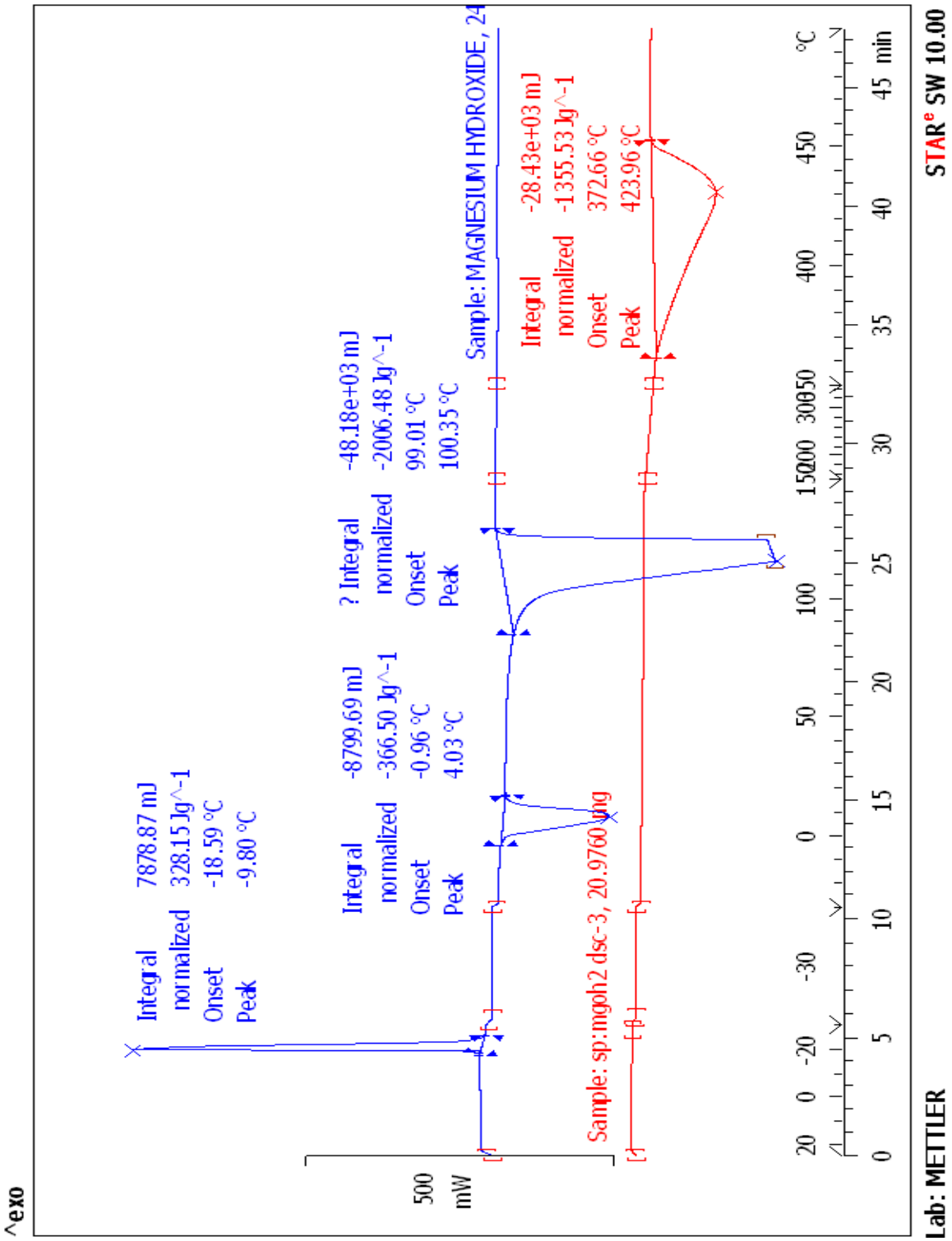

Figure 7-27: DSC thermogram of reference media and dried sediment of 1gm of magnesium hydroxide in water

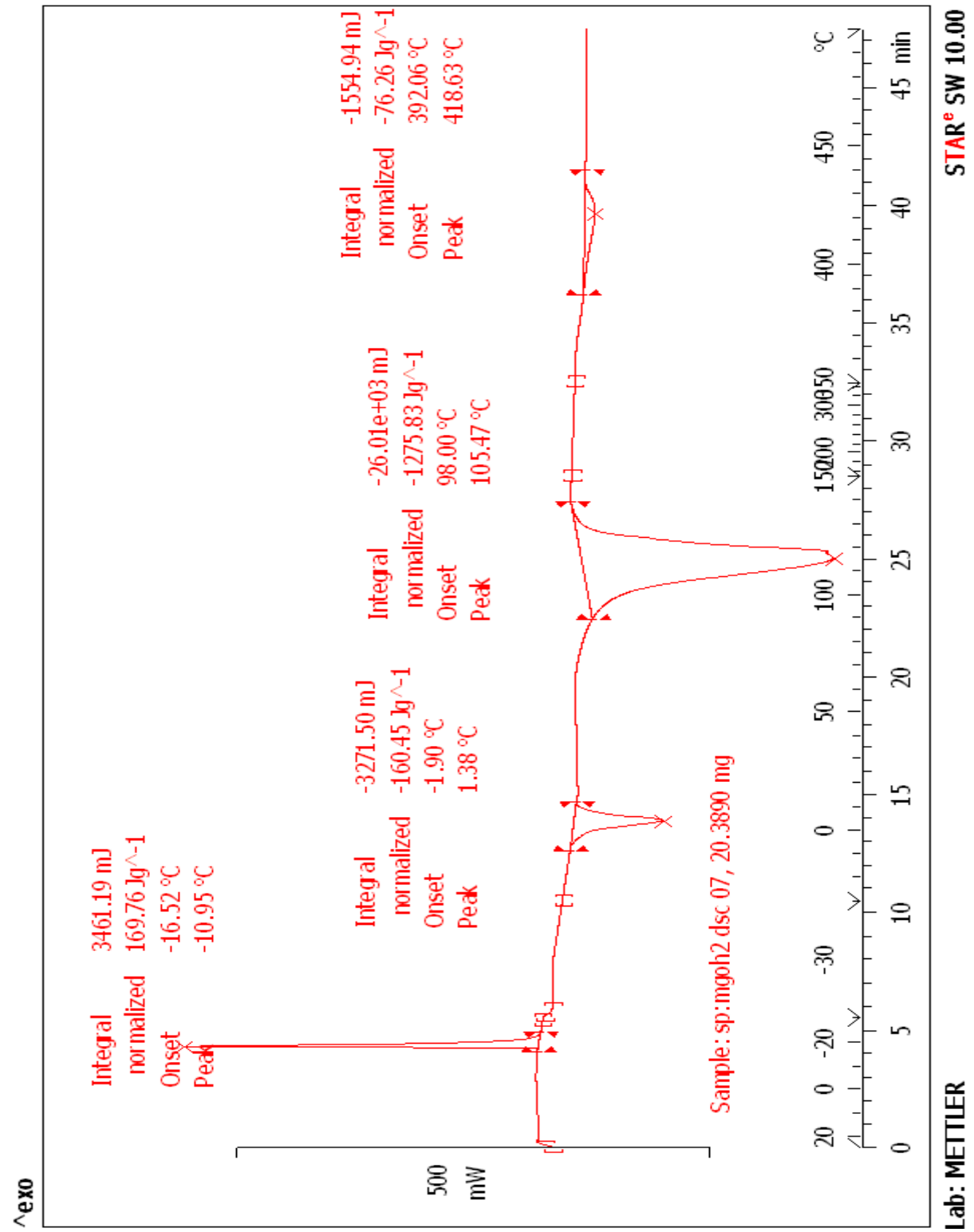

Figure 7-28: DSC thermogram of 1gm of magnesium hydroxide suspended in 0.025% Poloxamer

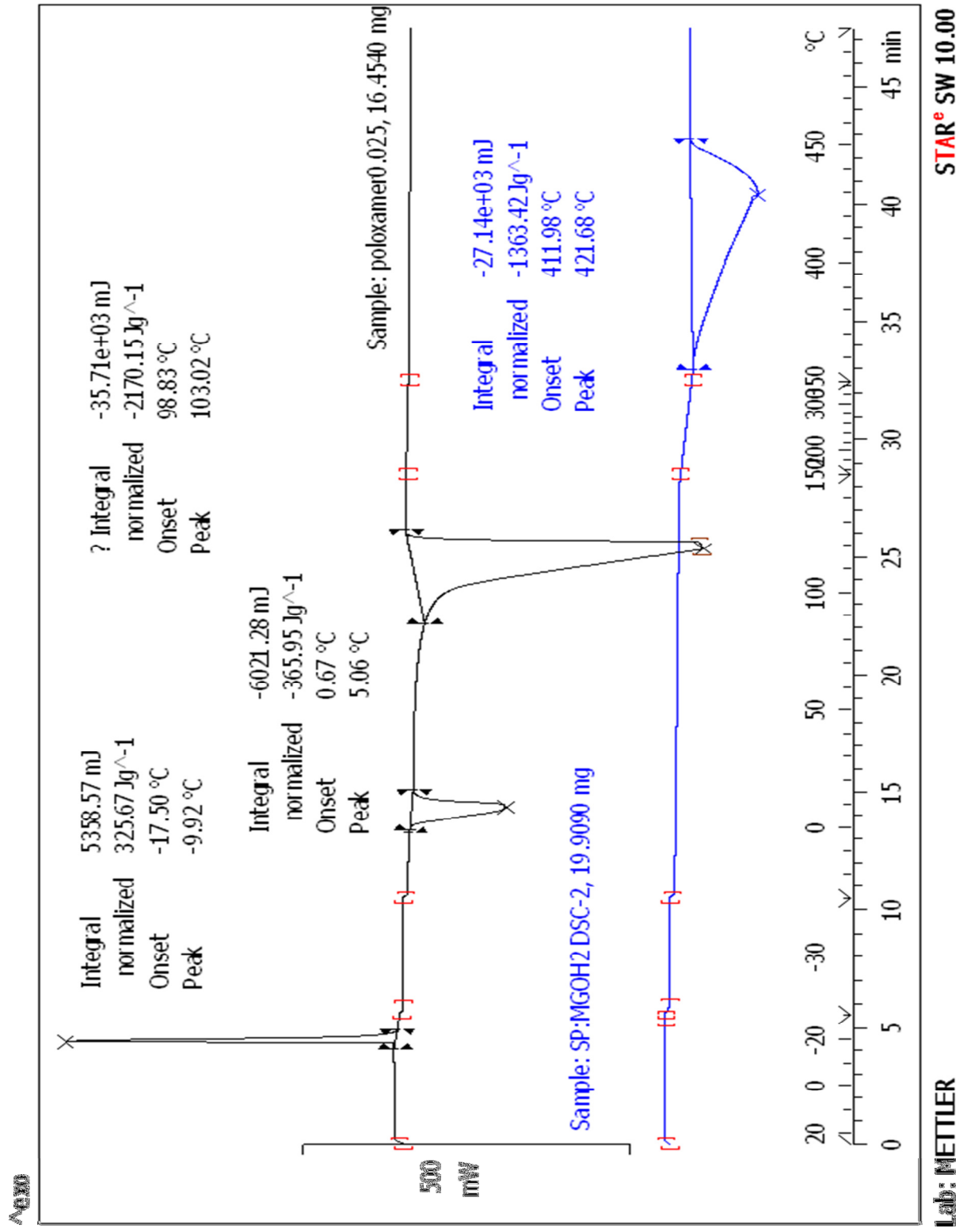

Figure 7-29: DSC thermogram of reference media and dried sediment of 1gm of magnesium hydroxide in 0.025% Poloxamer

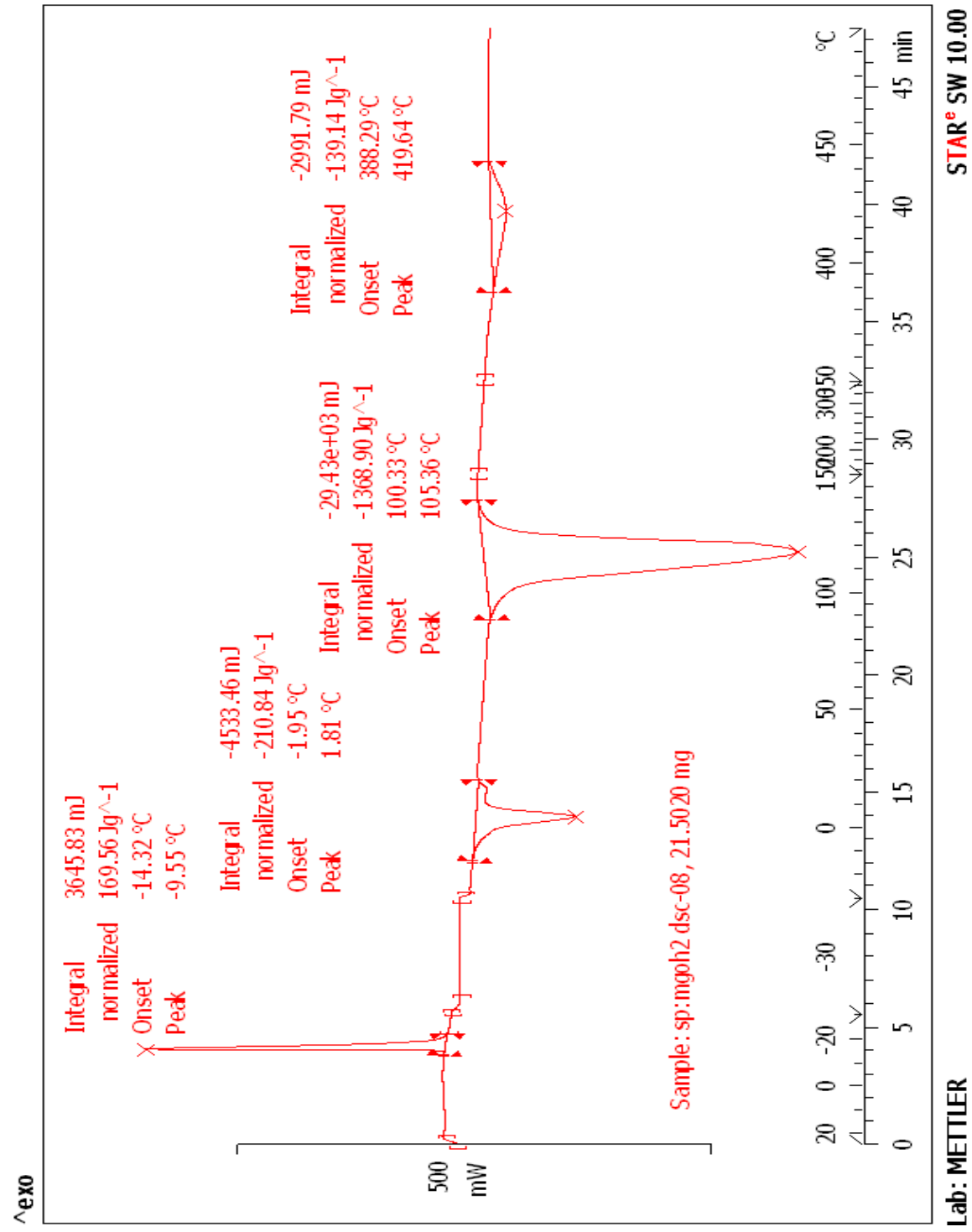

Figure 7-30: DSC thermogram of 1gm of magnesium hydroxide suspended in 0.05% Poloxamer

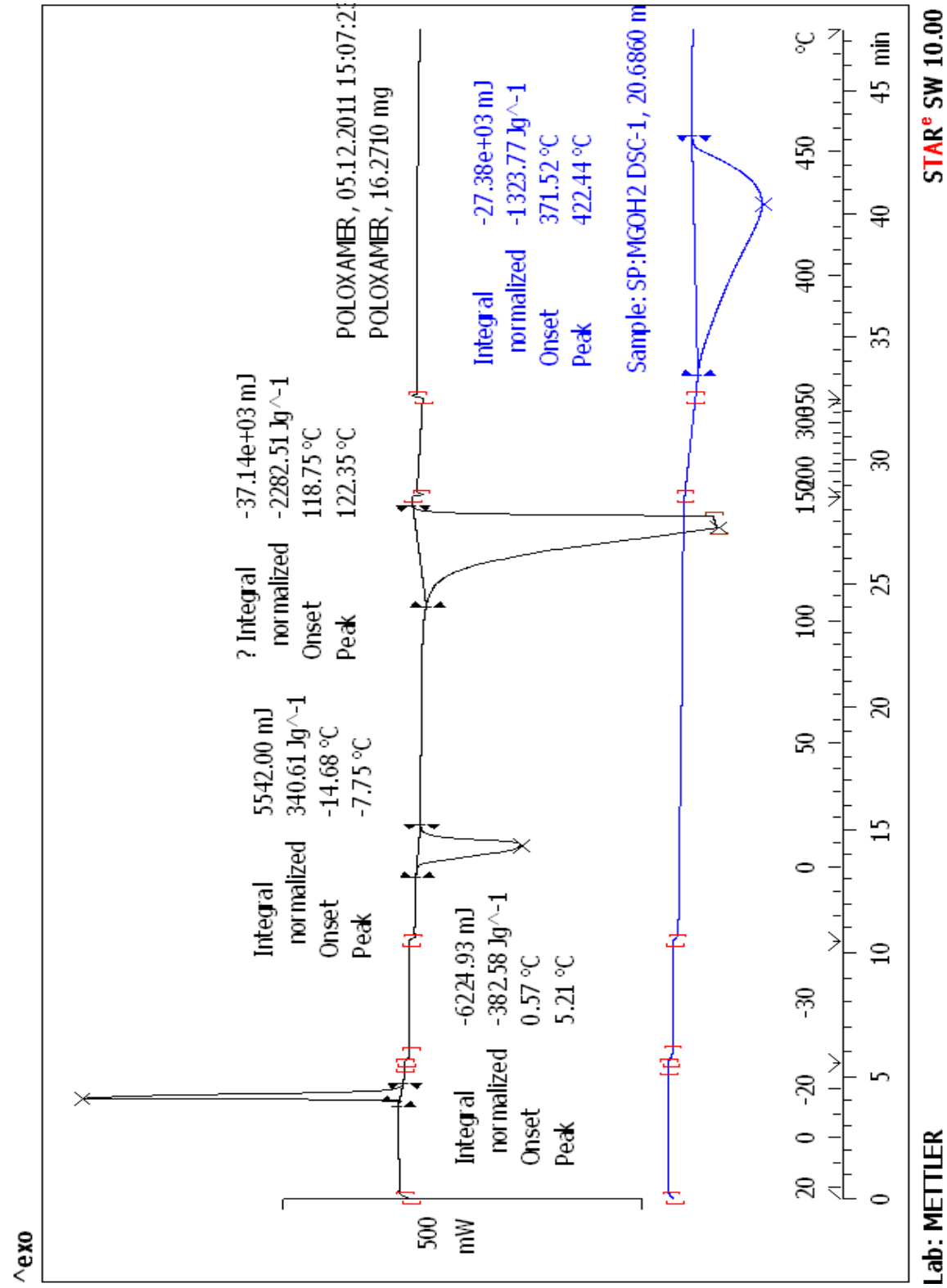

Figure 7-31: DSC thermogram of reference media and dried sediment of 1gm of magnesium hydroxide in 0.05% Poloxamer

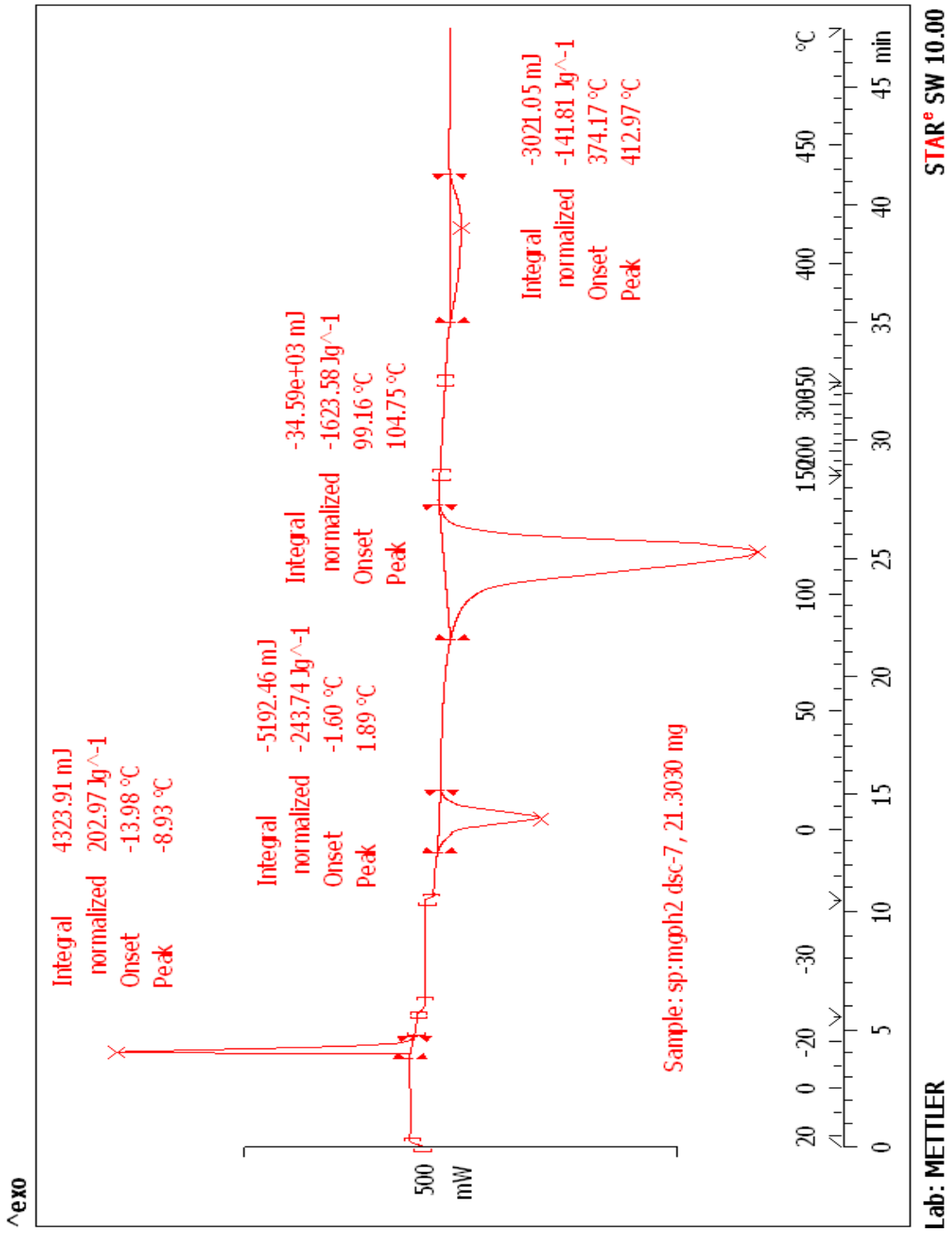

Figure 7-32: DSC thermogram of 1gm of magnesium hydroxide suspended in 0.075% Poloxamer

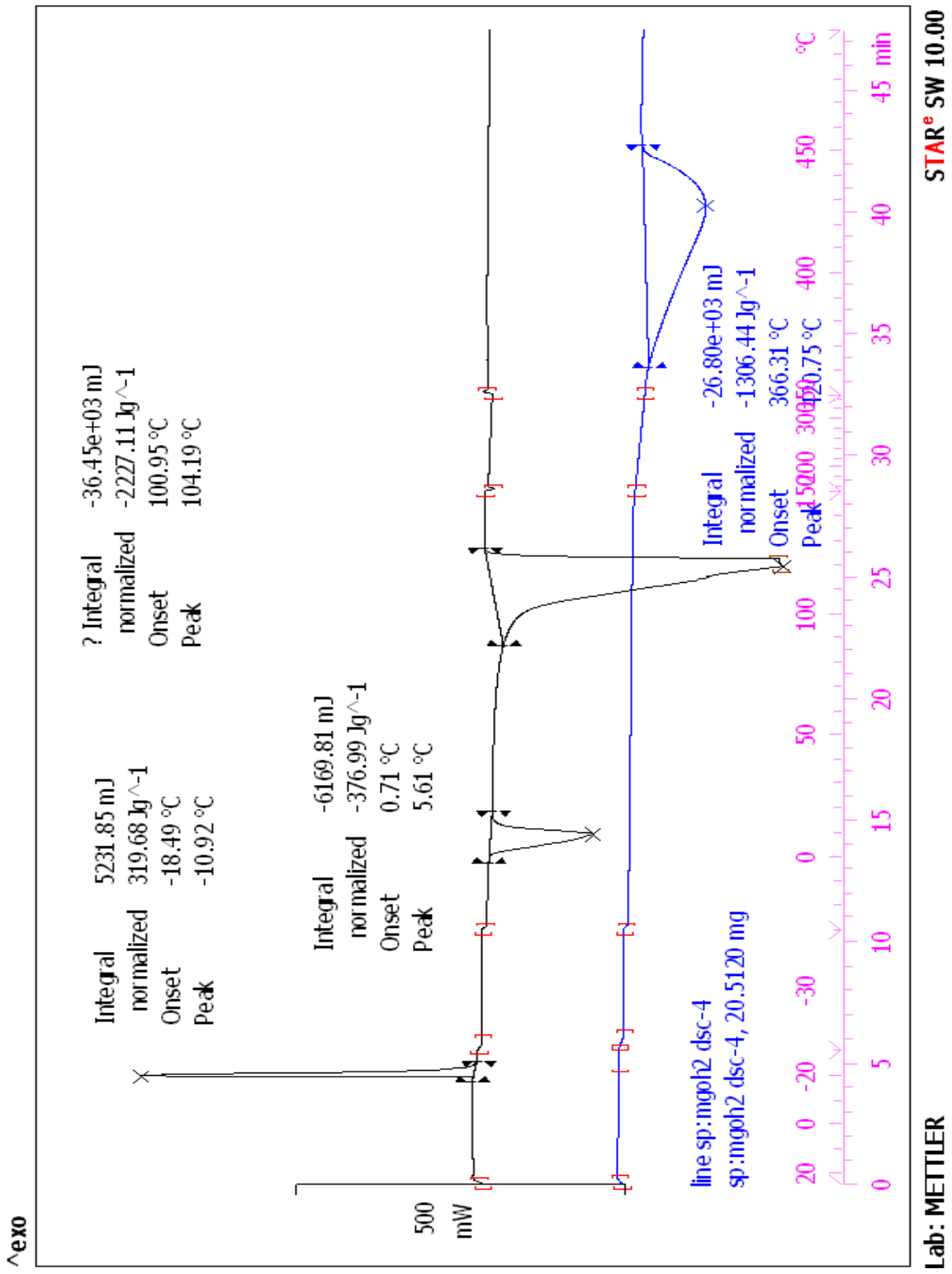

Figure 7-33: DSC thermogram of reference media and dried sediment of 1gm of magnesium hydroxide in 0.075% Poloxamer

The average water content for each of the suspensions was determined by the relative heat of crystallization and fusion by using the reference media and dried sediments. This water content is loosely bound water or unbound water present in the filtered sediments. This method cannot be used for the determination of bound water content in the sediments. From the Table 7.25, it was observed that there was an increase in water content of the suspensions as the concentration of Poloxamer increased.

Table 7.25: Average water content for 1gm magnesium hydroxide suspended in different media

Medium	Relative ΔH_c (%)	Relative ΔH_f (%)	Relative ΔH_v (%)	Average water content (%)
Water	15.78	11.03	42.49	23.10
0.025% Poloxamer	52.13	43.84	58.79	51.58
0.05% Poloxamer	49.78	55.11	59.97	54.95
0.075% Poloxamer	63.49	64.65	72.90	67.01

7.5 Thermogravimetry (TG) results:

TG was performed on 1gm magnesium hydroxide suspended in water, 0.025%, 0.05% and 0.075% Poloxamer as described in Chapter-6, Section 6.3.12.

Thermograms for all four suspensions are given in Figure 7.34 to 7.37. The first derivative of the thermogram was obtained to determine the water loss. Three different temperatures where water loss is observed for each of the suspensions is given in Table 7.26.

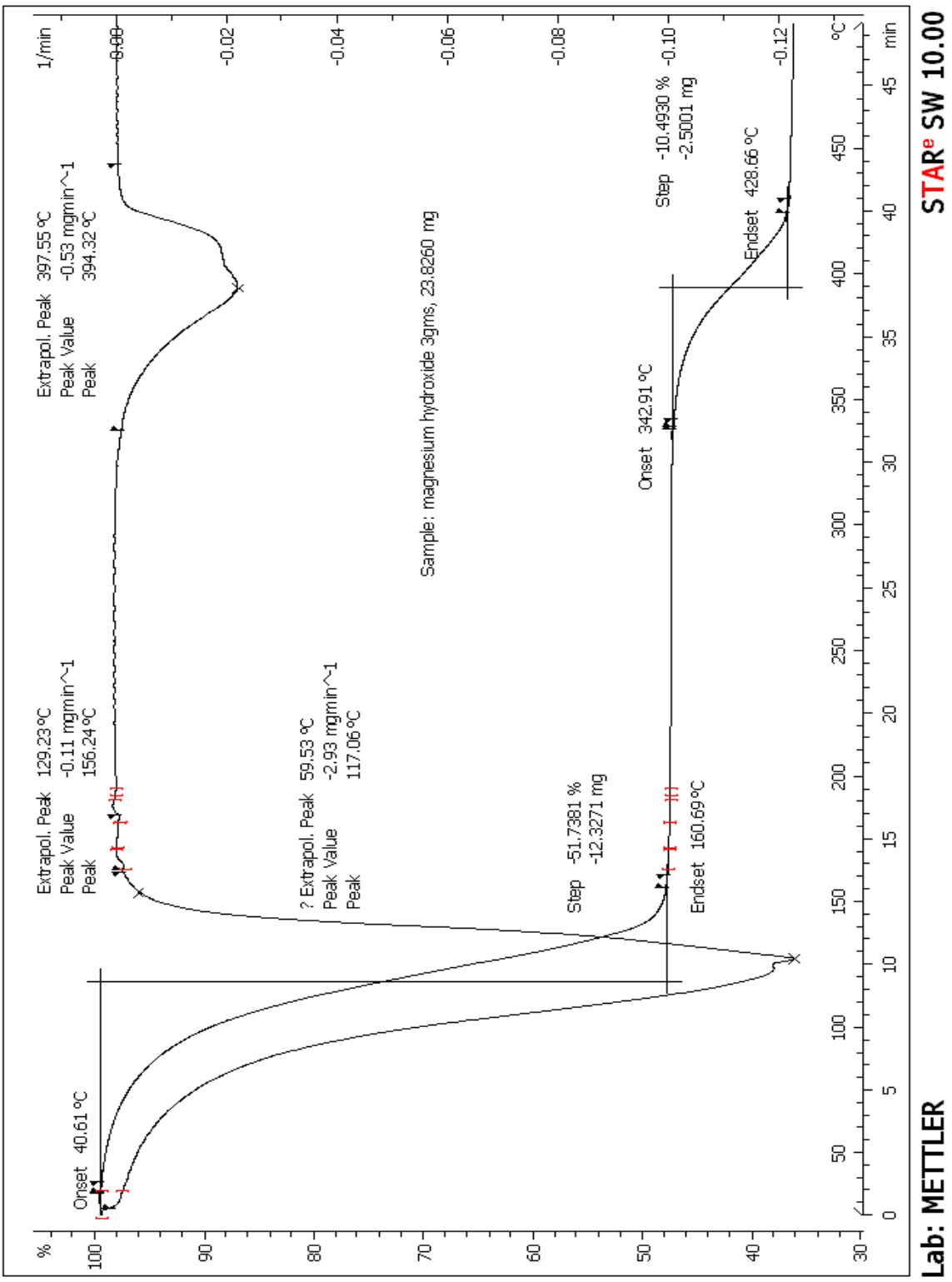

Figure 7-34: TG thermogram of 1gm of magnesium hydroxide suspended in water.

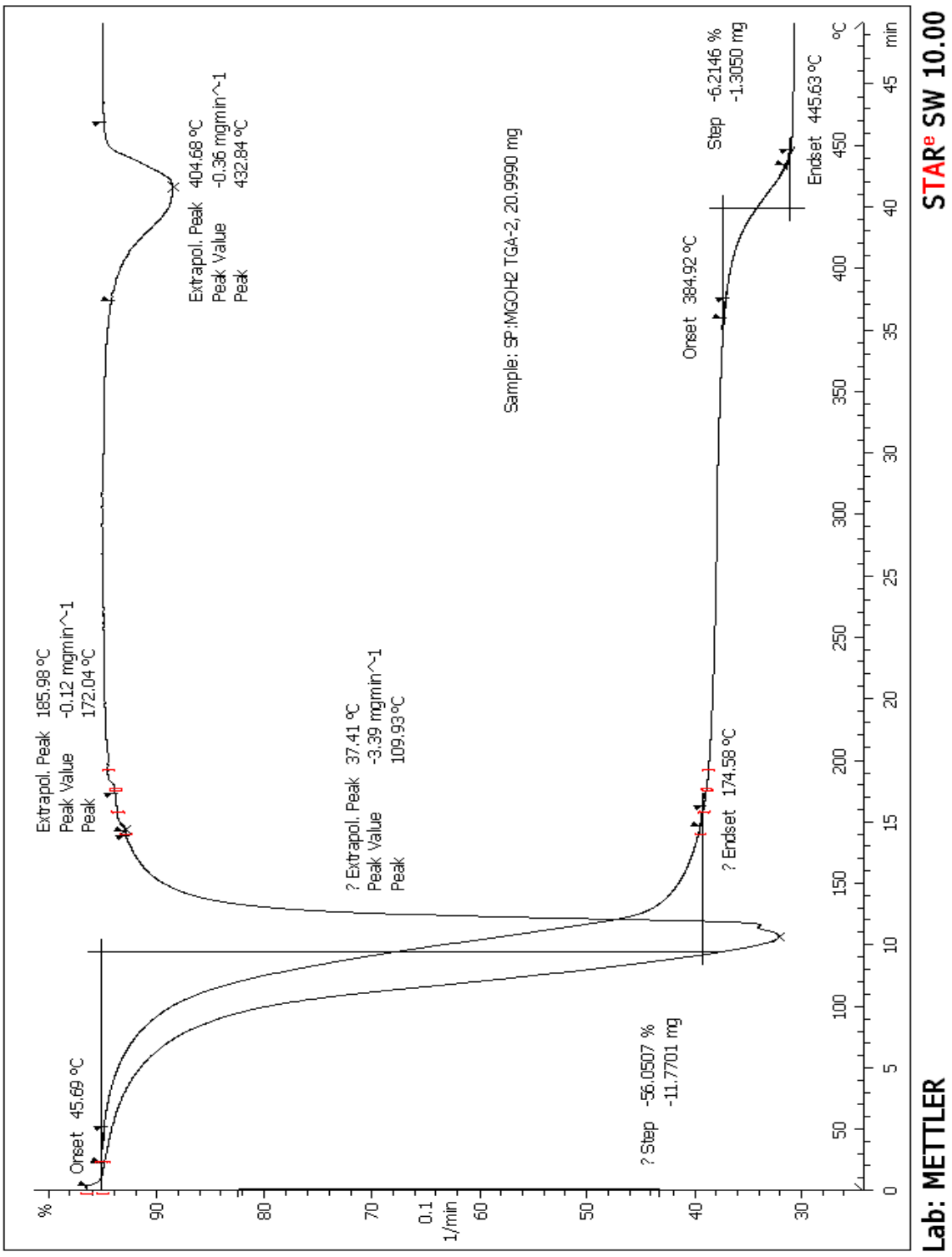

Figure 7-35: TG thermogram of 1gm of magnesium hydroxide suspended in 0.025% Poloxamer

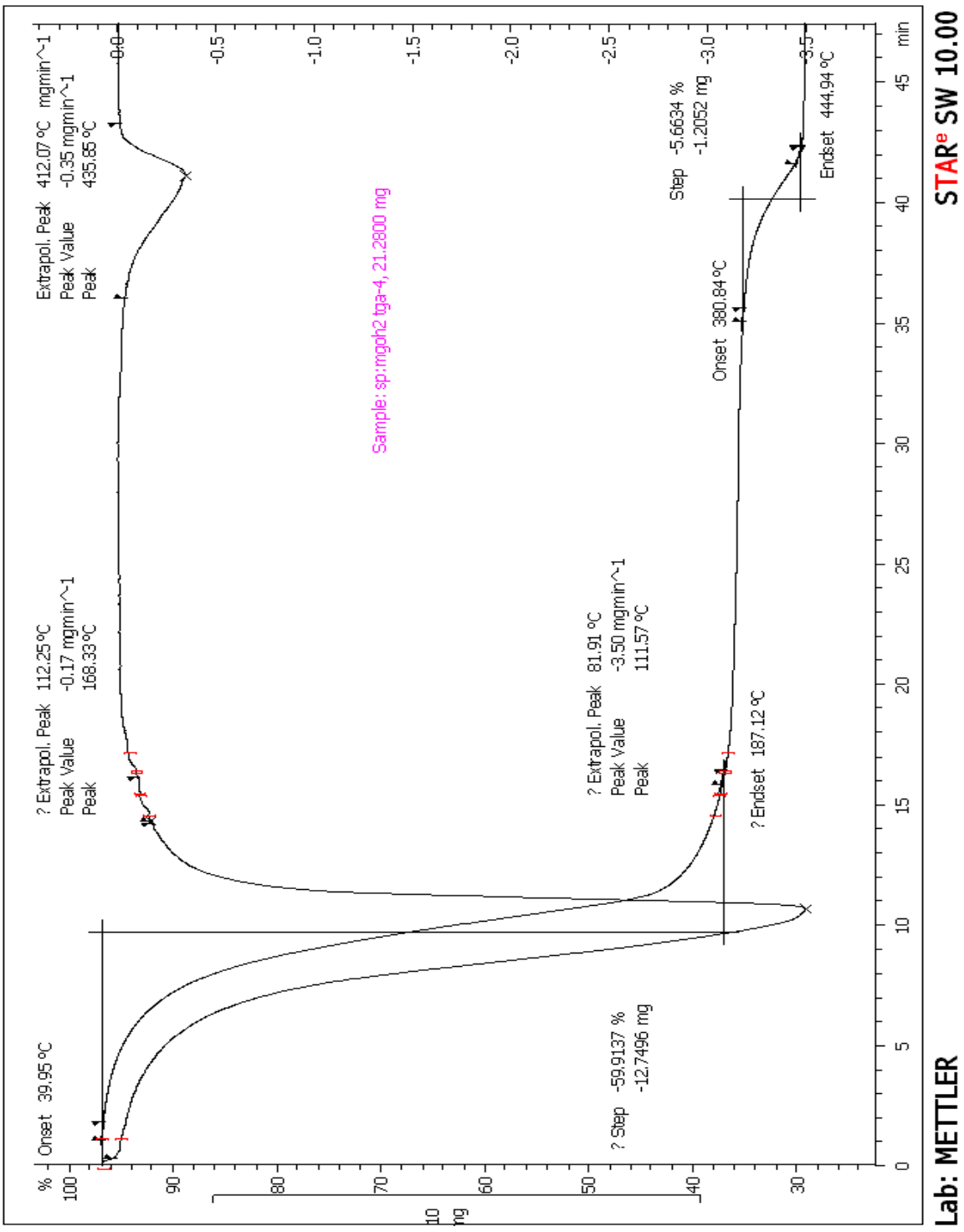

Figure 7-36: TG thermogram of 1gm of magnesium hydroxide suspended in 0.05% Poloxamer

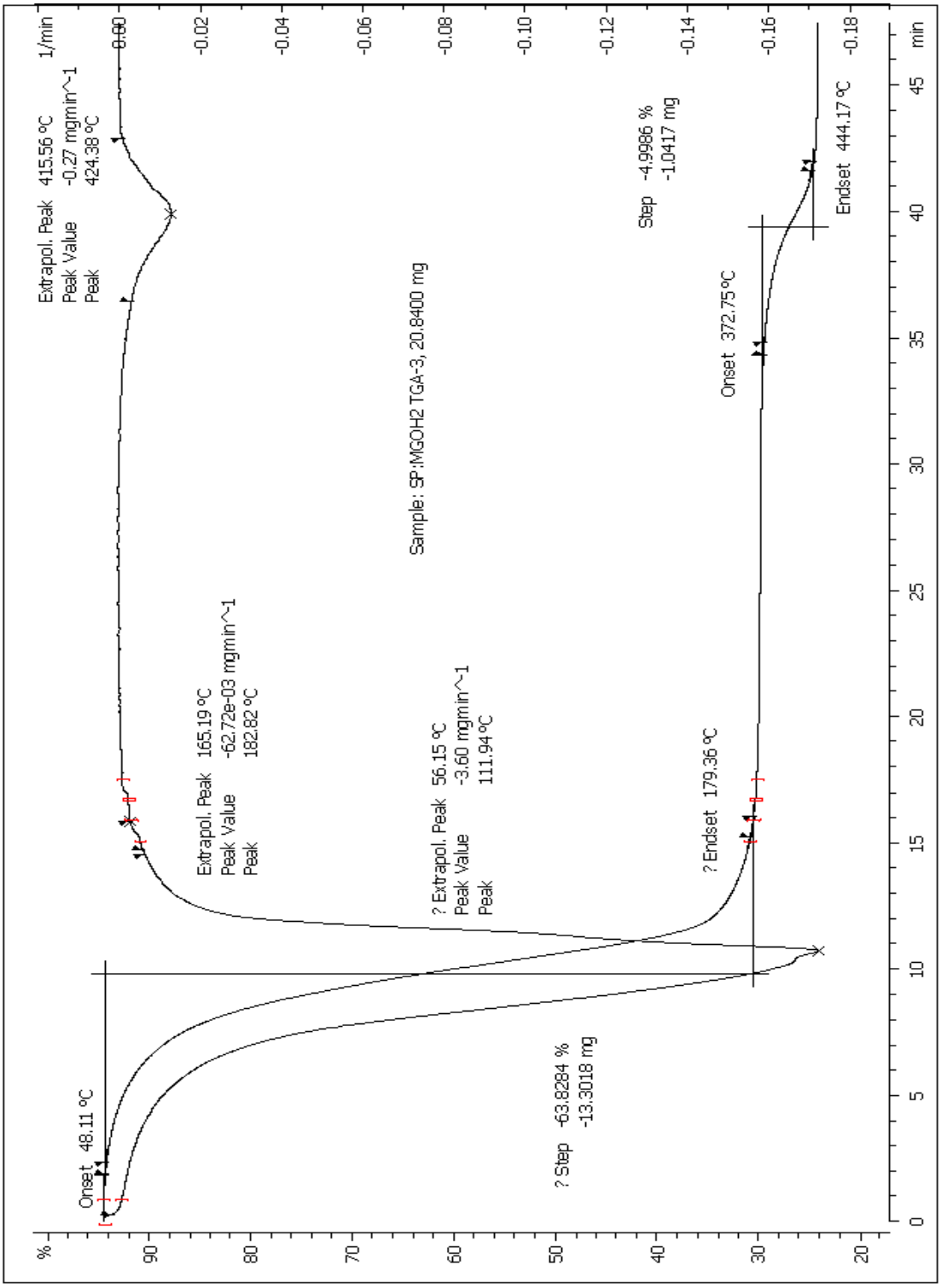

Figure 7-37: TG thermogram of 1gm of magnesium hydroxide suspended in 0.075% Poloxamer

Table 7.26: Peak temperatures for TG thermograms of magnesium hydroxide suspended in different media

Medium	$T_1(^0C)$	$T_2(^0C)$	$T_3(^0C)$
Water	117.06	156.24	394.32
0.025% Poloxamer	109.93	172.04	432.84
0.05% Poloxamer	111.57	168.33	435.85
0.075% Poloxamer	111.94	182.82	424.38

The percentage mass loss at different temperatures for all the suspensions is given in Table 7.27. The first derivative of the thermogram shows three different peaks, the first derivative peak at around 110^{o}C is due to the loss of unbound water, the second peak at around 160^{o}C is due to the loss of bound water; the third peak at 420^{o}C is because of degradation of magnesium hydroxide. The total percentage water loss with the percentage of bound and unbound water is given in Tables 7.28 and 7.29.

Table 7.27: Mass loss associated with the thermograms of magnesium hydroxide suspended in different media

Medium	Mass loss (%)	Onset (^{0}C)	Endset (^{0}C)
Water	51.7381	40.61	160.69
	10.4930	342.91	428.66
0.025% Poloxamer	56.0507	45.69	174.58
	6.2146	384.92	445.63
0.05% Poloxamer	59.9137	39.95	187.12
	5.6634	380.84	444.94
0.075% Poloxamer	63.8284	48.11	179.36
	4.9986	372.75	444.17

Table 7.28: Percentage of water loss along with percentage of unbound and bound water for magnesium hydroxide suspended in different media

Medium	Total mass loss (%)	Unbound (%)	Bound (%)
Water	51.7381	49.8660	1.8721
0.025% Poloxamer	56.0507	54.1344	1.9163
0.05% Poloxamer	59.9137	57.9137	2.7753
0.075% Poloxamer	63.8284	62.7354	1.0930

Table 7.29: Percentage of unbound and bound water content in magnesium hydroxide suspended in different media

Medium	Unbound (%)	Bound (%)
Water	96.38	3.62
0.025% Poloxamer	96.58	3.42
0.05% Poloxamer	96.66	3.34
0.075% Poloxamer	98.29	1.71

Although the total mass loss increased, the system was flocculated. The percentage of unbound water increases as the system is flocculated also as the concentration of Poloxamer increases. This may be due to the fact that Poloxamer causes bridging of magnesium hydroxide particles leading to decreased sites for the binding of water.

7.6 X-ray Powder Diffraction (PXRD) results:

PXRD was performed as described in Chapter-6 Section 6.3.13. PXRD was performed on commercial magnesium hydroxide, dried magnesium hydroxide suspended in water as well as with Poloxamer. The diffractograms indicate that the pattern is same for all three samples as seen in Figure 7.38.

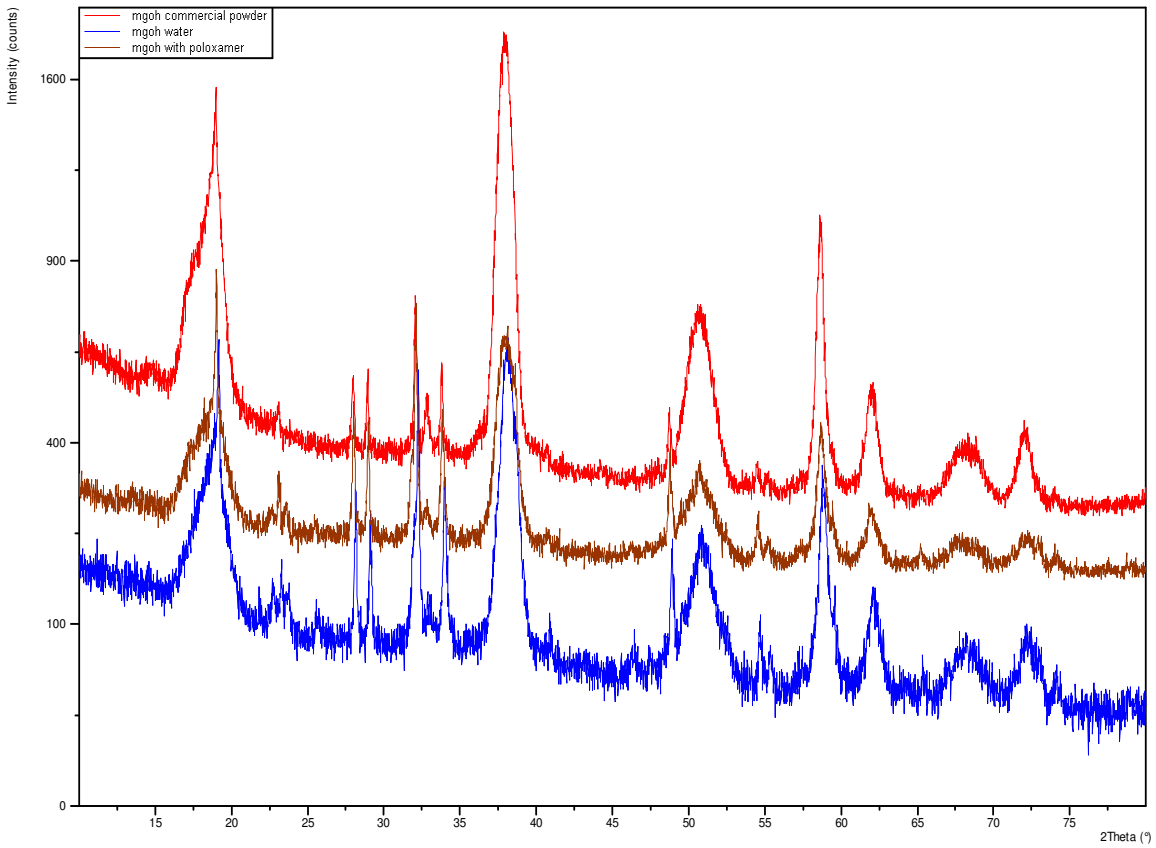

Figure 7-38: Diffractograms of dried commercial powder, dried magnesium hydroxide suspended in water and Poloxamer.

The diffractogram for magnesium hydroxide after it is heated till 500^0C using TG is shown in the Figure 7-39. The pattern in the diffractogram was compared to standard diffraction patterns for different substances. The presence of both magnesium hydroxide and magnesium oxide was observed from the Figure 7-40. Magnesium oxide was seen because of the degradation of magnesium hydroxide to magnesium oxide. Magnesium hydroxide was also seen because of its incomplete degradation.

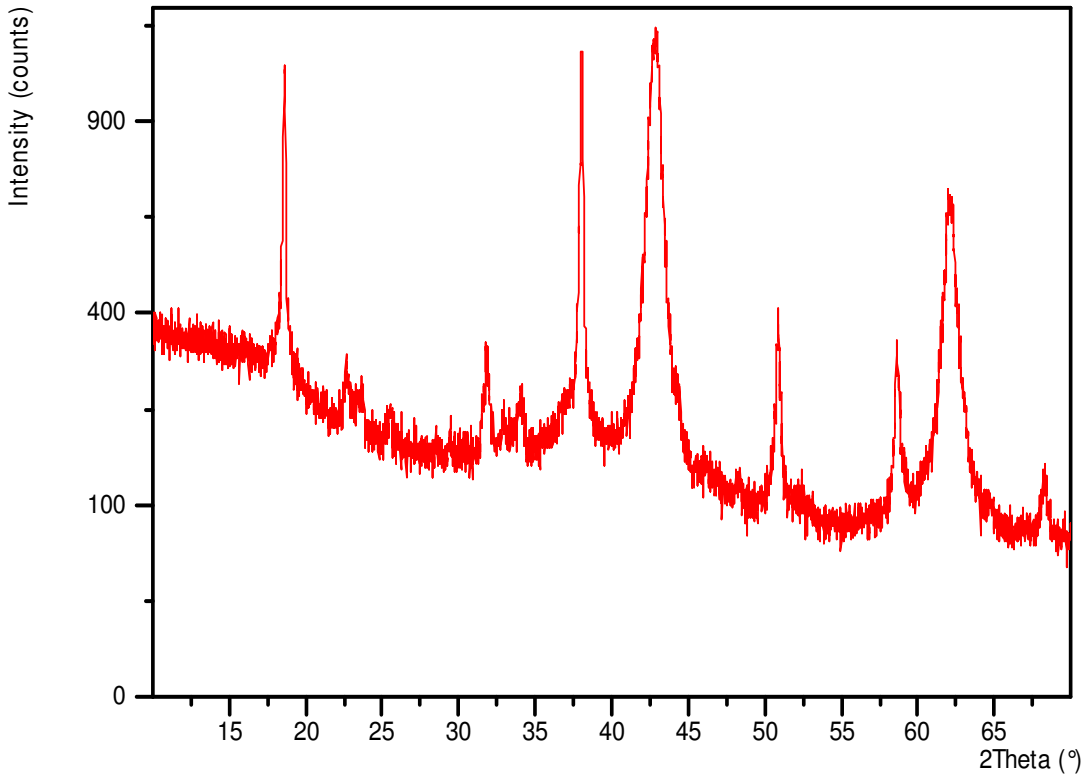

Figure 7-39: Diffractogram of the sample after heating using TG.

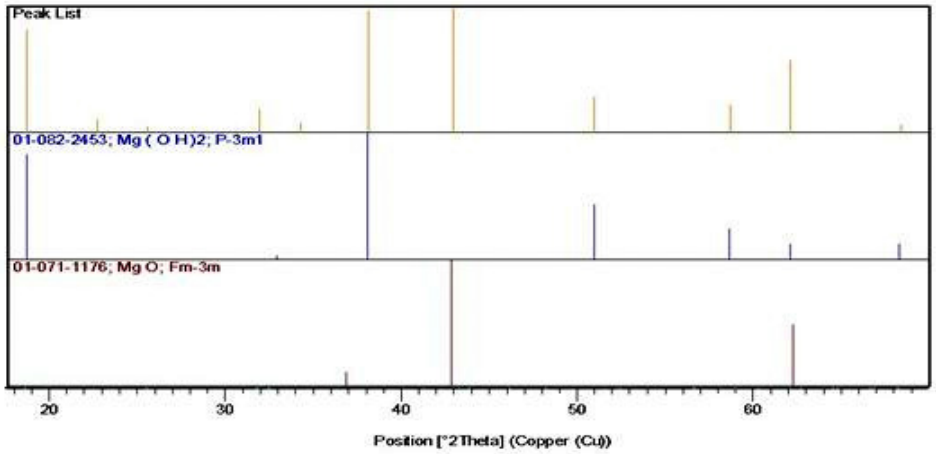

Figure 7-40: Peak list of the sample after heating using TGA.

Chapter 8

Conclusions and Future work

8.1 **Conclusions**

Never dried suspensions of magnesium hydroxide shows hindered settling behavior. Caking of the suspensions was not observed and was redispersible. Hindered settling proved to be an effective way of determining particle size for the suspensions. These suspensions obey the equations put forth by Steinour, Richardson & Zaki and Dollimore & McBride. There is also good correlation between all the three equations.

Magnesium hydroxide suspensions can be flocculated using Poloxamer 407. The effective concentration range was found to be 0.025% to 0.075% to achieve flocculation of the suspensions. As the concentration of the flocculant increased, particle size increased indicating maximum flocculation. When higher concentrations of Poloxamer were used, the system deflocculated. Flocculation is mainly achieved by polymer bridging between particles, thereby causing an increase in the particle size. Zeta potential measurements showed that increasing flocculation did not affect the zeta potential of the suspensions. The conclusion was that Poloxamer causes bridging between the particles by adsorption without involving any electrostatic interactions.

Permeability studies indicate that as flocculation increased permeability of the suspension decreases. This could be due to the fact that flocculation results in all particles attaching to one another leading to decreased pores through which the fluid can move.

By varying the rate of addition of Sodium hydroxide, particle size of the magnesium hydroxide can be modified. Slower addition causes larger particles because of the additional time needed for nucleation. SEM pictures show the presence of rod shaped crystals of magnesium hydroxide and depicted the formation of floccules where even the smallest particles come together to form a loose aggregate. Laser Diffraction results were not consistent with hindered settling results since the sample measurement involves a homogenizer which breaks up all the floccules and their exact size could not be determined.

DSC and TGA studies indicate that the water content increases with flocculation and the percentage of bound water content decreased because more particles get attached to the Poloxamer leading to fewer binding sites for water. Magnesium hydroxide starts degrading to magnesium oxide at around 420^{o}C and is confirmed by PXRD studies.

8.2 **Future Recommendations**

More studies should be performed to determine a more efficient way of producing never dried magnesium hydroxide suspensions since this method involves the tedious washing process to remove as much as the sodium sulfate as possible.

Other cationic and anionic flocculants can be used to produce flocculation of this system and their electrostatic interaction between the particles can be studied.

The effect of pH on the flocculation behavior of various ionic and nonionic polymers suspensions can also be studied.

A more sophisticated method of determining bound and unbound water content by DSC should be investigated.

References for Chapter-1

1. Kusolmanomai, N., The behavior of magnesium hydroxide suspensions in the never dried state and flocculated with polymer flocculants, 1993, University of Toledo. p. xiv, 171 leaves.

References for Chapter-2

1. Collins, A.G., *Geochemistry of oilfield waters*. Vol. 1. 1975: Elsevier Science & Technology.
2. Rogers, C.H., *A text-book of inorganic pharmaceutical chemistry*. 1943: Lea & Febiger.
3. Kusolmanomai, N., *The behavior of magnesium hydroxide suspensions in the never dried state and flocculated with polymer flocculants*. 1993, University of Toledo. p. xiv, 171 leaves.
4. Bothara, K., *Inorganic Pharmaceutical Chemistry*. 2008: Pragati Books Pvt. Ltd.
5. Wikipedia. *Magnesiumhydroxide*. 2012; Available from: http://en.wikipedia.org/wiki/Magnesium_hydroxide.
6. Gennaro, A.R., *Remington: the science and practice of pharmacy*. Vol. 20. 2000: Lippincott Williams & Wilkins Philadelphia.

References for Chapter-3

1. Basu, A., et al., *Extension of the compartment theory for hindered settling suspensions.* STP Pharma Sciences, 1997. **7**(3): p. 215-222.
2. Bhatty, J., L. Davies, and A. Dollimore, *The use of hindered settling data to evaluate particle size or floc size, and the effect of particle-liquid association on such sizes.* Surface Technology, 1982. **15**(4): p. 323-344.
3. Ramakrishna, V., S. Rao, and L. Ahuja, *Particle size determination by hindered settling and cluster formation.* Journal of Applied Chemistry, 1966. **16**(10): p. 310-312.
4. Majumder, A., *Settling velocities of particulate systems- a critical review of some useful models.* Minerals and Metallurgical Processing, 2007. **24**(4): p. 237-242.
5. Kusolmanomai, N., *The behavior of magnesium hydroxide suspensions in the never dried state and flocculated with polymer flocculants*. 1993, University of Toledo. p. xiv, 171 leaves.
6. Youssef, B., *The application of thermal analysis to the study of the behavior of concentrated aqueous suspensions of kaolin and talc*. 1996, University of Toledo. p. xxiii, 190 leaves.
7. Bhatty, J. and A. Dollimore, *Studies on the suspending properties of aqueous solutions of some natural and synthetic hydrocolloids on china clay suspensions.* Water Research, 1978. **12**(12): p. 1139-1148.

8. Bhatty, J.I., et al., *Suspensions and Sediments. Part I. Particle-Particle Interactions in Dilute Solid-Liquid Suspensions.* Separation Science and Technology, 1989. **24**(1-2): p. 1-14.

9. Zimmels, Y., *Theory of hindered sedimentation of polydisperse mixtures.* AIChE journal, 1983. **29**(4): p. 669-676.

10. Dollimore, D. and R. Karimian, *Sedimentation of suspensions: Factors affecting the hindered settling of alumina in a variety of liquids.* Surface Technology, 1982. **17**(3): p. 239-250.

11. Ramakrishna, V. and S. Rao, *Particle size determination and hindered settling.* Journal of Applied Chemistry, 1965. **15**(10): p. 473-479.

12. Tomkins, M.R., T.E. Baldock, and P. Nielsen, *Hindered settling of sand grains.* Sedimentology, 2005. **52**(6): p. 1425-1432.

13. Di Felice, R. and R. Kehlenbeck, *Sedimentation velocity of solids in finite size vessels.* Chemical engineering & technology, 2000. **23**(12): p. 1123-1126.

14. Davies, L., D. Dollimore, and J. Sharp, *Sedimentation of supsensions: implications of theories of hindered settling.* Powder Technology, 1975. **13**(1): p. 123-132.

15. Baldock, T., et al., *Settling velocity of sediments at high concentrations.* Coastal engineering, 2004. **51**(1): p. 91-100.

16. Davies, L., D. Dollimore, and G. McBride, *Sedimentation of suspensions: simple methods of calculating sedimentation parameters.* Powder Technology, 1977. **16**(1): p. 45-49.

17. Dollimore, D. and G. McBride, *Comparison of methods of calculating particle size from hindered settling results and its application to inorganic oxysalt precipitates.* Analyst, 1969. **94**(1122): p. 760-767.

18. Davies, L. and D. Dollimore, *Theoretical and experimental values for the parameter k of the Kozeny-Carman equation, as applied to sedimenting suspensions.* Journal of Physics D: Applied Physics, 1980. **13**: p. 2013.

19. Lea, F. and R. Nurse, *The specific surface of fine powders.* J. Soc. Chem. Ind, 1939. **58**: p. 277–283.

20. Rigden, P., *The specific surface of powders. A modification of the theory of the air-permeability method.* Journal of the Society of Chemical Industry, 1947. **66**(4): p. 130-136.

21. Allison, E. and P. Murray, *Sedimentation from Concentrated Suspensions in Relation to Particle Size*. 1951, Atomic Energy Research Establishment, Harwell, Berks,(England).

22. Azizi, J., et al., *The development of a permeability theory applied to concentrated suspensions.* Colloids and surfaces, 1992. **62**(1-2): p. 1-9.

23. Happel, J., *Viscous flow in multiparticle systems: slow motion of fluids relative to beds of spherical particles.* AIChE journal, 1958. **4**(2): p. 197-201.

24. Dollimore, D. and G. McBride, *Alternative methods of calculating particle size from hindered settling measurements.* Journal of Applied Chemistry, 1968. **18**(5): p. 136-140.

25. McKay, R.B., *Hindered settling of organic pigment dispersions in hydrocarbon liquids.* Journal of Applied Chemistry and Biotechnology, 1976. **26**(2): p. 55-66.

26. Rutgers, I.R., *Relative viscosity of suspensions of rigid spheres in Newtonian liquids.* Rheologica Acta, 1962. **2**(3): p. 202-210.

27. Simha, R., *The Influence of Brownian Movement on the Viscosity of Solutions.* The Journal of Physical Chemistry, 1940. **44**(1): p. 25-34.

28. Pendse, A., *Interpretations of hindered settling behavior of never dried magnesium carbonate suspensions*. 1995, University of Toledo. p. xiv, 110 leaves.

References for Chapter-4

1. Aulton, M.E. and J.W. Cooper, *Pharmaceutics: the science of dosage form design.* 2002.
2. Lachman, L., H.A. Lieberman, and J.L. Kanig, *The theory and practice of industrial pharmacy*1970, Philadelphia,: Lea & Febiger. xii, 811 p.
3. Martin, A.N., J. Swarbrick, and A. Cammarata, *Physical pharmacy : physical chemical principles in the pharmaceutical science*. 2d ed1969, Philadelphia: Lea & Febiger. vii, 637 p.
4. Bolt, G., *Analysis of the validity of the Gouy-Chapman theory of the electric double layer.* Journal of colloid science, 1955. 10(2): p. 206-218.
5. Li, L.C. and Y. Tian, *Zeta potential.* Encyclopedia of pharmaceutical technology, 2002. 2: p. 429–458.
6. Lyklema, J., H. Van Leeuwen, and M. Minor, *DLVO-theory, a dynamic re-interpretation.* Advances in colloid and interface science, 1999. 83(1-3): p. 33-69.
7. Malvern.2011;Availablefrom: http://www.malvern.com/LabEng/industry/colloids/dlvo_theory.htm.
8. Shin, W.W. and K.P. Lee, *Effect of electrolytes on rheological properties of Young-Il bentonite suspension.* Archives of Pharmacal Research, 1985. 8(2): p. 91-98.

9. Pharmainfo.net. 2005; Available from: http://www.pharmainfo.net/free-books/pharmaceutical-suspensionsa-review.

10. Nielloud, F. and G. Marti-Mestres, *Pharmaceutical emulsions and suspensions*. Vol. 105. 2000: Informa HealthCare.

11. Hiestand, E.N., *Theory of coarse suspension formulation.* Journal of Pharmaceutical Sciences, 1964. 53(1): p. 1-18.

12. Kusolmanomai, N., *The behavior of magnesium hydroxide suspensions in the never dried state and flocculated with polymer flocculants*, 1993, University of Toledo. p. xiv, 171 leaves.

13. Dollimore, D. and T. Horridge, *The optimum flocculant concentration for effective flocculation of china clay in aqueous suspension.* Water Research, 1972. 6(6): p. 703-710.

14. Pugh, T.L. and W. Heller, *Coagulation and stabilization of colloidal solutions with polyelectrolytes.* Journal of Polymer Science, 1960. 47(149): p. 219-227.

15. Kragh, A. and W. Langston, *The flocculation of quartz and other suspensions with gelatine.* Journal of colloid science, 1962. 17(2): p. 101-123.

References for Chapter-5

1. AZojomo, T.A.t.Z.o.M.a. *Particle Size Analysis - The Laser Diffraction Technique*. 2011; Available from: http://www.azom.com/article.aspx?ArticleID=1528.
2. Chu, B., *Laser light scattering.* NASA STI/Recon Technical Report A, 1974. **75**: p. 12150.
3. Torchilin, V. and M.M. Amiji, *Handbook of Materials for Nanomedicine*. Vol. 1. 2010: Pan Stanford Pub.
4. Dr Paul Kippax, E.B.P. *Measuring particle size using modern laser diffraction techniques*. 2011; Available from: http://www.chemeurope.com/en/whitepapers/61205/measuring-particle-size-using-modern-laser-diffraction-techniques.html.
5. Botiren, C. and D.R. Huffman, *Absorption and scattering of light by small particles.* J Wiley & Sons, New York, 1983.
6. Jones, R.M., *Particle size analysis by laser diffraction: ISO 13320, standard operating procedures, and Mie theory.* American Laboratory(USA), 2003. **35**(1): p. 44-47.
7. de Boer, G.B.J., et al., *Laser diffraction spectrometry: Fraunhofer diffraction versus Mie scattering.* Particle & Particle Systems Characterization, 1987. **4**(1-4): p. 14-19.
8. Blott, S.J., et al., *Particle size analysis by laser diffraction.* Geological Society, London, Special Publications, 2004. **232**(1): p. 63-73.

9. Malvern. 2011; Available from: http://www.malvern.com/LabEng/industry/colloids/dlvo_theory.htm.

10. Analyser, C.P.S. 2004; Available from: http://www.particle-size-analyzer.com/frequently_asked_questions.pdf.

11. Ltd, M.I., *Laser Diffraction Particle Sizing.* 2011.

12. Bürkholz, A. and R. Polke, *Laser diffraction spectrometers/experience in particle size analysis.* Particle & Particle Systems Characterization, 1984. **1**(1 4): p. 153-160.

13. Malvern. *Electrophoretic light scattering*. 2012; Available from: http://www.malvern.com/labeng/technology/electrophoretic-light-scattering.htm.

14. Ware, B., *Electrophoretic light scattering.* Advances in colloid and interface science, 1974. **4**(1): p. 1-44.

15. malvern. *Zeta potential measurement using laser doppler electrophoresis*. 2012; Availablefrom: http://www.malvern.com/labeng/technology/zeta_potential/zeta_potential_lde.htm.

16. Li, L.C. and Y. Tian, *Zeta potential.* Encyclopedia of pharmaceutical technology, 2002. **2**: p. 429–458.

17. manual, N.Z.U. *Zeta potential*. Available from: http://www.colorado.edu/ceae/environmental/ryan/research/pdfs/pss-zls-manual.pdf.

18. Wikipedia. *Electrophoretic light scattering*. 2012; Available from: http://en.wikipedia.org/wiki/Electrophoretic_light_scattering.

19. Goldstein, J., *Scanning electron microscopy and X-ray microanalysis*. Vol. 1. 2003: Springer Us.

20. University, M.S. 2011; Available from: http://serc.carleton.edu/research_education/geochemsheets/techniques/SEM.html.

21. Reimer, L., *Scanning electron microscopy: physics of image formation and microanalysis*. Vol. 45. 1998: Springer Verlag.

22. Hafner, B. 2007; Available from: http://www.charfac.umn.edu/sem_primer.pdf.

23. Bozzola, J.J., *Electron microscopy*1992: Wiley Online Library.

24. Wikipedia. 2011; Available from: http://en.wikipedia.org/wiki/Scanning_electron_microscope.

25. Gabriel, B.L., *SEM: A user's manual for materials science.* 1985.

26. University, P. 2010; Available from: http://www.purdue.edu/rem/rs/sem.htm.

27. Dubes, A., et al., *Scanning electron microscopy and atomic force microscopy imaging of solid lipid nanoparticles derived from amphiphilic cyclodextrins.* European Journal of Pharmaceutics and Biopharmaceutics, 2003. **55**(3): p. 279-282.

28. Wikipedia. *Differential Scanning Calorimetry*. 2011; Available from: http://en.wikipedia.org/wiki/Differential_scanning_calorimetry.

29. Höhne, G., W. Hemminger, and H.J. Flammersheim, *Differential scanning calorimetry*2003: Springer Verlag.

30. Mississippi, T.U.o.S. 2005; Available from: http://pslc.ws/macrog/dsc.htm.

31. Center, T.P.U. 2011; Available from: http://www.ms.ornl.gov/htmlhome/tpuc/dsc.html.

32. Boettinger, W.J., et al., *DTA and heat-flux DSC measurements of alloy melting and freezing*2006: US Department of Commerce, Technology Administration, National Institute of Standards and Technology.

33. Bratislava, S.u.o.t.i. *Laboratory of calorimetry*. 2012; Available from: http://www.fchpt.stuba.sk/generate_page.php?page_id=2890.

34. Reading, M., A. Luget, and R. Wilson, *Modulated differential scanning calorimetry.* Thermochimica acta, 1994. **238**: p. 295-307.

35. Simon, S.L., *Temperature-modulated differential scanning calorimetry: theory and application.* Thermochimica acta, 2001. **374**(1): p. 55-71.

36. Technology, D.o.F.a.C. 2004; Available from: http://www.chtf.stuba.sk/kach/lab_538.php.

37. Chemistry, P. 2011; Available from: http://www.lasalle.edu/academ/chem/ms/polymersRus/Resources/DSC.htm.

38. whisnantdm. *Polymer Chemistry*. 2001; Available from: http://faculty.uscupstate.edu/llever/Polymer%20Resources/DSC.htm.

39. Urbana-Champaign, U.o.I.a. 2011; Available from: http://scs.illinois.edu/microanalysis/dsc.php.

40. Giron, D., *Applications of thermal analysis in the pharmaceutical industry.* Journal of Pharmaceutical and Biomedical Analysis, 1986. **4**(6): p. 755-770.

41. Spink, C.H., *Differential scanning calorimetry.* Methods in cell biology, 2008. **84**: p. 115-141.

42. Chandrasekhar, S., B. Sadashiva, and K. Suresh, *Liquid crystals of disc-like molecules.* Pramana, 1977. **9**(5): p. 471-480.

43. Lopez, M.M. and G.I. Makhatadze, *Differential scanning calorimetry.* METHODS IN MOLECULAR BIOLOGY-CLIFTON THEN TOTOWA-, 2002. **173**: p. 113-120.

44. Wikipedia. *Thermogravimetric analysis*. 2011; Available from: http://en.wikipedia.org/wiki/Thermogravimetric_analysis.

45. Odlyha, M., R.P.W. Scott, and C. Simpson, *The hydroxyl content of silica gel.* Journal of Thermal Analysis and Calorimetry, 1993. **40**(3): p. 1197-1212.

46. Barron, C.d.F.a.A.R. *Thermogravimetric Analysis of Single Walled Carbon Nanotubes*. 2009; Available from: http://cnx.org/content/m22972/latest/.

47. Rawlinson, C. *Differential Scanning Calorimeter*. 2006; Available from: http://www.mmsconferencing.com/pdf/eyp/c.rawlinson.pdf.

48. University, C.S. *Thermogravimetry*. 2011.

49. Scott, R.P.W. *Physical chmeistry resources*. 2011; Available from: http://physicalchemistryresources.com/Book5_sections/TA_SilanolGroupsSurfaceSilicaGelHTML_1.htm.

50. Anderson Materials Evaluation, I. *Thermogravimetry*. 2007; Available from: http://www.andersonmaterials.com/tga.html.

51. Barnes, A., M. Hardy, and T. Lever, *A review of the applications of thermal methods within the pharmaceutical industry.* Journal of Thermal Analysis and Calorimetry, 1993. **40**(2): p. 499-509.

52. Barbara L Dutrow, C.M.C. *X-ray Powder Diffraction*. 2011; Available from: http://serc.carleton.edu/research_education/geochemsheets/techniques/XRD.html.

53. Whittingham, S. *X-ray analysis of a solid*. 1997; Available from: http://materials.binghamton.edu/labs/xray/xray.html.

54. Wikipedia. *Bragg's law*. 2011; Available from: http://en.wikipedia.org/wiki/Bragg's_law.

55. Guinier, A., *X-ray diffraction in crystals, imperfect crystals, and amorphous bodies*1994: Dover Publications.

56. Connolly, J.R. *Introduction to X-ray Powder Diffraction*. 2007; Available from: http://epswww.unm.edu/xrd/xrdclass/01-XRD-Intro.pdf.

57. S. Motamarri, S.L.A. *Structure Determination from X-Ray Powder Diffraction*. 2011; Available from: http://www2.egr.uh.edu/~smotamar/XRay/XRay.html.

58. Warren, B.E., *X-ray Diffraction*1990: Dover Pubns.

59. Chung, F.H. and D.K. Smith, *Industrial applications of X-ray diffraction*1999: CRC.

60. Suryanarayana, C. and M.G. Norton, *X-ray diffraction: a practical approach.* Microscopy and Microanalysis, 1998. **4**: p. 513-515.

61. Chiou, W.L., *Pharmaceutical applications of solid dispersion systems: x ray diffraction and aqueous solubility studies on griseofulvin polyethylene glycol 6000 systems.* Journal of Pharmaceutical Sciences, 1977. **66**(7): p. 989-991.

62. Khan, A.I., et al., *Intercalation and controlled release of pharmaceutically active compounds from a layered double hydroxideElectronic supplementary information (ESI) available: Fig. S1: X-ray diffraction patterns of (a)[LiAl2 (OH) 6] Cl· H2O and (b) LDH/Ibuprofen intercalate. See http://www. rsc.*

org/suppdata/cc/b1/b106465g. Chemical Communications, 2001(22): p. 2342-2343.

References for Chapter-6

1. Kuznetsov, S. and V. Dereogankin, *Physical Chemistry of Alumina Production by the Bayer Method.* Metallurgizdat, Moscow, 1964.

References for Chapter-7

1. Revision, U.S.P.C.C.o. *United States pharmacopeia, the national formulary*. 1985. United States Pharmacopeial Convention, Inc.